HYDRODYNAMIC STUDY OF SAIPAN'S WESTERN LAGOON

February 2019

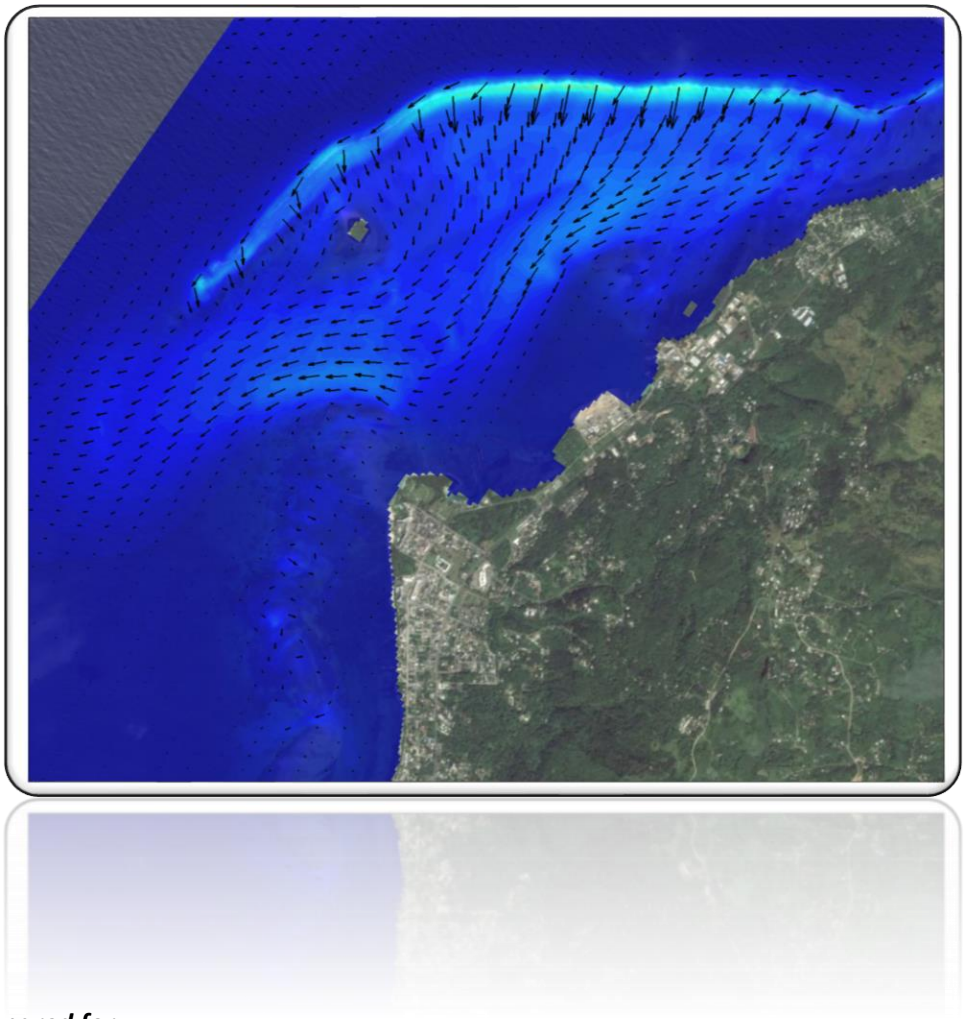

Prepared for:

Commonwealth of the Northern Mariana Islands
Bureau of Environmental and Coastal Quality
Caller Box 10007
Saipan, MP 96950

Prepared by:

Sea Engineering, Inc.
Makai Research Pier
Waimanalo, HI 96795

Job No. 25582

TABLE OF CONTENTS

LIST OF FIGURES

LIST OF TABLES

1. INTRODUCTION

Saipan, an island in the Commonwealth of the Northern Mariana Islands (CNMI), is located at approximately 15° 11' north latitude and 145° 43' east longitude. The Northern Mariana Islands are a group of fourteen islands, aligned north-south in a chain 708 kilometers (440 miles) long. Saipan, the largest island in the group, is also the center of government, business and population. The island is about 20.1 kilometers (12.5 miles) long and 8.9 kilometers (5.5 miles) wide. Saipan consists of a volcanic core capped by limestone (calcareous reef rock) terraces. Limestone cliffs, which also include local deposits of volcanic origin, line the eastern, northern and southern coasts of the island. The western coast, however, is composed of a narrow coastal plain of calcareous sand, mixed with volcanic alluvium. Offshore of the west coast, there is a broad, shallow lagoon sheltered from the ocean by a barrier reef. The lagoon is broadest and deepest immediately north of American Memorial Park at Puntan Muchot where the distance from the shore to the barrier reef is about 3 kilometers (2 miles) and the maximum water depth is about 12 to 15 meters (40 to 50 feet). A wide pass interrupts the barrier reef offshore and the commercial harbor and entrance channel are located in this area, taking advantage of the reef pass. To the south and north, the lagoon transitions into a fringing reef from 0.5 to 1.3 kilometers (0.3 to 0.8 miles) wide with water depths typically less than 3 meters (10 feet).

Saipan's Bureau of Environmental and Coastal Quality, Division of Coastal Resource Management (BECQ-DCRM) has contracted Sea Engineering, Inc. (SEI) to conduct a hydrodynamic study of Saipan's western lagoon. The study approach included measuring waves and currents in the lagoon, and then using that data to develop and calibrate combined wave and hydrodynamic models of current and circulation in the lagoon. The field measurements included deployment of 9 wave and current meters throughout the lagoon for a three-month period during summer of 2017. A summary report of the field data was completed in March 2018. This report present results of the wave and hydrodynamic numerical modeling. The model provides a basic understanding of the primary currents and circulation patterns within the lagoon and will assist BECQ-DCRM with the development of sampling and protocols for marine and water quality monitoring in the lagoon.

There are many driving factors to circulation over a reef environment, however the waves are usually the dominant forces. Other factors such as wind, tides, and buoyancy forcing can influence flows but are typically not the main driving factors. In wave theory, it is known that a decrease in wave height, typically from wave breaking, increases the mean water level. This phenomenon is known as wave setup. In the case where there is a fringing reef with a lagoon behind it, waves breaking on the reef increases the mean water level in the surf zone resulting in a net flow into the lagoon. For lagoons bounded by land, the net inflow of water results in an increase in the mean water level of the lagoon relative to the ocean. The raised mean water level in the lagoon generates a return flow to the open ocean through channels in the reef to reestablish equilibrium (Lowe, 2008). A simplified visualization of wave driven circulation in a lagoon from Lowe (2008) is presented in Figure 1-1.

The geometry of parts of the lagoon with a shallow fringing reef along the border and a deep channel in the middle allows for tide to influence currents similar to those of an enclosed bay where the rising and lowering of the tides generates flooding and ebbing flow patterns depicted in Figure 1-2.

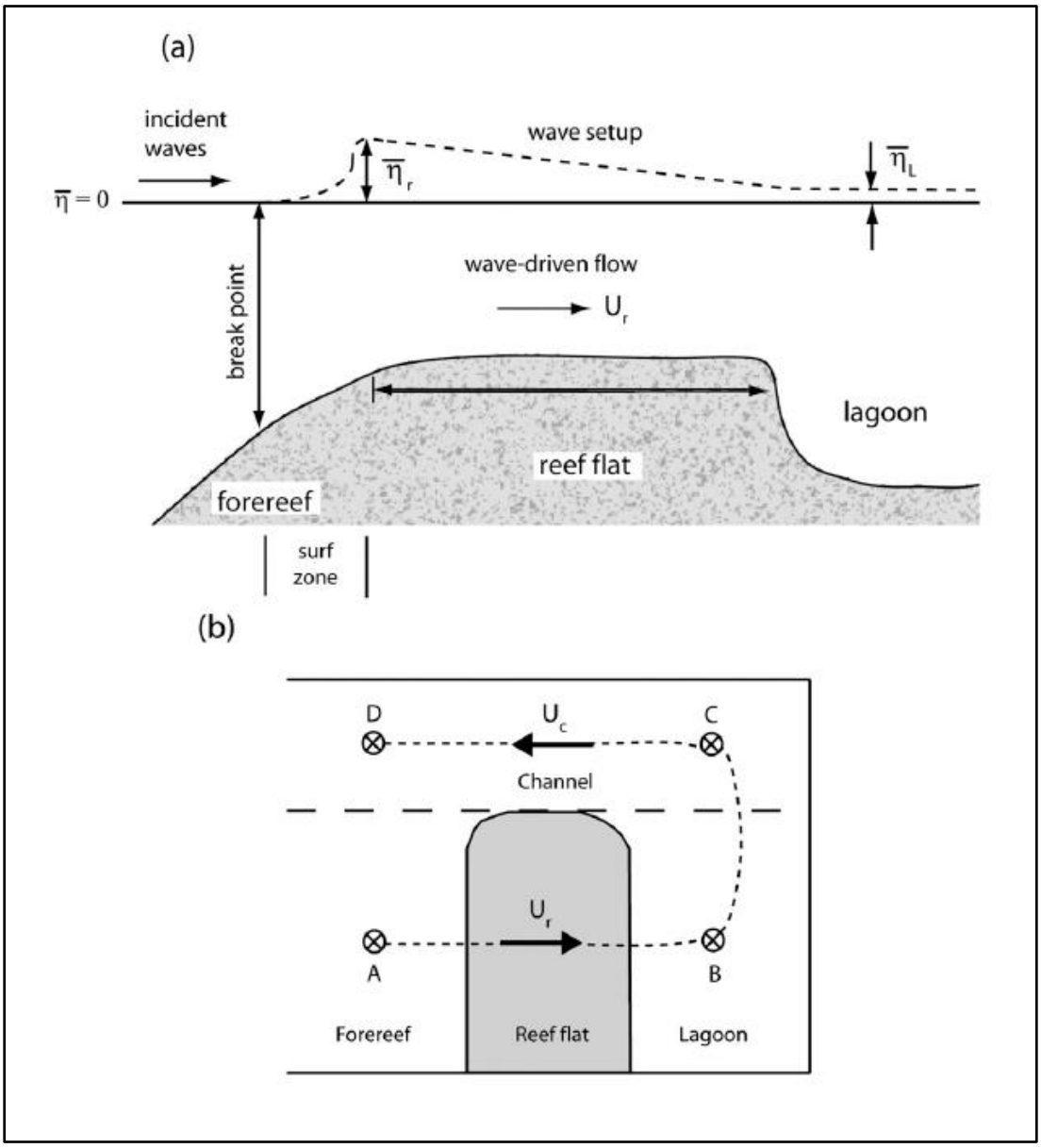

Figure 1-1. Idealized wave driven circulation in a lagoon.

Note vertical scales of the bathymetry and wave setup are both highly exaggerated (Lowe, 2008). In the figure $\bar{\eta}$= mean water level, $\bar{\eta}_r$ = mean water over the reef, $\bar{\eta}_L$ = mean water level in the lagoon, and U_r = flow over the reef, U_c = flow out of the channel.

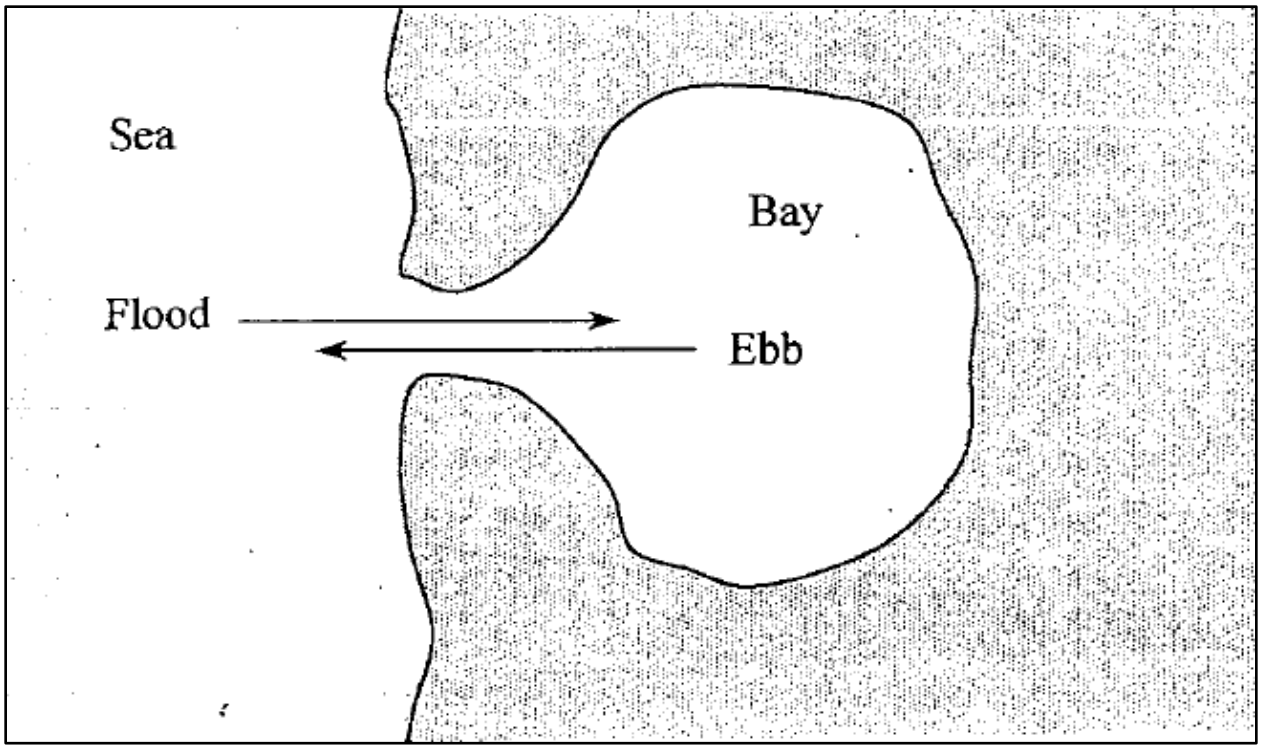

Figure 1-2. Idealized tidal flow in an enclosed bay (Kamphuis 2010)

2. CLIMATE AND OCEANOGRAPHIC CONDITIONS

2.1 Tide

The tides in Saipan waters are semi-diurnal, with pronounced diurnal inequalities (two tidal cycles each day with the range of high and low water levels being unequal). Tidal data from the tide station at Saipan Harbor are as follows:

Table 2-1. Saipan Tidal Ranges.

Datum	MLLW Datum (m)	MSL Datum (m)
Mean High Water (MHHW)	0.67	0.28
Mean High Water (MHW)	0.63	0.24
Mean Sea Level (MSL)	0.39	0.00
Mean Low Water (MLW)	0.19	-0.21
Mean Lower Low Water (MLLW)	0.00	-0.39

The mean tide range is .45 m (1.5 ft), with a maximum diurnal range of .67 m (2.2 ft).

2.2 Currents

The focus of this report is the hydrodynamics inside of Saipan Lagoon; however, there are strong regional currents offshore the west coast of Saipan. An SEI report in 2004 studied the currents around the Garapan Anchorage. The Garapan Anchorage is located off the southern half of the west coast of Saipan. Figure 2-1 shows the location of the anchorage relative to Saipan and Tinian. The two islands are oriented along a north-northeast to south-southwest azimuth, and the distance from the south end of Tinian to the north end of Saipan is 25 nautical miles (nm) (46 km). The Saipan Channel separating the two islands is 3 nm (5.5 km) wide.

The available information indicates that the primary potential driving forces for the circulation around the Garapan Anchorage are the underlying North Equatorial Current and the semidiurnal tide. The North Equatorial Current, generated by the northeast trade winds, generally sets in a westerly direction near Saipan, with speeds of up to 1 knot (.5 m/s). The Sailing Directions for the Pacific Islands (1976) and available anecdotal information indicate that this current is stronger in the winter months when the trade winds are prevalent. According to the Sailing Directions, "In the vicinity of Saipan the flood current generally sets westward and the ebb current eastward. The tidal currents usually turn at the times of high and low water. The tidal currents in Saipan Channel set northwest at 2.5 knots (1.3 m/s) on the rising tide, and southeast at 1.25 knots (0.6 m/s) on the falling tide. During the Northeast Trades, the tidal currents set

northwest almost continuously at a rate of 2.5 to 4 knots (1.3 to 2.0 m/s). The ebb current is hardly noticeable at this time. In the outer anchorage of Saipan Harbor, the tidal currents are irregular, with a maximum west-northwest set of about 2 knots (1 m/s) during rising tide. In Garapan Anchorage, the tidal currents set north at rates of 0.5 to 1.0 knot (0.25 to 0.5 m/s) during the rising tide and southwest at rates of 0.5 to 0.75 knot (0.25 to 0.4 m/s) during falling tide." Anecdotal information, based on historical observations of the headings of the ships at anchor and local fishermen, also indicates that the flow of water through the Saipan Channel has a major influence on currents at the Garapan Anchorage. Flows in the channel have been reported to be as high as 3 to 4 knots 1.5 to 2.0 m/s), which is in agreement with the summary in the Sailing Directions. The currents have significant seasonal variations and are greatly modified by the complex bathymetry of the Garapan Anchorage.

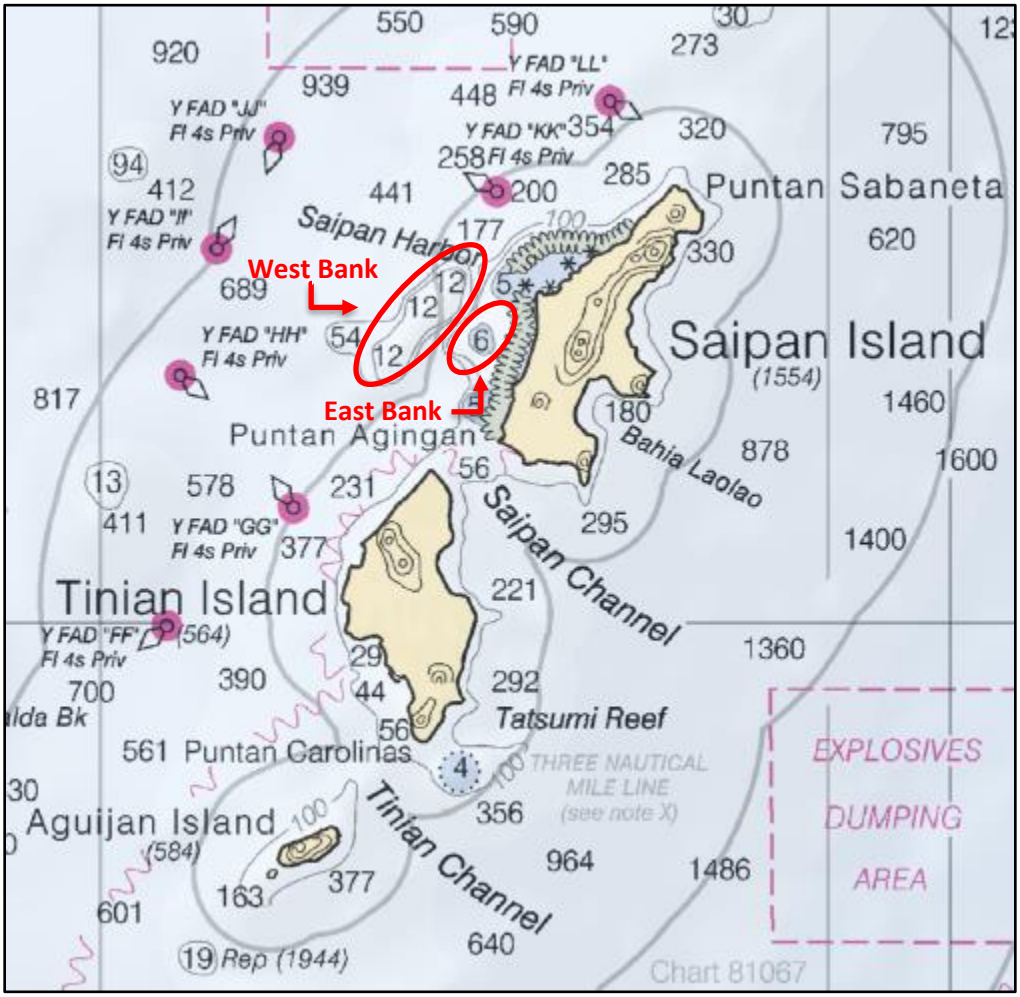

Figure 2-1. Location map (https://nauticalcharts.noaa.gov).

The 2004 SEI study results found similar results to those descriptions above, and also found that the currents also vary seasonally, and the tradewinds are the driving factor. During the winter months the North Equatorial Current approaches Saipan from the east with the speed enhanced by the prevailing trade winds. The approaching water is blocked by the island masses of Saipan and Tinian, and as a result, water is funneled at 3 to 4 knots (1.5 to 2.0 m/s) through the Saipan Channel. Once through the channel, the current hits the south end of the two banks and is modified by the complex bathymetry. The water flows into the narrow channel between the two banks, but spills up and over the West Bank, resulting in almost unidirectional flow patterns on the West Bank for the entire winter season. Only the seaward bulge of the East Bank is impacted by this northward flowing current; elsewhere on the East Bank, the reversing tidal currents predominate. Current flow directions reverse regularly with the periodicity of the semidiurnal tide. The currents become weaker and more variable at all locations during the summer months, and the semidiurnal tide appears to be the primary driving force on both banks.

2.3 Wind

The Marianas experience three wind patterns; trade winds, doldrums and typhoons. The islands lie near the border between the Asiatic monsoon and the belt of northeast trade winds. The predominant winds are the easterly trade winds, which approach from the northeast through east-southeast sectors. The trades are stronger and steadier in the winter (January to April) and light and variable winds with intermittent trades occur during the summer typhoon season (July to October). The spring and fall months are transition periods.

Figure 2-2 presents the wind rose for Saipan based on 30-years of hourly hindcasted wind data from 1985 to 2015. The winds around Saipan are primarily from the east-northeast and northeast with speeds from 12 to 24 mile per hour (mph) (5.3 to 10.6 m/s) occurring approximately 50 percent of the time.

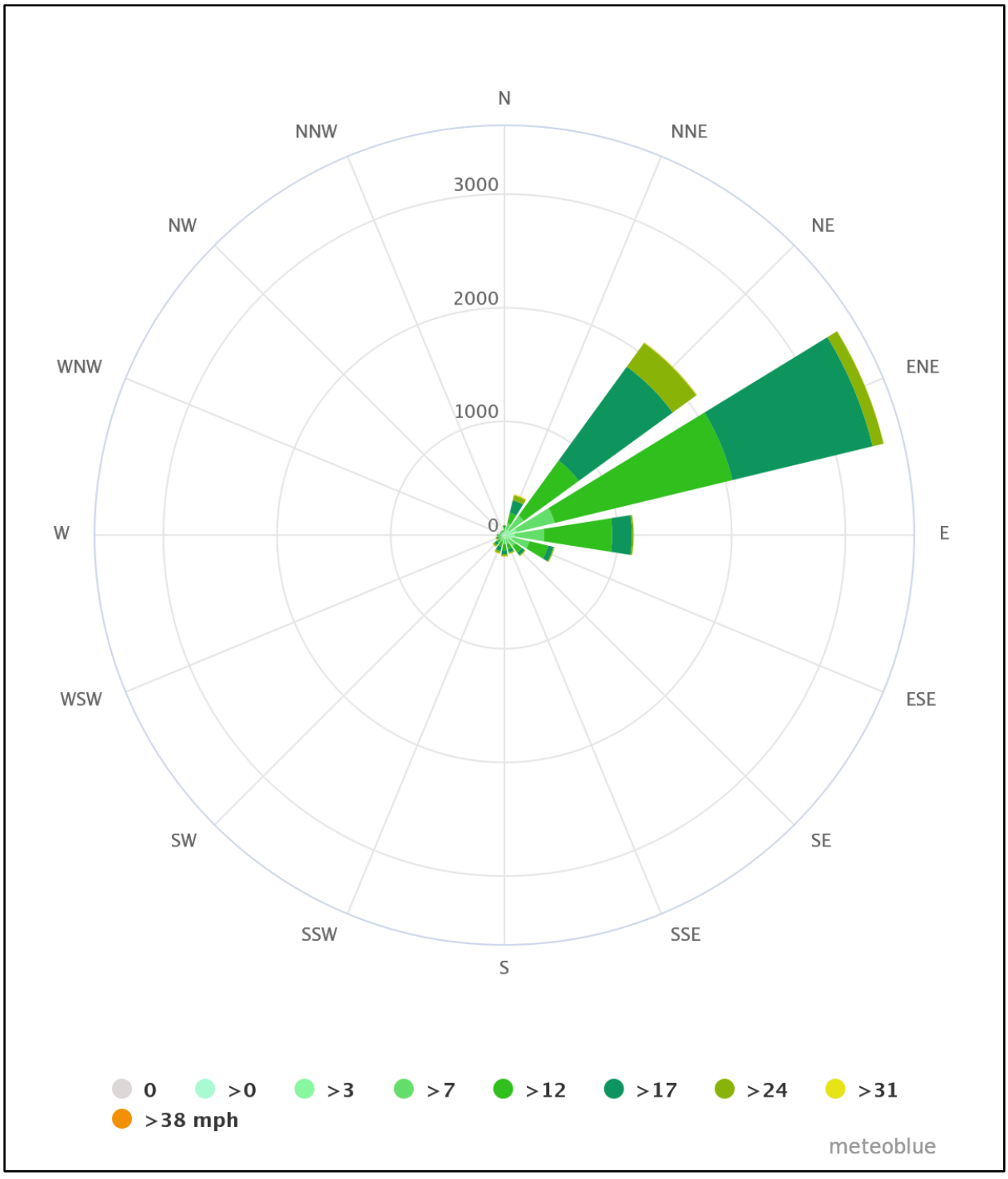

Figure 2-2. Saipan wind rose. The rose shows the number of hours per year of the wind direction and speed (meteoblue.com).

2.4 Typhoons

Due to its proximity to typhoon generation zones, Saipan is subject to the year-round passage of developing tropical storms and typhoons. In October 2018, super typhoon Yutu made landfall on the island of Saipan causing wide spread damage. Typhoons generally move from east to west; however, the tracks often curve so that the typhoon moves south to north, or even doubles back. Figure 2-3 illustrates the entire tropical storm record of the International Best Track Archive for Climate Stewardship (IBTrACS). The IBTrACS record shows that 22 hurricanes and 42 tropical storms passed within 60 nautical miles (111 kilometers) between 1946 to 2016, as shown in Figure 2-4. The National Ocean and Atmospheric Administration (NOAA) records storm intensities based on the Saffir-Simpson Hurricane Intensity Scale. Hurricane and typhoons are the same type of storm, the difference in naming comes from where the storm is formed. The defining wind speeds for hurricanes from the National Hurricane Center (NHC) are listed in Table 2-2 and defining winds speeds for typhoons from the Joint Typhoon Warning Center (JTWC) are listed in

Table 2-3.

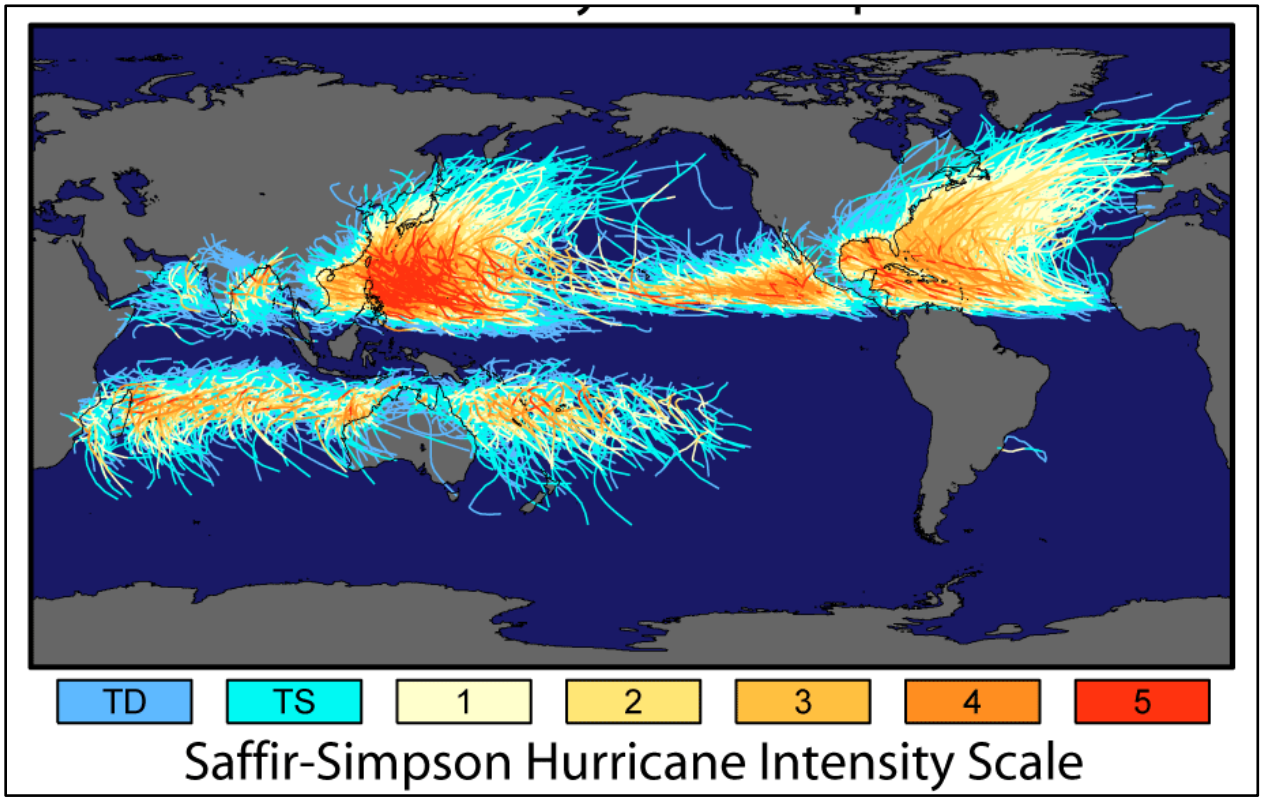

Figure 2-3. Global tropical storm track record
Source: https://earthobservatory.nasa.gov/images/7079/historic-tropical-cyclone-tracks

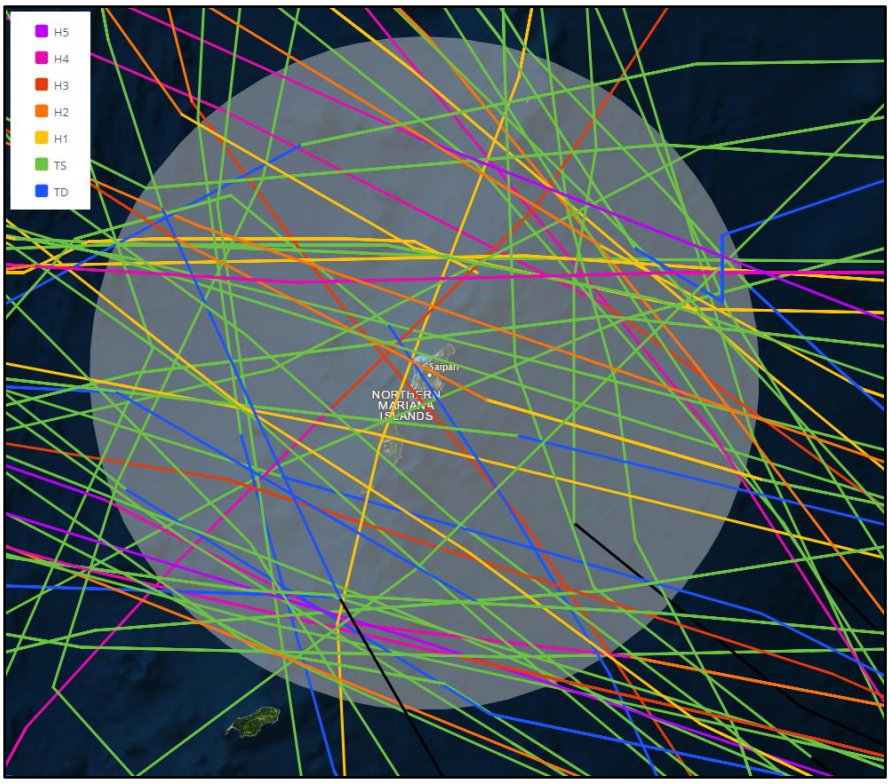

Figure 2-4. Historical tropical storm tracks passing within a 60 nautical mile radius of Saipan.
Source: https://coast.noaa.gov/hurricanes/

Table 2-2. NHC and CPHC Classification of Tropical Storms.

Classification	Wind Speed	
	km/hr	knots
Tropical Depression	62 or less	33 or less
Tropical Storm	63-118	34–63
Category 1 Hurricane	119–153	64-82
Category 2 Hurricane	154–177	83-95
Category 3 (Major) Hurricane	178–208	96-112
Category 4 (Major) Hurricane	209–251	113-136
Category 5 (Major) Hurricane	252 or higher	137 or higher

Note: Listed wind speeds are 1-minute averages

Table 2-3. JTWC Classification of Tropical Storms.

Classification	Wind Speed	
	km/hr	knots
Tropical Depression	62 or less	33 or less
Tropical Storm	63-118	34–63
Typhoon	119-240	64-129
Super Typhoon	241 or higher	130 or higher

Note: Listed wind speeds are 1-minute averages

2.5 Waves

2.5.1 Deepwater Wave Climate

2.5.1.1 Wave Information Studies (WIS) Data

Wave information is available in the form of hindcast data sets provided by the U.S. Army Corps of Engineers' Wave Information Studies (WIS). WIS provides records of wave conditions based on historical wind and wave conditions at numerous virtual stations around the Marianas chain by running numerical wave models driven by historical wind conditions. These hourly model hindcast records of wave conditions are available for the 32-year period from 1980 through 2011.

Figure 2-5. WIS 81104 and CDIP 197 station location (Image from Bing Satellite).

Hourly deepwater wave characteristics were determined for the 32-year period for WIS Station 81104 located 84 kilometers (52 miles) southwest of Garapan. The wave climate in Saipan can be divided into two distinct wave types; seas generated by the prevailing tradewinds and waves from tropical storms or typhoons (either near or distant). The percent occurrences of wave height by direction and wave period by direction are presented below. Figure 2-6 and Table 2-4 are the wave height rose diagram and histogram, respectively. Figure 2-7 and Table 2-5 are the wave period rose diagram and histogram, respectively. Note the color scheme on the histograms is a visual aid to view the differences in percent occurrence by time. The diagrams show that waves are predominantly from the east-northeast and have a significant wave height (Hs) less than 2.4 m (8 ft) occurring 87 percent of the time. Wave heights are between 0.8 to 1.9 meters (3 to 6 feet), occurring 60 percent of the time. The peak period (Tp) is generally between 6 and 12 seconds (s) occurring 89 percent of the time. Approximately 52 percent of waves have a period between 8-10 seconds.

The deepwater wave climate in the vicinity of Saipan is dominated by the occurrence of trade wind waves with a peak direction (Dp) from northeast through east-northeast directions, clockwise. The west coast of Saipan is largely sheltered from these waves by the island itself; the wave energy is reduced when waves refract around to the west side of the island. The hindcast data shows rare but extremely large waves that approach from all direction, as indicated by the maximum wave heights listed in the last row of Table 2-4. These large wave events are generated by passing typhoons. The large, energetic waves have direct exposure to the west side of the island. A hindcast forced by WIS buoy data was used to model variations in the wave climate just off west coast of Saipan and is discussed in Section 2.5.3.

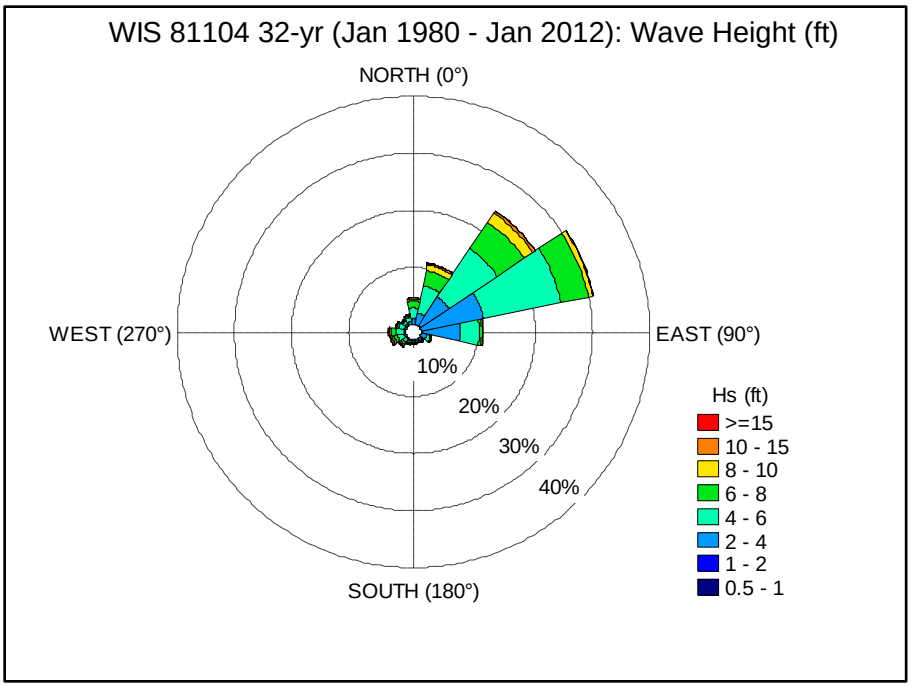

Figure 2-6 WIS 81104 Wave rose.

Table 2-4 WIS 81104 Wave Height Percent Frequency of Occurrence.

Hs (ft)\Dp(deg)	0	22.5	45	67.5	90	112.5	135	157.5	180	202.5	225	247.5	270	292.5	315	337.5	Total
1-2		0.0	0.0	0.1	0.1	0.0											0.17
2-3	0.2	0.5	1.4	3.4	2.4	0.3	0.1	0.1	0.0	0.0	0.0	0.0	0.0	0.0	0.0	0.1	8.72
3-4	0.8	1.6	4.7	7.7	4.3	0.8	0.3	0.2	0.2	0.2	0.2	0.3	0.3	0.3	0.3	0.5	22.61
4-6	2.0	4.9	10.1	13.8	3.4	0.7	0.4	0.3	0.3	0.4	0.7	1.1	1.5	1.0	0.7	0.7	41.99
6-8	1.2	2.7	5.7	4.9	0.5	0.1	0.1	0.1	0.1	0.1	0.4	0.7	0.7	0.4	0.2	0.3	18.19
8-10	0.4	1.0	1.8	0.7	0.2	0.1	0.1	0.1	0.1	0.1	0.2	0.3	0.3	0.1	0.0	0.1	5.67
10-12	0.1	0.2	0.4	0.1	0.0	0.0	0.0	0.0	0.0	0.1	0.1	0.2	0.1	0.0	0.0	0.1	1.54
12-14	0.0	0.1	0.1	0.0	0.0	0.0	0.0	0.0	0.0	0.0	0.1	0.1	0.1	0.0	0.0	0.0	0.59
14-16	0.0	0.0	0.0	0.0	0.0	0.0	0.0	0.0	0.0	0.0	0.1	0.0	0.1	0.0	0.0	0.0	0.26
16-20	0.0	0.0	0.0	0.0	0.0	0.0	0.0	0.0	0.0	0.0	0.0	0.0	0.0	0.0	0.0	0.0	0.20
20+	0.0	0.0	0.0	0.0	0.0	0.0	0.0	0.0	0.0	0.0	0.0	0.0	0.0		0.0	0.0	0.07
Total	4.62	11.03	24.29	30.76	10.90	1.99	0.98	0.77	0.82	1.02	1.85	2.84	3.05	1.90	1.35	1.84	100.00

	0	22.5	45	67.5	90	112.5	135	157.5	180	202.5	225	247.5	270	292.5	315	337.5	Overall
Mean	5.69	5.66	5.40	4.72	3.95	4.54	5.10	5.55	6.16	6.29	6.80	6.75	6.24	5.39	5.15	5.37	5.16
StDev	2.04	1.96	1.92	1.57	1.58	2.28	2.79	3.04	3.21	3.16	3.00	3.07	2.62	1.76	2.08	2.38	2.07
Min	2.00	1.84	1.67	1.61	1.80	1.94	2.00	2.03	2.10	2.20	2.26	2.36	2.26	2.43	2.33	2.26	1.61
Max	22.24	23.03	39.66	43.27	43.86	38.29	33.99	27.76	24.47	21.69	22.70	26.34	22.11	18.01	21.75	23.59	43.86

Note: The color scheme on the histogram is a visual aid to help view the differences in percent occurrence. Empty cells indicate where the value is precisely zero. Cells ranging from green to yellow to red indicate lower to intermediate to higher values, respectively.

Legend: Hs (ft) = wave height in feet; Dp = peak direction; deg = degree

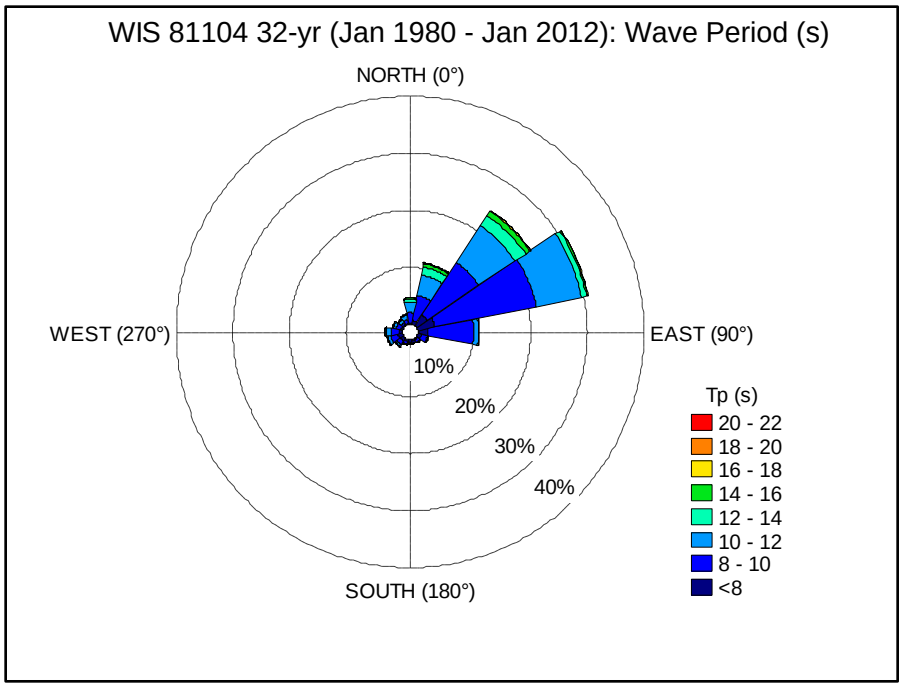

Figure 2-7. WIS 81104 Period rose.

Table 2-5. WIS 81104 Wave Period Percent Frequency of Occurrence.

Tp (s)\Dir (deg)	0	22.5	45	67.5	90	112.5	135	157.5	180	202.5	225	247.5	270	292.5	315	337.5	Total
3-6	0.0	0.0	0.2	0.8	0.4	0.2	0.1	0.1	0.0	0.0	0.1	0.1	0.0	0.0	0.0	0.0	2.03
6-8	0.2	0.7	2.1	2.4	1.4	0.5	0.3	0.3	0.3	0.4	0.5	0.7	0.5	0.3	0.1	0.2	11.02
8-10	1.9	4.5	11.0	18.3	8.2	1.1	0.5	0.3	0.3	0.4	0.9	1.3	1.5	0.9	0.6	0.7	52.36
10-12	1.9	3.7	7.7	8.2	0.9	0.1	0.1	0.1	0.1	0.1	0.3	0.6	0.9	0.5	0.5	0.8	26.31
12-14	0.5	1.5	2.2	0.9	0.1	0.0	0.0	0.0	0.0	0.0	0.0	0.1	0.1	0.2	0.1	0.2	5.84
14-16	0.2	0.6	1.0	0.2	0.0	0.0	0.0	0.0	0.0	0.0	0.0	0.0	0.0	0.0	0.0	0.0	2.15
16-18	0.0	0.1	0.1	0.0	0.0												0.26
18-20	0.0	0.0	0.0														0.02
20+		0.0															0.00
Total	4.62	11.03	24.29	30.76	10.90	1.99	0.98	0.77	0.82	1.02	1.85	2.84	3.05	1.90	1.35	1.84	100.00

	0	22.5	45	67.5	90	112.5	135	157.5	180	202.5	225	247.5	270	292.5	315	337.5	Overall
Mean	10.43	10.45	10.07	9.45	8.78	8.29	8.38	8.19	8.31	8.42	8.74	8.89	9.40	9.65	9.93	10.09	9.61
StDev	1.73	1.96	1.88	1.45	1.20	1.50	1.52	1.58	1.57	1.55	1.54	1.67	1.55	1.85	1.67	1.56	1.75
Min	5.14	4.65	4.23	4.18	3.86	3.87	4.17	4.29	4.23	4.33	4.27	4.59	4.60	4.65	4.31	5.17	3.86
Max	18.52	20.56	19.48	17.93	17.79	15.98	15.95	15.00	15.18	15.18	15.47	15.39	15.36	15.92	14.89	15.27	20.56

Note: The color scheme on the histogram is a visual aid to help view the differences in percent occurrence. Empty cells indicate where the value is precisely zero. Cells ranging from green to yellow to red indicate lower to intermediate to higher values, respectively.

Legend: Tp (ft) = peak wave period in seconds; Dp = peak direction; deg = degree

Seasonal variation in the wave climate can be shown by filtering data based on seasonal variability in tradewinds and typhoon season. As previously stated, the tradewinds are stronger and steadier in the winter (January to April) and light and variable winds with intermittent trades occur during the summer typhoon season (July to October). The spring and fall months are transition periods. Figure 2-8 and Figure 2-9 plot the wave roses for the winter season and the summer typhoon season, respectively. Table 2-6 presents the corresponding wave height histogram for winter months and Table 2-7 presents the corresponding wave height histogram for summer/typhoon months. There are two noticeable difference between the summer and winter seasons. The first is a pronounced difference in the percent occurrence and size of the tradewind waves. During the winter months waves approach from the 0˚ clockwise to 90˚approximately 98 percent of the time compared to approximately 57 percent of the time during the summer months. Also, the trade wind waves are consistently larger during the winter months compared to the summer. During the winter waves from 0˚ clockwise to 90 ˚ are greater than 4 ft (1.2 meters) approximately 85 percent of the time compared to 21 percent of the timer during the summer months.

Winter period wave period and the corresponding histogram are presented in Figure 2-10 and Table 2-8, respectively. Figure 2-11 and Table 2-9 present the wave period rose and wave period histogram for the peak summer/typhoon season, respectively. Wave period is relatively constant from winter to summer. Tradewind waves with longer periods than 12 seconds are slightly more common during the winter months than in the summer.

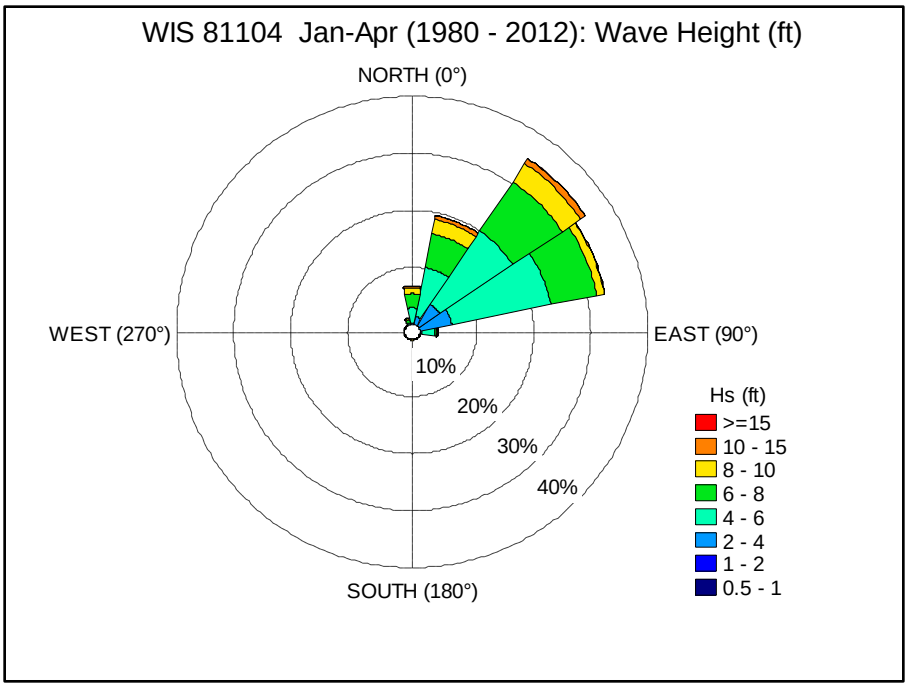

Figure 2-8. Wave rose for the months of January, February, March, and April between January 1, 1980 to January 1, 2012.

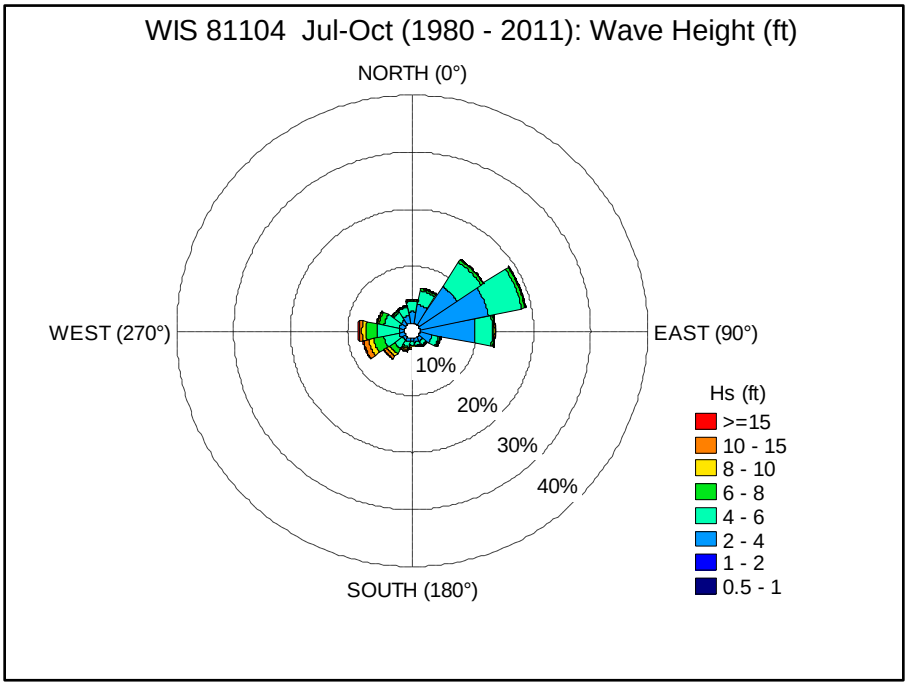

Figure 2-9. Wave rose a for the months of July, August, September, and October between January 1, 1980 to January 1, 2012.

Table 2-6. Wave Height Percent Frequency of Occurrence During the Seasonal Strong Tradewinds (January, February, March, and April Between January 1, 1980 to January 1, 2012).

Hs (ft)\Dp(deg)	0	22.5	45	67.5	90	112.5	135	157.5	180	202.5	225	247.5	270	292.5	315	337.5	Total
1-2																	0.00
2-3		0.0	0.3	0.8	0.1	0.0											1.22
3-4	0.3	1.5	4.1	5.0	0.4	0.0	0.0	0.0							0.0	0.0	11.41
4-6	2.6	8.7	15.5	17.7	2.1	0.1	0.1	0.0	0.0	0.1	0.1	0.1	0.1	0.1	0.1	0.3	47.57
6-8	2.5	6.0	10.4	8.2	0.3	0.0	0.0	0.0	0.0	0.0	0.0	0.0	0.0	0.0	0.0	0.5	28.31
8-10	1.0	2.6	3.8	1.3	0.1	0.0	0.0	0.0	0.0	0.0	0.0	0.0	0.0	0.0	0.0	0.3	9.25
10-12	0.2	0.5	0.9	0.0	0.0		0.0								0.0	0.1	1.78
12-14	0.1	0.1	0.1	0.0			0.0								0.0	0.0	0.36
14-16		0.0	0.0	0.0		0.0	0.0								0.0		0.05
16-20			0.0	0.0	0.0	0.0									0.0	0.0	0.02
20+	0.0	0.0	0.0	0.0	0.0											0.0	0.03
Total	6.65	19.49	35.25	33.13	3.11	0.19	0.15	0.06	0.10	0.11	0.09	0.12	0.11	0.08	0.14	1.21	100.00
	0	22.5	45	67.5	90	112.5	135	157.5	180	202.5	225	247.5	270	292.5	315	337.5	Overall
Mean	6.53	6.21	5.94	5.33	5.02	5.93	6.81	6.91	7.14	6.07	5.89	6.00	5.84	5.54	7.23	7.14	5.82
StDev	1.81	1.86	1.85	1.41	1.39	2.25	2.85	1.62	1.51	1.42	1.27	1.00	0.91	0.76	3.38	2.28	1.77
Min	3.02	2.49	2.43	2.17	2.72	2.95	3.41	3.97	4.17	4.20	4.23	4.30	4.43	4.13	3.90	3.18	2.17
Max	22.24	23.03	23.56	23.26	21.29	17.65	14.76	9.42	9.06	8.99	8.43	8.43	8.04	8.43	18.41	22.08	23.56

Note: The color scheme on the histogram is a visual aid to help view the differences in percent occurrence. Empty cells indicate where the value is precisely zero. Cells ranging from green to yellow to red indicate lower to intermediate to higher values, respectively.

Table 2-7. Wave Height Percent Frequency of Occurrence During Seasonal Lighter Trades and Typhoon Season (July, August, September, and October between January 1, 1980 to January 1, 2012).

Hs (ft)\Dp(deg)	0	22.5	45	67.5	90	112.5	135	157.5	180	202.5	225	247.5	270	292.5	315	337.5	Total
1-2		0.0	0.1	0.1	0.1	0.0											0.29
2-3	0.4	1.1	2.4	5.0	4.1	0.6	0.3	0.2	0.1	0.1	0.1	0.1	0.1	0.1	0.1	0.3	15.19
3-4	1.6	2.3	5.6	7.2	5.5	1.6	0.7	0.5	0.5	0.5	0.5	0.8	0.9	0.9	0.9	1.2	31.18
4-6	1.7	2.5	5.1	6.0	3.0	1.2	0.7	0.6	0.6	1.0	1.7	2.8	3.9	2.8	1.7	1.5	36.74
6-8	0.2	0.4	0.5	0.6	0.3	0.3	0.1	0.2	0.3	0.3	1.0	1.8	1.9	0.9	0.3	0.2	9.24
8-10	0.1	0.1	0.1	0.1	0.1	0.1	0.1	0.1	0.1	0.3	0.7	0.9	0.8	0.3	0.1	0.0	3.71
10-12	0.0	0.0	0.0	0.0	0.0	0.0	0.1	0.1	0.1	0.2	0.3	0.5	0.3	0.1	0.1	0.0	1.77
12-14	0.0	0.0	0.0	0.0	0.0	0.0	0.0	0.0	0.1	0.1	0.2	0.3	0.2	0.0	0.0	0.0	1.00
14-16		0.0	0.0	0.0	0.0	0.0	0.0	0.0	0.0	0.0	0.1	0.1	0.1	0.0	0.0	0.0	0.52
16-20	0.0	0.0	0.0	0.0	0.0	0.0	0.0		0.0	0.0	0.0	0.1	0.1	0.0	0.0	0.0	0.35
20+	0.0		0.0	0.0	0.0	0.0	0.0	0.0	0.0			0.0				0.0	0.03
Total	4.11	6.36	13.82	19.01	13.25	3.84	1.97	1.71	1.81	2.43	4.69	7.49	8.19	4.99	3.11	3.22	100.00
	0	22.5	45	67.5	90	112.5	135	157.5	180	202.5	225	247.5	270	292.5	315	337.5	Overall
Mean	4.31	4.15	3.97	3.80	3.64	4.28	4.65	4.94	5.78	6.15	6.77	6.74	6.26	5.33	4.93	4.49	4.69
StDev	1.67	1.44	1.25	1.19	1.41	1.98	2.29	2.48	2.98	3.11	2.99	2.94	2.58	1.67	1.76	1.76	2.22
Min	2.00	1.84	1.67	1.84	1.80	1.94	2.00	2.03	2.10	2.20	2.26	2.36	2.26	2.43	2.33	2.26	1.67
Max	21.10	19.91	29.63	32.09	33.10	32.84	27.92	24.08	21.33	19.03	18.90	20.18	18.27	18.01	19.19	20.18	33.10

Note: The color scheme on the histogram is a visual aid to help view the differences in percent occurrence. Empty cells indicate where the value is precisely zero. Cells ranging from green to yellow to red indicate lower to intermediate to higher values, respectively.

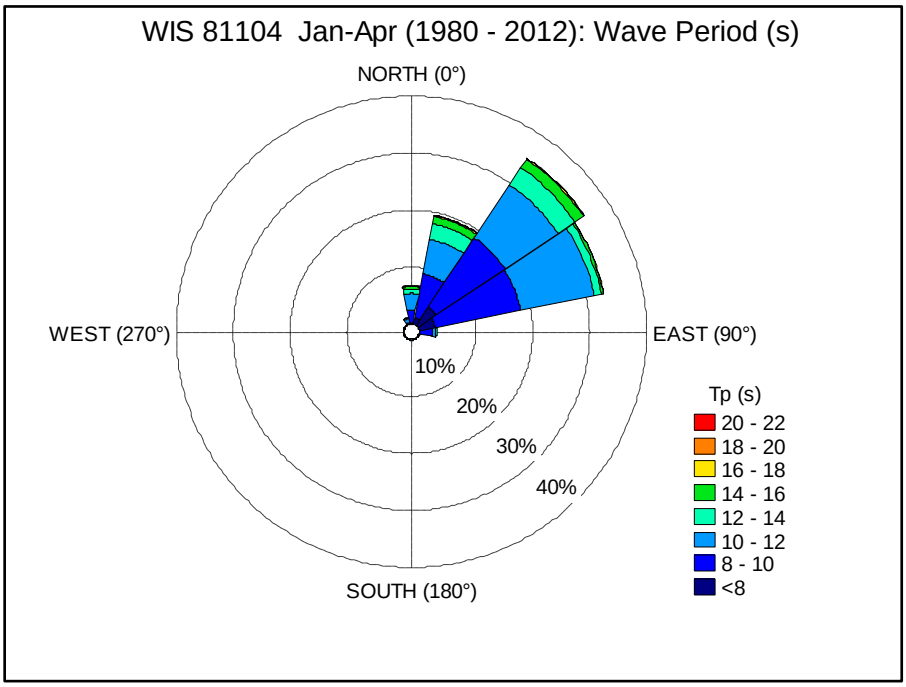

Figure 2-10 Period rose the months of January, February, March, and April between January 1, 1980 to January 1, 2012.

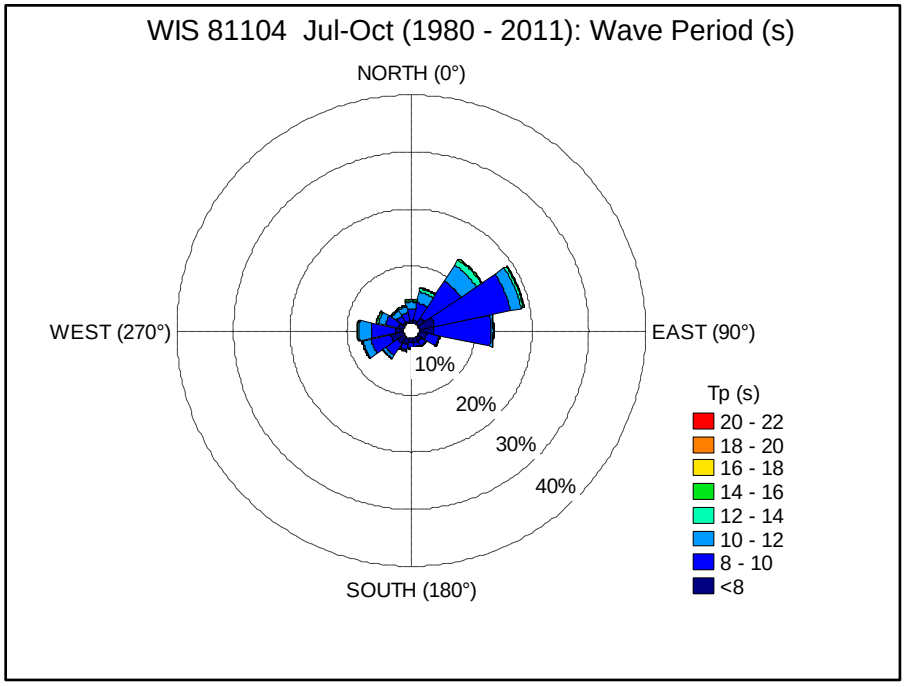

Figure 2-11 Period rose for the months of July, August, September, and October between January 1, 1980 to January 1, 2012.

Table 2-8. Wave Period Percent Frequency of Occurrence During the Seasonal Strong Tradewinds (January, February, March, and April between January 1, 1980 to January 1, 2012).

Tp (s)\Dir (deg)	0	22.5	45	67.5	90	112.5	135	157.5	180	202.5	225	247.5	270	292.5	315	337.5	Total
3-6	0.0	0.1	0.4	0.7	0.1	0.0	0.0	0.0	0.0	0.0	0.0	0.0	0.0	0.0	0.0	0.0	1.38
6-8	0.1	1.1	3.5	2.1	0.1	0.0	0.0	0.0	0.0	0.0	0.0	0.0	0.0		0.0	0.0	7.17
8-10	2.3	7.8	14.6	15.4	2.1	0.1	0.1	0.0	0.0	0.0	0.0	0.0	0.0	0.0	0.1	0.3	42.91
10-12	3.0	6.2	11.2	13.2	0.8	0.0	0.0	0.0	0.1	0.0	0.0	0.1	0.1	0.0	0.1	0.8	35.52
12-14	0.7	2.7	3.6	1.3	0.1		0.0	0.0	0.0	0.0	0.0	0.0	0.0	0.0		0.1	8.60
14-16	0.5	1.3	1.8	0.4												0.0	3.95
16-18	0.0	0.2	0.2	0.0													0.43
18-20	0.0	0.0	0.0														0.05
20+		0.0															0.00
Total	6.65	19.49	35.25	33.13	3.11	0.19	0.15	0.06	0.10	0.11	0.09	0.12	0.11	0.08	0.14	1.21	100.00

	0	22.5	45	67.5	90	112.5	135	157.5	180	202.5	225	247.5	270	292.5	315	337.5	Overall
Mean	10.79	10.56	10.14	9.83	9.54	9.03	8.85	8.70	10.00	9.11	9.30	10.07	9.89	9.66	9.47	10.70	10.14
StDev	1.75	2.06	2.00	1.48	1.04	1.46	1.16	1.92	1.72	1.96	2.32	2.39	2.00	1.62	1.16	1.13	1.84
Min	5.77	4.65	4.29	4.20	4.76	4.81	5.73	5.04	5.11	4.85	5.20	5.26	5.25	5.27	5.28	5.98	4.20
Max	18.52	20.56	19.48	17.43	13.43	11.47	12.65	13.05	13.23	13.08	12.94	13.13	13.02	13.08	11.82	14.23	20.56

Note: The color scheme on the histogram is a visual aid to help view the differences in percent occurrence. Empty cells indicate where the value is precisely zero. Cells ranging from green to yellow to red indicate lower to intermediate to higher values, respectively.

Table 2-9. Wave Period Percent Frequency of Occurrence During Seasonal Lighter Trades and Typhoon Season (July, August, September, and October between January 1, 1980 to January 1, 2012).

Tp (s)\Dir (deg)	0	22.5	45	67.5	90	112.5	135	157.5	180	202.5	225	247.5	270	292.5	315	337.5	Total
3-6	0.0	0.0	0.1	0.6	0.5	0.4	0.1	0.1	0.1	0.1	0.2	0.3	0.1	0.1	0.0	0.0	2.75
6-8	0.4	0.6	1.3	2.3	2.1	1.1	0.7	0.8	0.8	1.0	1.4	2.1	1.3	0.9	0.4	0.4	17.35
8-10	2.2	3.1	7.8	13.6	10.2	2.2	1.0	0.7	0.7	1.1	2.4	3.6	4.2	2.3	1.4	1.5	58.07
10-12	1.2	1.9	3.3	1.9	0.4	0.1	0.1	0.1	0.1	0.2	0.7	1.4	2.2	1.3	1.1	1.1	17.15
12-14	0.3	0.6	1.1	0.4	0.1	0.0	0.0	0.0	0.0	0.0	0.1	0.2	0.3	0.3	0.2	0.2	3.77
14-16	0.1	0.1	0.2	0.1	0.0	0.0	0.0	0.0	0.0	0.0	0.0	0.0	0.1	0.1	0.0	0.0	0.85
16-18		0.0	0.0	0.0	0.0												0.07
18-20																	0.00
20+																	0.00
Total	4.11	6.36	13.82	19.01	13.25	3.84	1.97	1.71	1.81	2.43	4.69	7.49	8.19	4.99	3.11	3.22	100.00

	0	22.5	45	67.5	90	112.5	135	157.5	180	202.5	225	247.5	270	292.5	315	337.5	Overall
Mean	9.80	9.93	9.67	8.93	8.55	8.14	8.21	7.94	8.09	8.20	8.59	8.75	9.36	9.52	9.81	9.79	9.08
StDev	1.66	1.72	1.66	1.38	1.12	1.51	1.50	1.41	1.44	1.45	1.41	1.59	1.52	1.79	1.61	1.59	1.61
Min	5.14	4.73	4.23	4.31	3.86	3.87	4.21	4.29	4.23	4.33	4.27	4.59	4.60	4.65	4.31	5.17	3.86
Max	15.96	16.94	17.55	16.18	17.45	15.98	15.95	15.00	15.18	15.18	15.47	15.34	15.36	15.92	14.89	15.27	17.55

Note: The color scheme on the histogram is a visual aid to help view the differences in percent occurrence. Empty cells indicate where the value is precisely zero. Cells ranging from green to yellow to red indicate lower to intermediate to higher values, respectively.

2.5.1.2 Recorded Buoy Data

In addition to the WIS virtual buoy 81104, CDIP buoy 197 is located 9 kilometers (5.6 miles) to the northwest of Garapan (Figure 2-5). The buoy was installed in October 2012 and has been recording data since that time, with occasional data gaps due to maintenance. The CDIP buoy recorded data during the same period SEI instruments were deployed in Saipan Lagoon, and was therefore used to force the offshore wave model during calibration discussed in Section 3.3.

Despite CDIP 197 being slightly more sheltered from easterly trade winds, the statistics from CDIP 197 agree with those from WIS 81104 - waves are predominantly from the northeast with wave heights less than 2.4 meters (8 feet) and wave periods less than 12 seconds. Wave height statistics are summarized by a wave rose and histogram in Figure 2-12 and Table 2-10, respectively. Wave period statistics are shown by the period rose and histogram in Figure 2-13 and Table 2-11. Similar to the WIS data, the CDIP buoy recorded large waves from all directions generated by passing typhoons. Wave heights are slightly less from the east-southeast clockwise to the south due to sheltering from Saipan and Tinian.

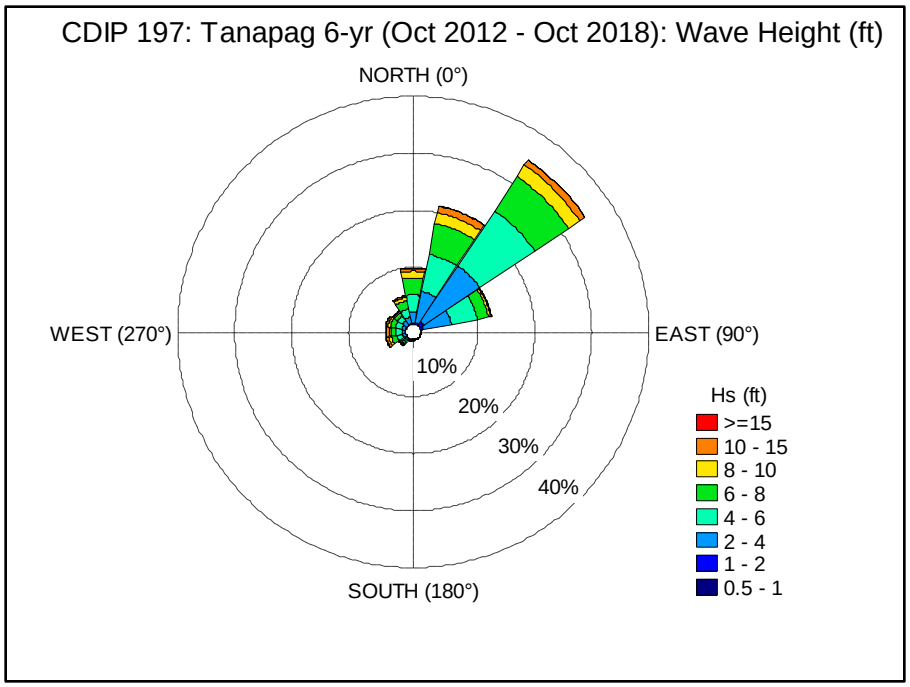

Figure 2-12. CDIP 197 Wave rose.

Table 2-10. CDIP 197 Wave Height percent frequency of occurrence.

Hs (ft)\Dir (deg)	0	22.5	45	67.5	90	112.5	135	157.5	180	202.5	225	247.5	270	292.5	315	337.5	Total
0.5-1.0																	0.00
1-2	0.2	0.4	0.9	0.5	0.0	0.0	0.0	0.0	0.0	0.0	0.0	0.0	0.0	0.0	0.1	0.1	2.28
2-3	0.9	2.3	5.5	2.2	0.0	0.0	0.0	0.0	0.0	0.0	0.1	0.1	0.1	0.2	0.5	0.6	12.56
3-4	1.2	3.3	6.2	2.9	0.1	0.0	0.0	0.0	0.0	0.1	0.3	0.5	0.4	0.5	0.5	0.5	16.58
4-6	3.0	6.6	11.6	4.6	0.0	0.0	0.0	0.0	0.0	0.1	0.4	1.0	1.1	1.2	0.9	1.5	32.08
6-8	3.0	5.5	7.2	2.0	0.0	0.0	0.0	0.0	0.0	0.1	0.4	0.9	0.9	0.9	0.7	1.5	23.14
8-10	1.2	1.9	2.4	0.4	0.0	0.0	0.0	0.0	0.0	0.0	0.2	0.5	0.4	0.5	0.2	0.6	8.27
10-12	0.5	0.9	0.8	0.1	0.0	0.0		0.0	0.0	0.0	0.1	0.3	0.3	0.2	0.1	0.2	3.54
12-14	0.1	0.2	0.2	0.0	0.0					0.0	0.1	0.1	0.1	0.1	0.0	0.0	0.98
14-16	0.0	0.0	0.0	0.0						0.0	0.0	0.1	0.1	0.0	0.0	0.0	0.34
16-20		0.0	0.0	0.0	0.0					0.0	0.0	0.0	0.1	0.0	0.0	0.0	0.17
20+	0.0		0.0	0.0							0.0	0.0	0.0		0.0	0.0	0.05
Total	9.88	21.22	34.93	12.67	0.21	0.07	0.04	0.05	0.09	0.32	1.64	3.56	3.48	3.61	3.09	5.15	100.00

	0	22.5	45	67.5	90	112.5	135	157.5	180	202.5	225	247.5	270	292.5	315	337.5	Overall
Mean	5.92	5.65	5.09	4.55	4.24	3.99	4.27	4.16	4.96	6.05	6.53	6.84	6.86	6.21	5.26	5.80	5.45
StDev	2.32	2.39	2.22	1.89	2.19	1.69	1.71	2.03	2.07	3.23	3.33	3.17	3.23	2.59	2.34	2.52	2.44
Min	1.35	1.28	1.28	1.25	1.48	1.44	1.64	1.61	1.64	1.54	1.44	1.87	1.51	1.38	1.35	1.35	1.25
Max	24.51	19.55	20.14	21.36	16.93	10.10	9.38	10.10	10.99	17.36	28.35	25.66	21.69	17.09	21.92	23.39	28.35

Note: The color scheme on the histogram is a visual aid to help view the differences in percent occurrence. Empty cells indicate where the value is precisely zero. Cells ranging from green to yellow to red indicate lower to intermediate to higher values, respectively.

Legend: Hs (ft) = wave height in feet; Dp = peak direction; deg = degree

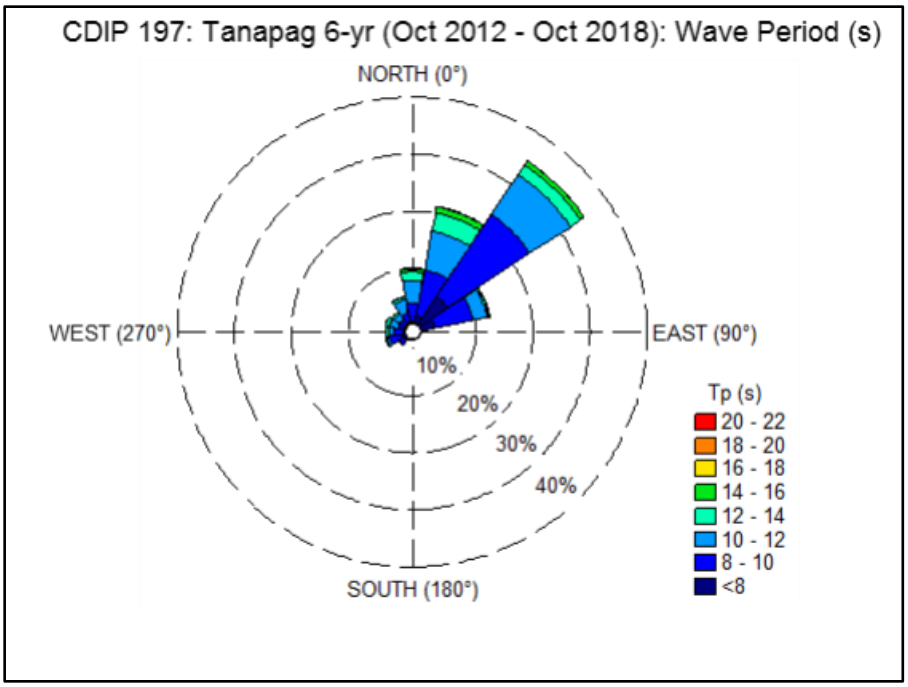

Figure 2-13. CDIP 197 Wave period rose.

Table 2-11. CDIP 197 Wave Period Percent Frequency of Occurrence.

Tp (s)\Dir (deg)	0	22.5	45	67.5	90	112.5	135	157.5	180	202.5	225	247.5	270	292.5	315	337.5	Total
3-6	0.0	0.1	0.7	0.3	0.0	0.0		0.0	0.0	0.0	0.1	0.1	0.0	0.0	0.0	0.0	1.37
6-8	0.4	1.5	5.6	2.5	0.1	0.0	0.0	0.0	0.0	0.1	0.4	0.5	0.3	0.1	0.1	0.2	12.27
8-10	3.5	8.3	17.2	6.8	0.1	0.0	0.0	0.0	0.0	0.2	0.9	2.2	1.6	1.1	1.0	2.0	44.95
10-12	3.9	6.9	8.5	2.5	0.0				0.0	0.0	0.2	0.5	0.9	1.6	1.4	2.4	28.66
12-14	1.5	3.3	2.1	0.3	0.0					0.0	0.1	0.2	0.5	0.7	0.4	0.5	9.63
14-16	0.5	1.0	0.8	0.2	0.0						0.0	0.0	0.1	0.0	0.1	0.1	2.88
16-18	0.0	0.1	0.0	0.0									0.0	0.0	0.0		0.22
18-20	0.0	0.0	0.0	0.0											0.0		0.02
20+																	0.00
Total	9.88	21.22	34.93	12.67	0.21	0.07	0.04	0.05	0.09	0.32	1.64	3.56	3.48	3.61	3.09	5.15	100.00

	0	22.5	45	67.5	90	112.5	135	157.5	180	202.5	225	247.5	270	292.5	315	337.5	Overall
Mean	10.76	10.55	9.57	9.20	8.15	7.65	8.16	8.16	8.43	8.64	8.69	9.15	10.26	10.75	10.63	10.44	9.96
StDev	1.78	1.92	1.81	1.67	1.62	0.89	0.90	1.02	1.28	1.51	1.64	1.63	1.93	1.60	1.71	1.48	1.89
Min	4.76	4.55	3.33	3.33	4.76	5.26	6.67	5.88	5.26	4.35	4.00	4.35	5.26	4.00	5.26	5.56	3.33
Max	18.18	18.18	18.18	18.18	14.29	9.09	9.88	9.88	11.76	13.33	14.29	15.38	16.67	16.67	18.18	15.38	18.18

Note: The color scheme on the histogram is a visual aid to help view the differences in percent occurrence. Empty cells indicate where the value is precisely zero. Cells ranging from green to yellow to red indicate lower to intermediate to higher values, respectively.

Legend: Tp (ft) = peak wave period in seconds; Dp = peak direction; deg = degree

2.5.2 Return Period

Waves at sea are composed of a spectrum of wave heights and wave lengths. The hourly record of the spectrum of wave heights at WIS station 81104 were used as a statistical basis for generating return period wave information, using the Weibull extreme event distribution. The return period, or recurrence interval value is a useful concept for engineering design, as it forms a statistical basis for establishing a level of design criteria as well. It is also useful to gauge the severity of storm events relative to other historical events. For this study, a direction filter from 215˚ to 15˚ was applied to only consider waves which can impact the west coast of Saipan. The wave heights are plotted with their calculated return periods in Figure 2-14, and return periods and the associated wave heights are listed in Table 2-12. While the Weibull distribution is able to generate information on return period wave heights, it cannot predict wave period or direction. The wave period and direction are determined from actual recorded large events. The 10 largest events on record, listed in Table 2-13, show relatively constant period and show most typhoon waves approach from the southwest or north-northwest.

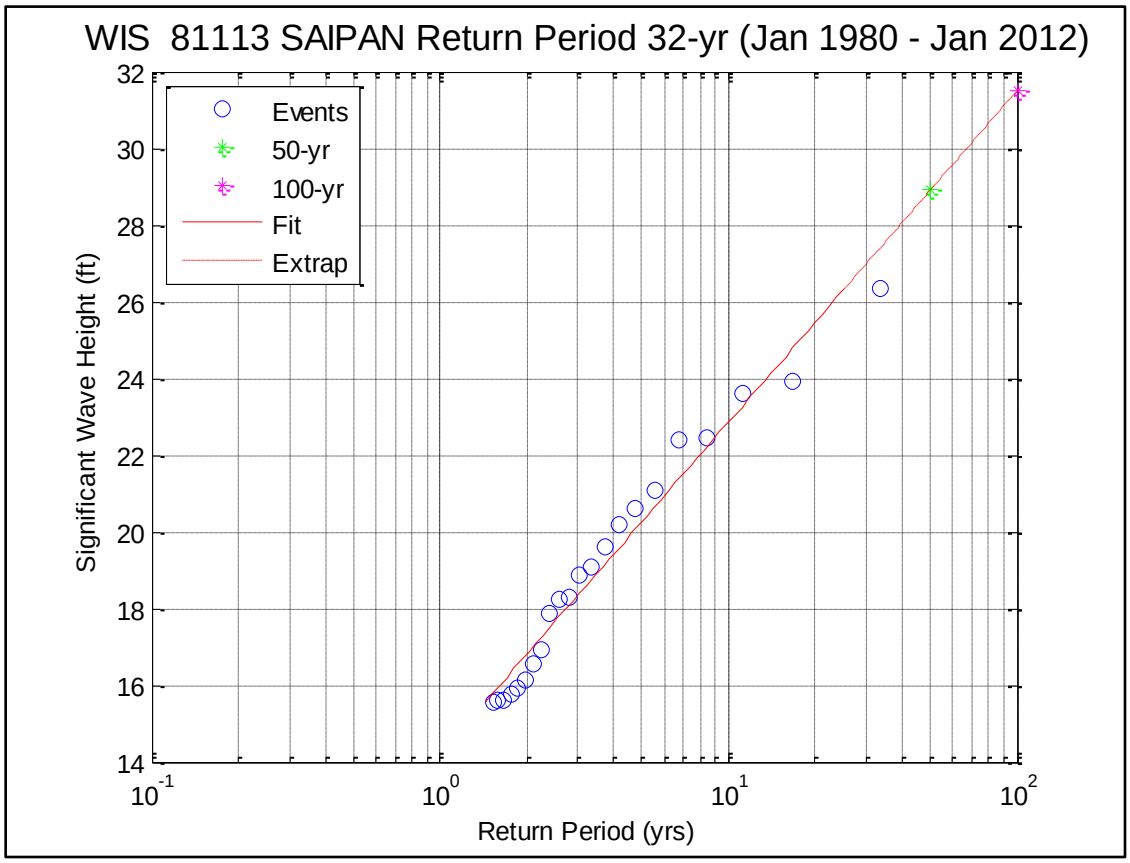

Figure 2-14. Return period wave height.

Table 2-12. Return Period Wave Heights Calculated from WIS 81104 Time Series.

Return Period (years)	Hs (m)	Hs (ft)
1	4.3	14.2
2	5.1	16.8
5	6.2	20.3
10	7.0	22.9
25	8.0	26.3
50	8.8	28.9
100	9.6	31.5

Table 2-13. Ten Largest Wave Heights Recorded at WIS 81104.

Date (yyyy-mm-dd)	Hs (m)	Hs (ft)	Tp (s)	Dp (deg)
2004-06-29	8.0	26.3	12	244
1996-12-29	7.3	23.9	12	243
1986-12-03	7.2	23.6	12	344
1990-01-14	6.8	22.4	11	13
1991-11-03	6.8	22.4	12	330
1987-10-18	6.4	21.1	9	5
1991-09-19	6.3	20.6	13	354
2001-08-17	6.1	20.2	13	246
1996-09-25	6.0	19.6	14	7
1994-11-03	5.8	19.1	12	354

2.5.3 Deepwater Hindcast

There are a number of phenomena that apply to the behavior of water waves in shallow nearshore water that are important for understanding coastal processes. As deepwater waves propagate toward shore they begin to encounter and be transformed by the ocean bottom. The 3rd generation spectral wave model SWAN (Simulating WAves Nearshore) developed by Delft Institute of Hydraulics was used to transform the deepwater waves from WIS station 81104 to shallower water off the west coast of Saipan.

The purpose of the hindcast was to determine how wave heights varied off the west coast of Saipan before they encountered the shallow fringing reef at the edge of the lagoon. The hindcast model was driven by a two-dimensional wave spectrum generated at WIS station 81104. The model was configured to calculate hourly wave parameters (wave height, period, and direction) at five virtual buoy locations at depths between 20 and 30 meters (66 to 98 feet) along the coast from January 1980 through

December 2011. The locations of the virtual buoys are spaced along the coast to represent wave climate off the northern end lagoon (Northern), the middle of the northern half lagoon (Middle Northern), the middle of lagoon (Middle), the middle of the southern half of the lagoon (Middle Southern), and the southern end of the lagoon (Southern). The locations of the virtual buoys are shown in Figure 2-15. For this study, the wave climate at WIS station 81104 was assumed to adequately describe the deepwater wave climate for this region of the Northern Mariana Islands.

Figure 2-15. Virtual buoy location (Image from Bing Satellite).

The percent occurrence of wave heights at WIS 81104 and the virtual buoys off of Saipan are listed in Table 2-14. The results show that the west side of Saipan is sheltered from tradewind waves (Figure 2-16); the wave heights and direction typically change as prevailing tradewind waves wrap to the west side of Saipan. The virtual buoys at the Southern and Middle Southern locations are the most sheltered from the prevailing conditions with wave heights less than 2 ft more than 54 and 59 percent of the time, respectively. The Middle and the Middle Northern virtual buoys are the least sheltered from tradewind wave wrap with wave heights ranging between 2 to 4 feet over 54 and 55 percent of the time, respectively. The Northern virtual buoy shows intermediate sheltering with wave heights ranging from 1 to 3 feet approximately 63 percent of the time. It should be noted that all locations are exposed to the occasional large wave heights from passing typhoons as seen in Figure 2-17. Figure 2-18 shows the wave roses

for all five locations, while Figure 2-19 shows the period roses for all five locations. The figures show the expected drop in trade wind waves observed at WIS 81104 and that waves primarily wrap around the north end of the island.

Table 2-14. Percent Frequency of Occurrence of Wave Heights at Virtual Buoys.

Hs (ft)	WIS 81104	Northern	Middle Northern	Middle	Middle Southern	Southern
0-1	0.0	3.4	0.1	0.7	16.4	12.8
1-2	0.2	33.3	12.6	23.1	42.2	41.7
2-3	8.7	30.3	30.0	32.6	22.2	22.0
3-4	22.6	17.3	24.5	21.2	10.0	11.1
4-6	42.0	12.7	24.2	16.9	6.5	8.4
6-8	18.2	2.4	6.8	4.1	1.8	2.5
8-10	5.7	0.5	1.4	0.9	0.5	0.8
10-12	1.5	0.1	0.3	0.3	0.3	0.4
12-14	0.6	0.0	0.1	0.1	0.1	0.2
14-16	0.3	0.0	0.0	0.0	0.0	0.1
16-20	0.2	0.0	0.0	0.0	0.0	0.1
20+	0.1	--	0.0	0.0	0.0	0.0

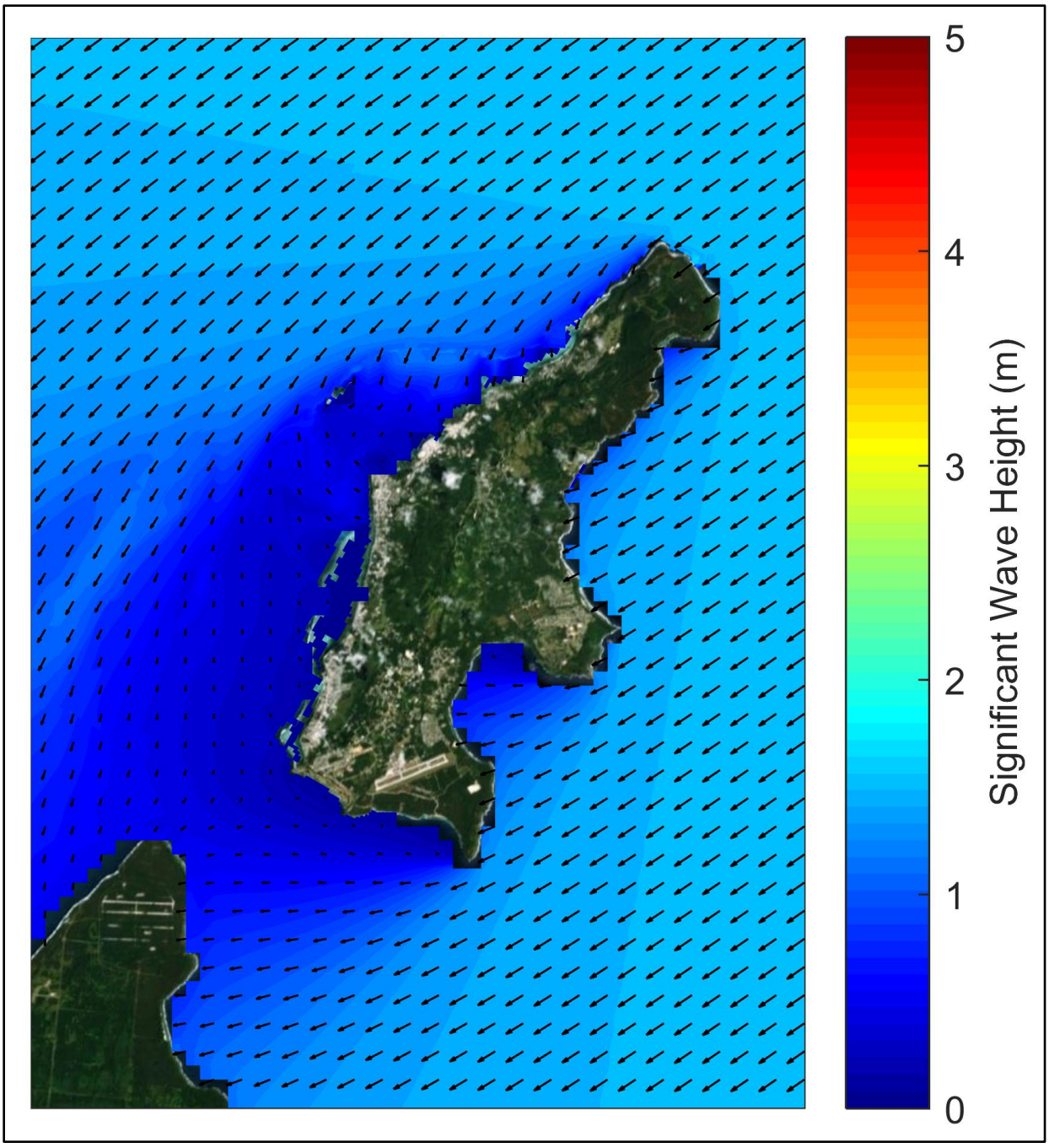

Figure 2-16. Prevailing tradewind waves patterns.

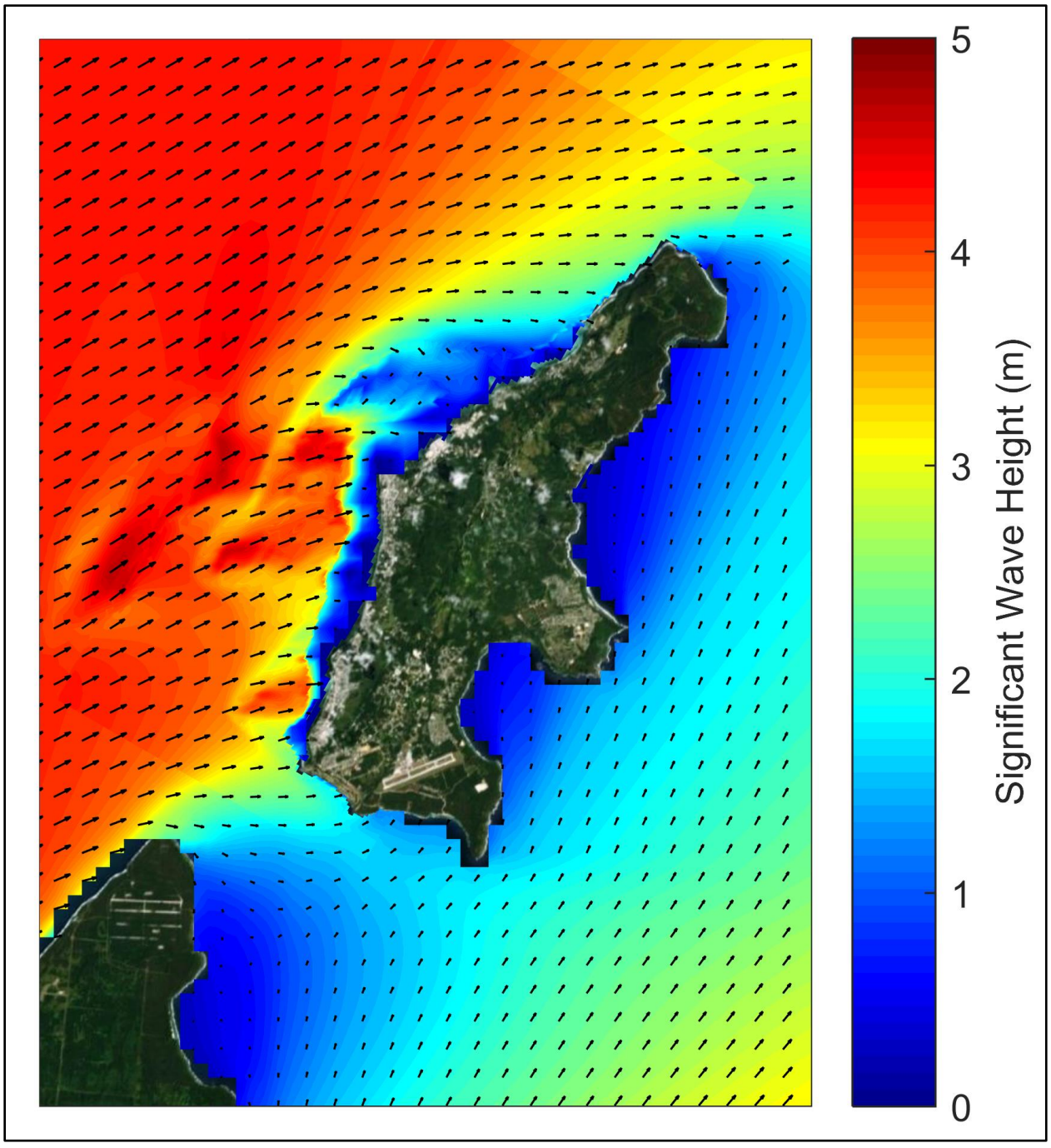

Figure 2-17. Typhoon generated waves approaching from the southwest.

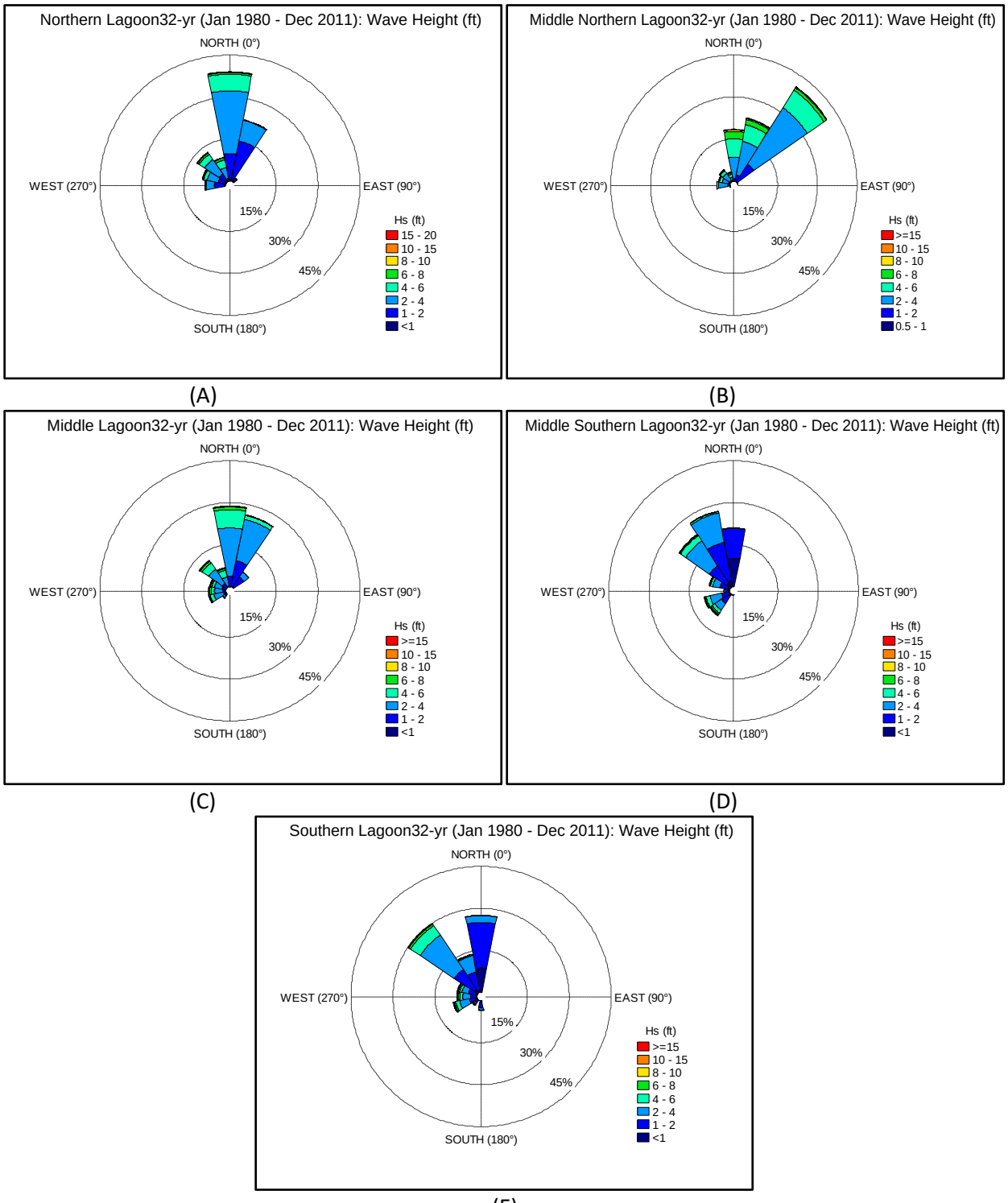

Figure 2-18. Wave Roses for (A) Northern virtual buoy, (B) Middle Northern virtual buoy, (C) Middle virtual buoy, (D) Middle Southern virtual buoy, (E) Southern virtual buoy.

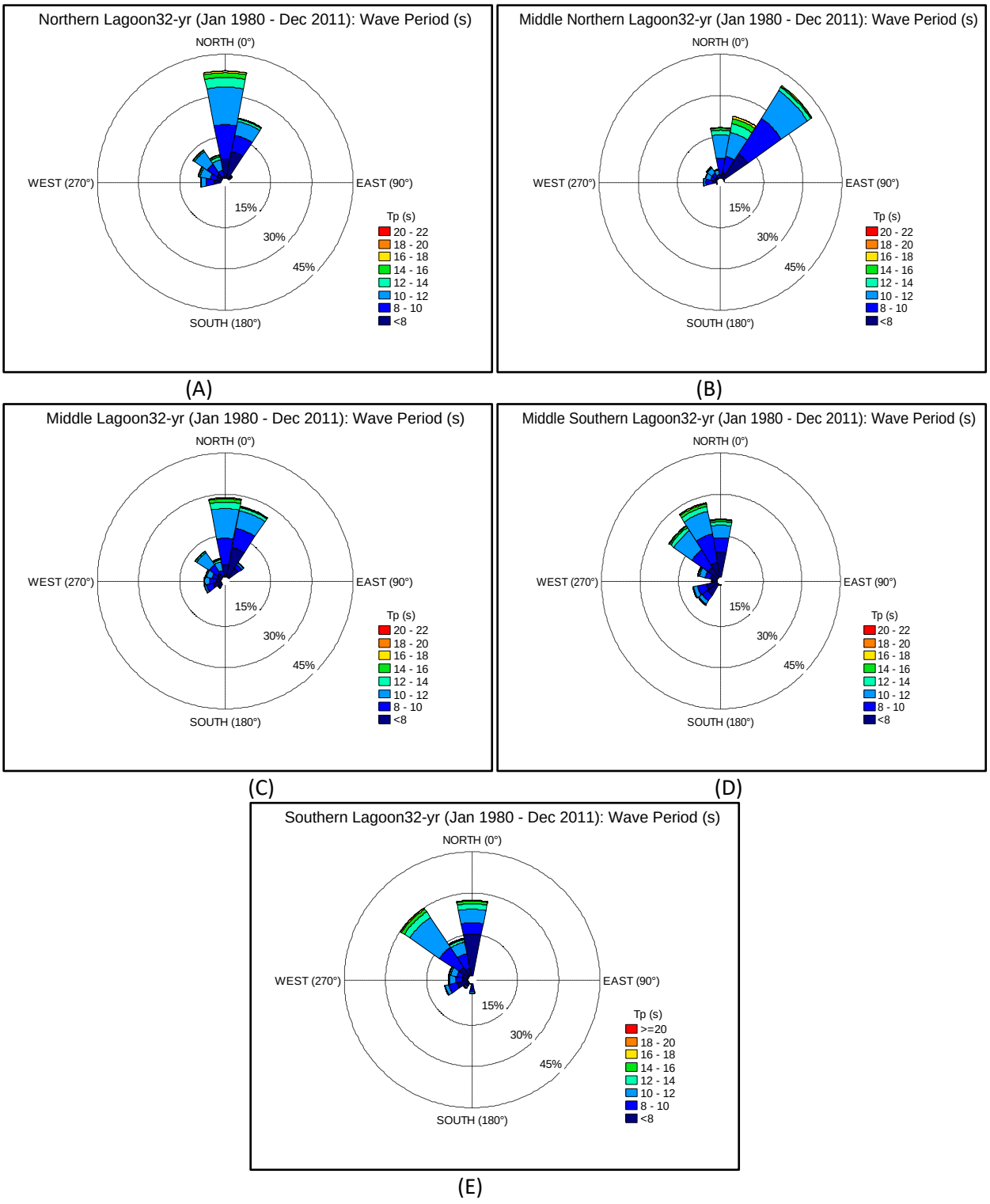

Figure 2-19. Period Roses for (A) Northern virtual buoy, (B) Middle Northern virtual buoy, (C) Middle virtual buoy, (D) Middle Southern virtual buoy, (E) Southern virtual buoy.

3. LAGOON HYDRODYNAMIC MODELING

The hydrodynamic modeling process involves several steps: 1) applying a deepwater numerical wave model to propagate and transform deep ocean waves to the project area; 2) developing a nearshore coupled wave and circulation model that uses the output of the deepwater wave model to drive the nearshore waves and currents; 3) calibrating and validating the models by using the measured wave conditions during summer of 2017 at CDIP buoy 197 as input to the deepwater wave model, using the output of the deepwater wave model to drive the nearshore wave-circulation model, and comparing the results to actual wave and currents measured by SEI at nine locations in the project area; 4) based on the wave climate analysis presented in Section 2, selecting and running 5 model cases that represent the most typical conditions in the lagoon. These steps and results are described below.

3.1 Model Descriptions

3.1.1 Deepwater Wave Model - SWAN

The SWAN (Simulating Waves Nearshore) model was used to model propagation and transformation of wave energy from the open ocean to the project area. SWAN is a third-generation wave model developed by Delft University of Technology (Netherlands) that computes random, short-crested, wind-generated waves in coastal regions and inland waters. The SWAN model can be applied as a steady state or non-steady state model, and is fully spectral (i.e., it covers the total range of wave frequencies/periods). Wave propagation is based on linear wave theory and includes the effects of wave generated currents (i.e., Doppler effect). SWAN provides many output quantities including two-dimensional spectra, significant wave height and mean wave period, and average wave direction and directional spreading.

3.1.2 Nearshore Coupled Wave & Circulation Models – Delft3D-Wave+Delft3D-Flow

Because wave conditions affect currents, and the currents they produce may then affect the waves themselves, a coupled wave and circulation model was used for this study. The strength of coupled models is the capability for steering results from one model to the other. This interaction means that for every time step in the simulation, the wave model can pass calculated wave height and other parameters to the flow model for its calculations, which in turn can pass back wave-induced current data to the wave model, enabling a direct solution for a seemingly difficult iterative process.

Nearshore wave heights and wave-generated currents were analyzed numerically using the coupled Delft3D-Wave and Delft3D-Flow models as part of the Delft3D modeling suite, developed by Deltares. Delft3D is an industry-leading 3D modeling suite used globally to investigate ocean hydrodynamics, sediment transport and morphology and water quality for fluvial, estuarine and coastal environments. Delft3D-Wave relies on the previously mentioned spectral wave model SWAN, while Delft3D-Flow is a multi-dimensional (2D depth-averaged or 3D) hydrodynamic and transport simulation model which solves the non-steady shallow-water equations with the hydrostatic and Boussinesq assumptions.

3.2 Model Domain and Flow Forcing

3.2.1 Model Domain

A 3-grid nesting scheme in SWAN was utilized for this study to propagate deepwater offshore waves to the nearshore regions around Saipan's lagoons. The nesting scheme consists of a course 500-meter grid, an intermediate 120-meter grid, and a fine 30-meter grid near shore. The fine wave grid and flow grid are identical which allows for wave and current data to be passed between the two grids without interpolation.

Table 3-1 summarizes each of the domains used in this study. Figure 3-1 shows the boundaries of each of the domains in relation to Saipan.

Table 3-1. Summary of Model Domain Characteristics

Domain	Model	Number of Cells	Resolution (m)	Nested In Domain
1	Delft3D-WAVE (SWAN)	10624	500x500	N/A
2	Delft3D-WAVE (SWAN)	24544	120x120	1
3	Delft3D-WAVE (SWAN)	113315	50x30	2
4	Delft3D-FLOW	113315	50x30	3

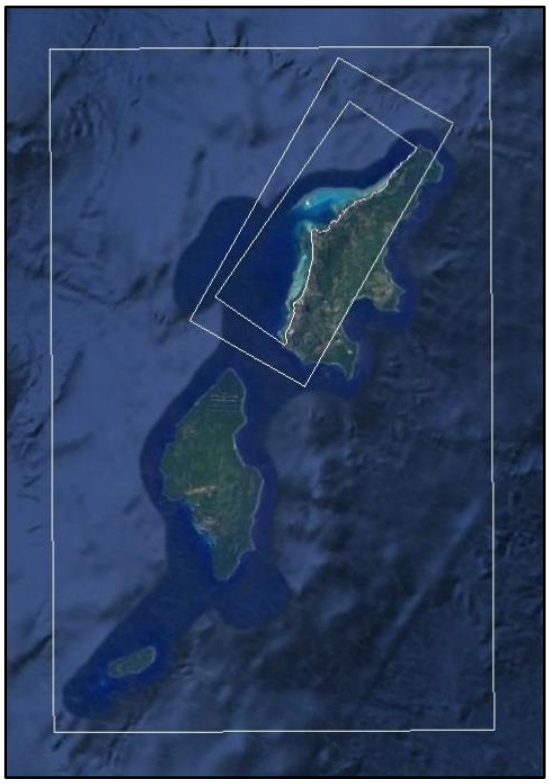

Figure 3-1. Grid nesting scheme.

3.2.2 Bathymetry

Bathymetry plays a critical role in modeling wave transformation and hydrodynamics. The Pacific Island Benthic Habitat Mapping Center has compiled hydrographic surveys to generate a 5-meter resolution digital elevation map (DEM) for the waters surrounding Saipan (Figure 3-2). The data set compiles ship based multibeam data collected by 2007, airplane-based Lidar data collected in 2001, and IKONOS satellite imagery data. Figure 3-3 shows the coverage area for each data set. Of the three sources, IKONOS is the least accurate. In deep water, error on the order of meters is insignificant; however, in a shallow reef environment, such as Saipan's lagoon, error on the order of meters could have significant impact on model results. Color contours for depths from 0 to 5 meters for the northern half of lagoon are shown Figure 3-4. At this scale it becomes clear the low level of accuracy from the IKONOS data along the northern end of the lagoon and along the reef crest where there is a distinct color lineation marking an erroneous offset in the bathymetry. A transect marked in Figure 3-4 and plotted in Figure 3-5 shows that there is a deep trench recorded in the IKONOS data set in the middle of the reef crest which actually does not exist. For the numerical model, this error in the bathymetry data was adjusted by raising the elevations to match the average elevation of the reef crest along the southern half of the lagoon. The large area to the north was also smoothed and changed to match the adjacent lidar data. The adjusted bathymetry in the northern part of the lagoon that is used in the model is presented in Figure 3-6. It should be noted that the Lidar data which covers most of the lagoon is over 17-years old and would not represent any changes in the bathymetry that may have occurred over this time span. The bathymetry of the hydrodynamic domain shown in Figure 3-7 plots the depth up to 15 meters (49 feet) in the lagoon. The figure highlights the complex bathymetry of the project area that steers currents forced by waves and tides.

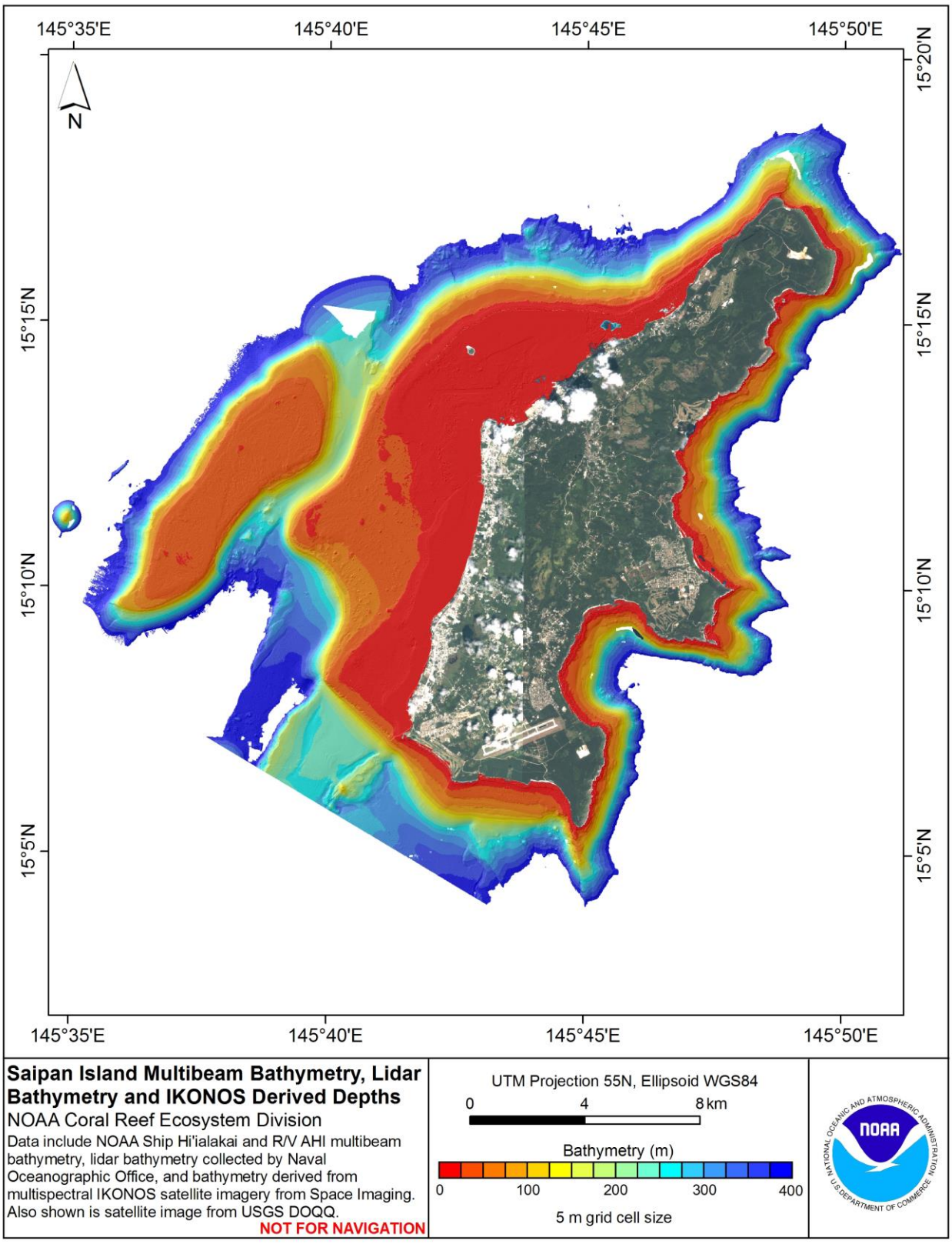

Figure 3-2. Saipan Island bathymetry.

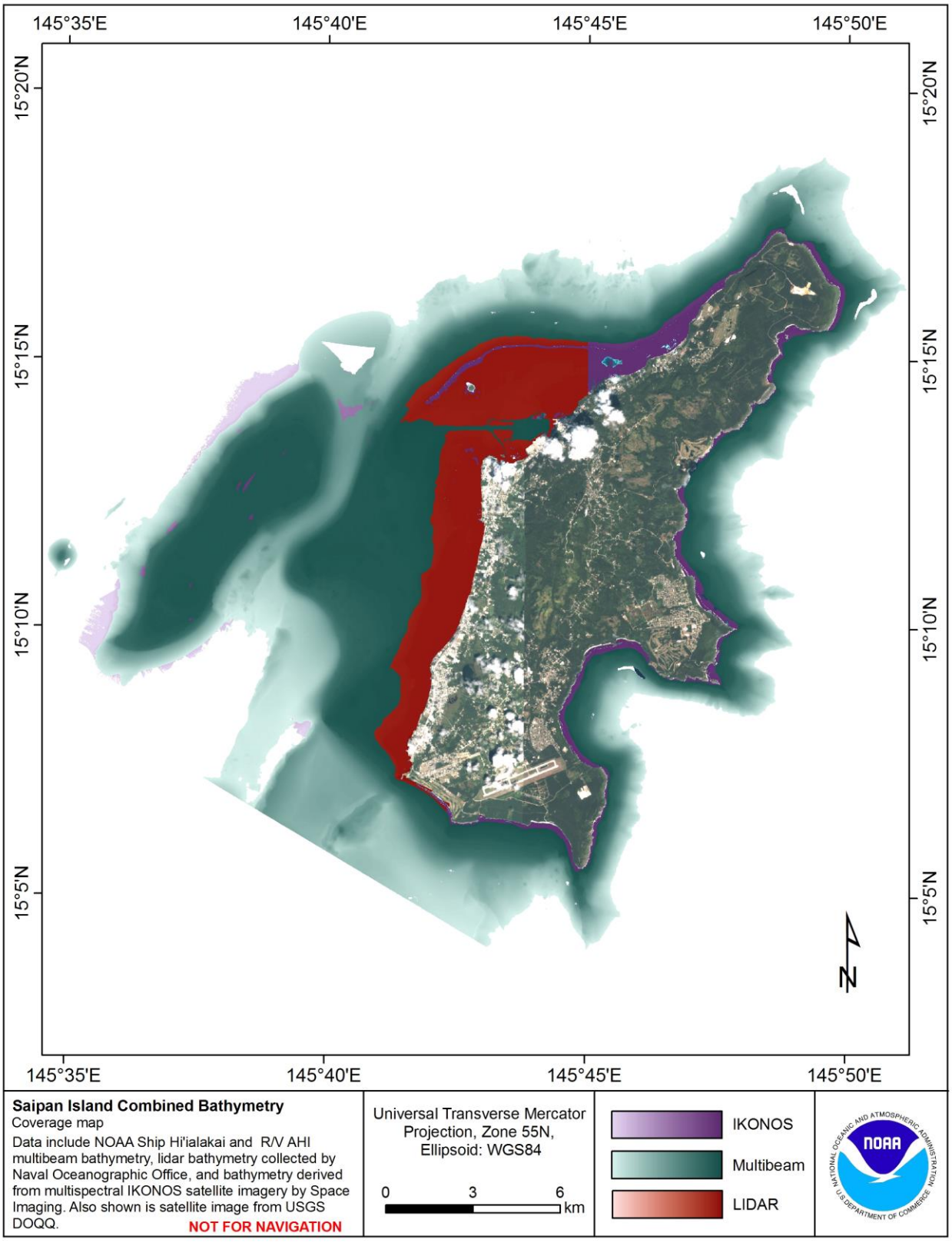

Figure 3-3. Bathymetric data around Saipan.

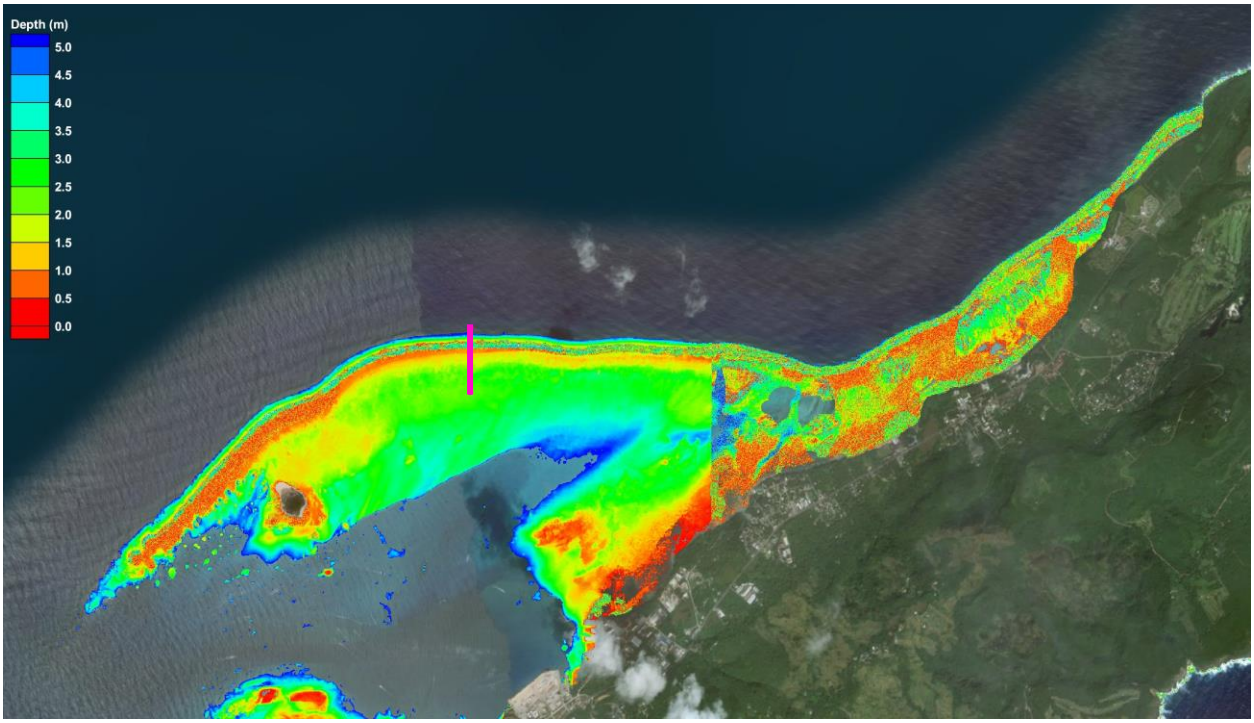

Figure 3-4. Unadjusted bathymetry at the north end of the lagoon showing erroneous offset.

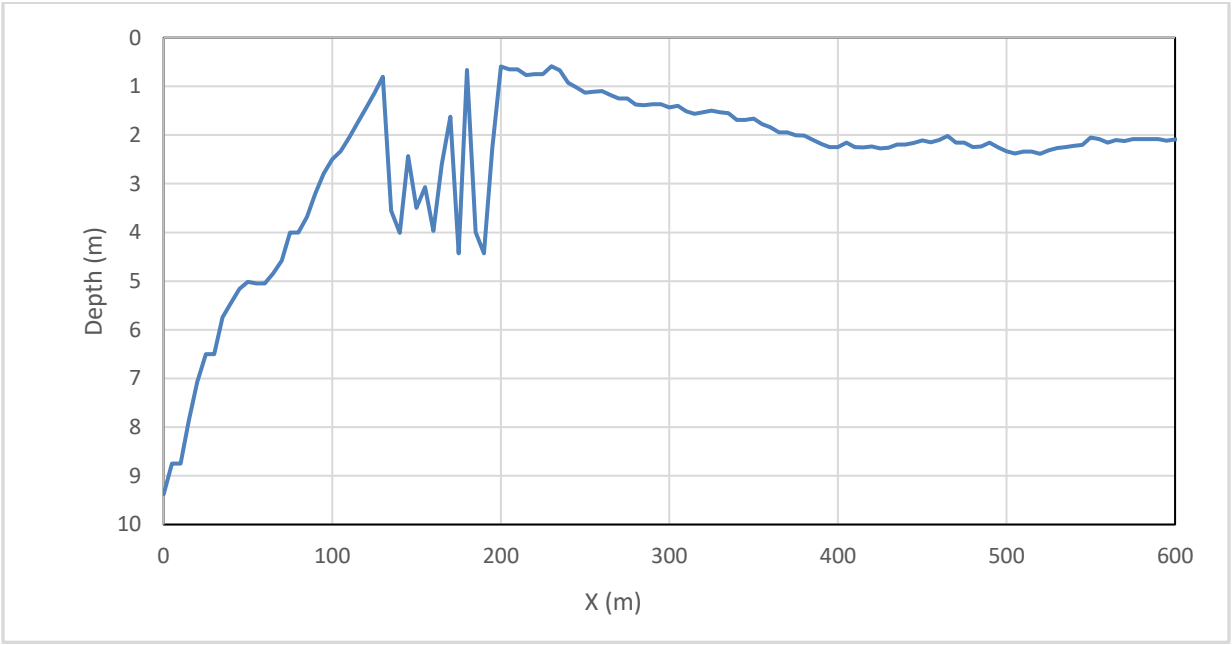

Figure 3-5. Cross section of reef flat bathymetry showing erroneous trench.

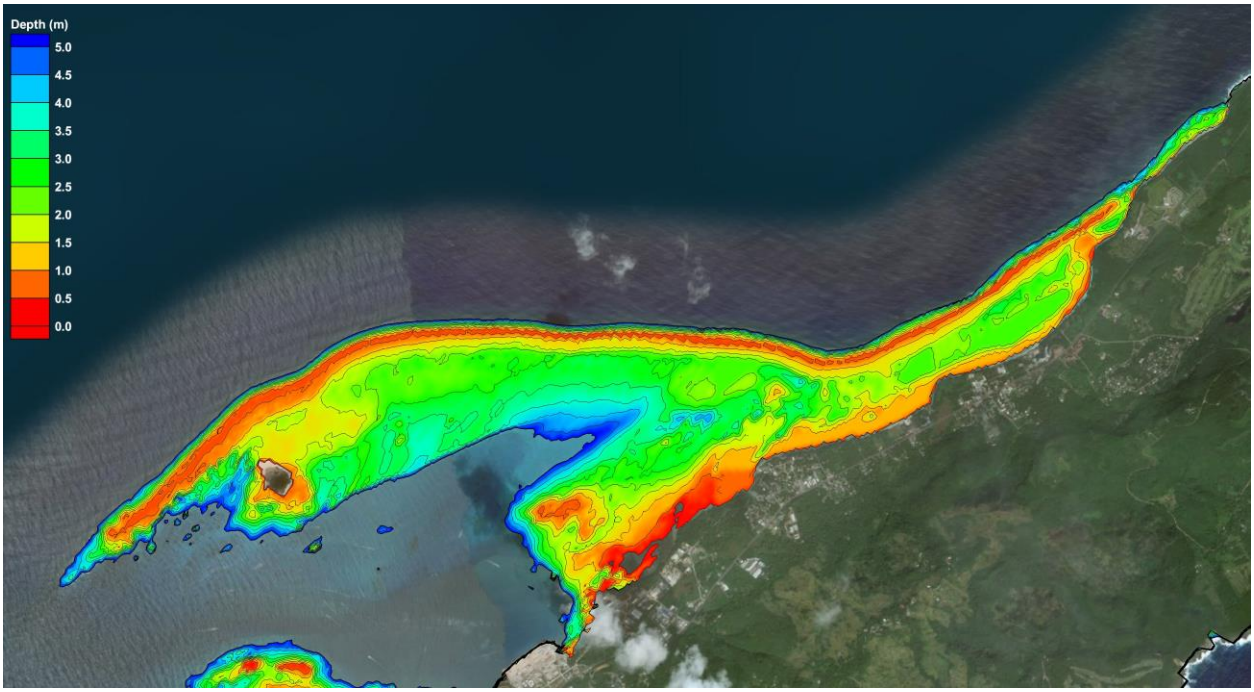

Figure 3-6. Adjusted bathymetry along reef crest and northeast reef flat.

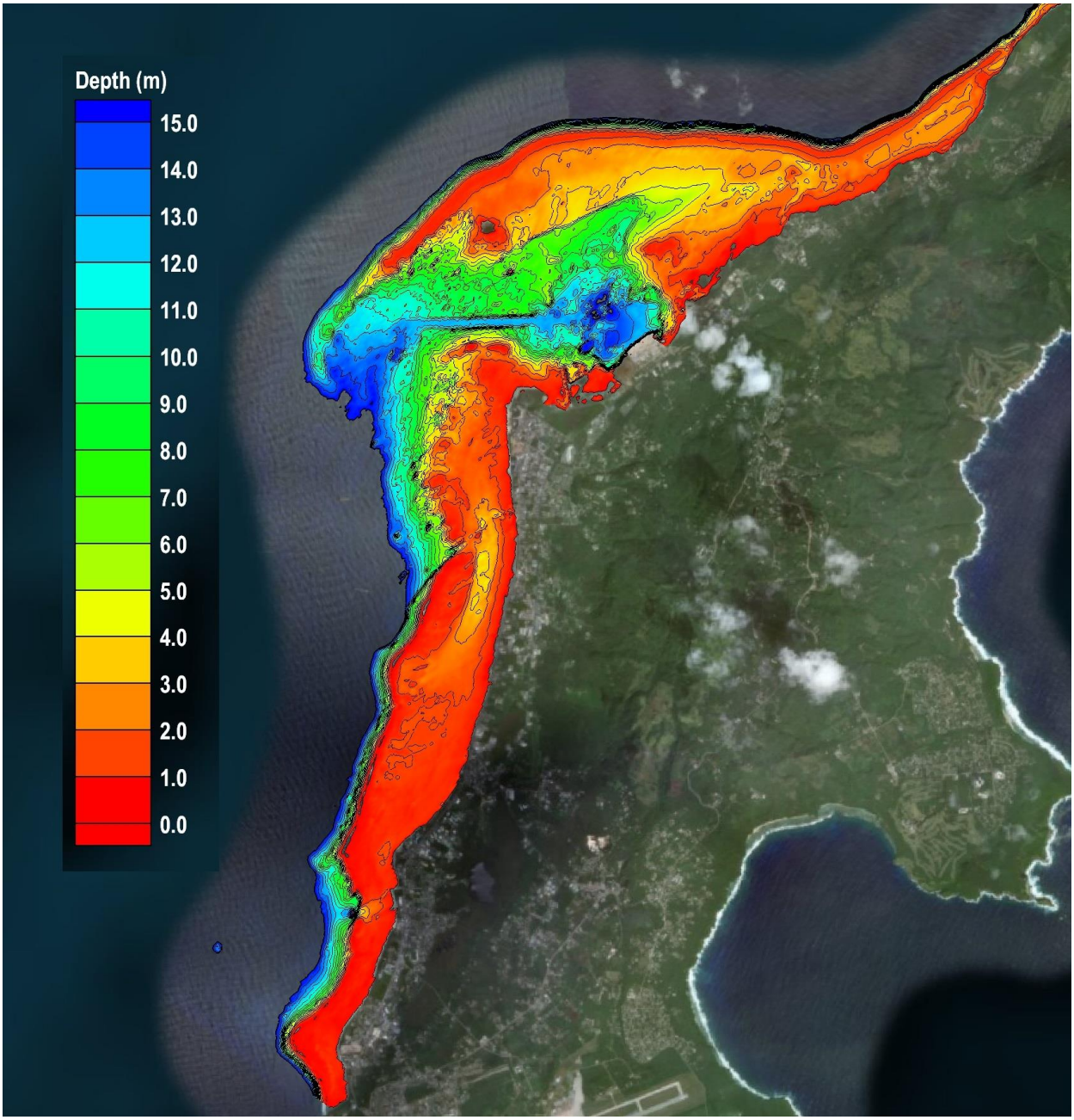

Figure 3-7. Model bathymetry for Saipan Lagoon.

3.2.3 Boundary Conditions

3.2.3.1 Tide

The open boundaries of the Delft3D-FLOW model were specified as water level boundaries defined by the TPXO8 global tide model. The TPXO8 model provides tidal constituents and their corresponding amplitudes and phases at a 1/6-degree resolution over the globe. A snapshot of the TPXO8 model output is shown in Figure 3-8.

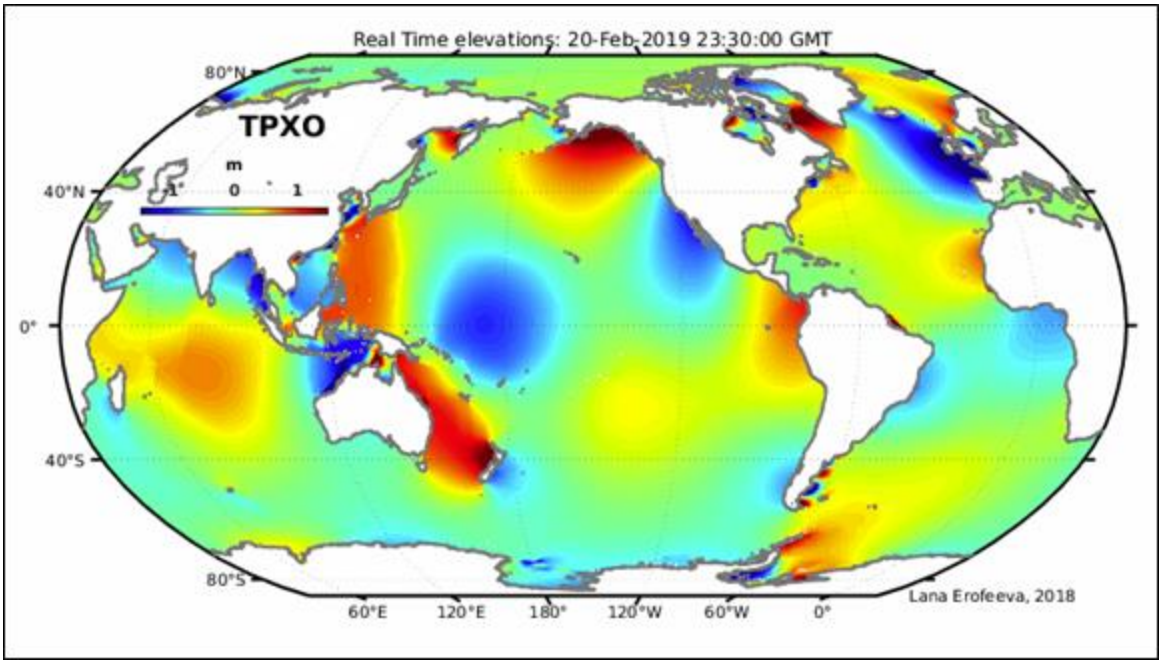

Figure 3-8. Snapshot of tidal elevation from the TPXO8 model.

Source: http://volkov.oce.orst.edu/tides/global.html

Tidal constituents along with their amplitudes and phases were extracted from the TPXO8 model at multiple locations along the open boundaries of the flow model. Over the simulation period the spatially varying tidal heights were generated by the amplitude and phases of each constituent (Egbert, 2002).

3.2.3.2 Deepwater Waves

The wave model was driven by a two-dimensional wave spectrum recorded at CDIP 197. The 2D wave spectrum incorporates the full wave climate recorded at the buoy rather than peak parametric data, which allows for a more accurate model result.

3.2.4 Wave Model Parameters

A key parameter for the wave model is bottom roughness, which results in friction. Parameterization of wave energy dissipation due to bottom friction has been derived from the equations employed for bottom friction in open channel flow and was adapted for use in linear wave theory. Natural coral reef structures may commonly have roughness heights that are orders of magnitude greater than adjacent channel bottom areas or sandy regions. Roughness heights are essentially the heights of individual structural elements that rise above the average surrounding bottom. Roughness is expressed in the model as bottom friction coefficients. There have been various studies attempting to calibrate roughness parameters for coral reefs; however, the roughness of coral reefs is often highly variable from location to location resulting in a wide range of values with no intuitive way to quantify and apply them. In order to obtain a representative distribution of bottom friction coefficients, it was first necessary to assign roughness heights to all regions in the model domain; the roughness height values are simply the

vertical difference between local minima and maxima in the bathymetry data. Assignment of the roughness heights was primarily based on physical features in the bathymetry data, as well as from limited observations made during the site visit and from satellite imagery.

3.2.5 Flow Model Parameters

The roughness parameter for the flow model was specified based on the White-Colebrook formulation using a Nikuradse value, k_s, of 0.5m. This roughness was chosen based on the work by Lowe et al. (2009) where a similar model setup was calibrated in Kaneohe Bay on the Island of Oahu, Hawaii (Lowe et al, 2009). All other flow parameters were kept at their default values for this study.

3.3 Model Validation

The wave and hydrodynamic model were validated by running the model with wave conditions recorded at CDIP buoy 197, comparing model results with the wave and currents measured during summer of 2017 at the nine locations shown in Figure 3-9. The results of this field measurement program are summarized in the 2018 SEI report *Hydrodynamic Study of Saipan's Western Lagoon - Data Report*.

Table 3-2 summarizes the location and deployment duration of the nine instruments SEI deployed for the study. The validation included both comparing model computed wave heights in the lagoon with the measurements and comparing model computed currents in the lagoon with the measurements. For further discussion, the lagoon to the north of the main channel will be referred to as Tanapag Lagoon and the lagoon area to the south will be referred to as the Garapan Lagoon, as it is marked in NOAA charts.

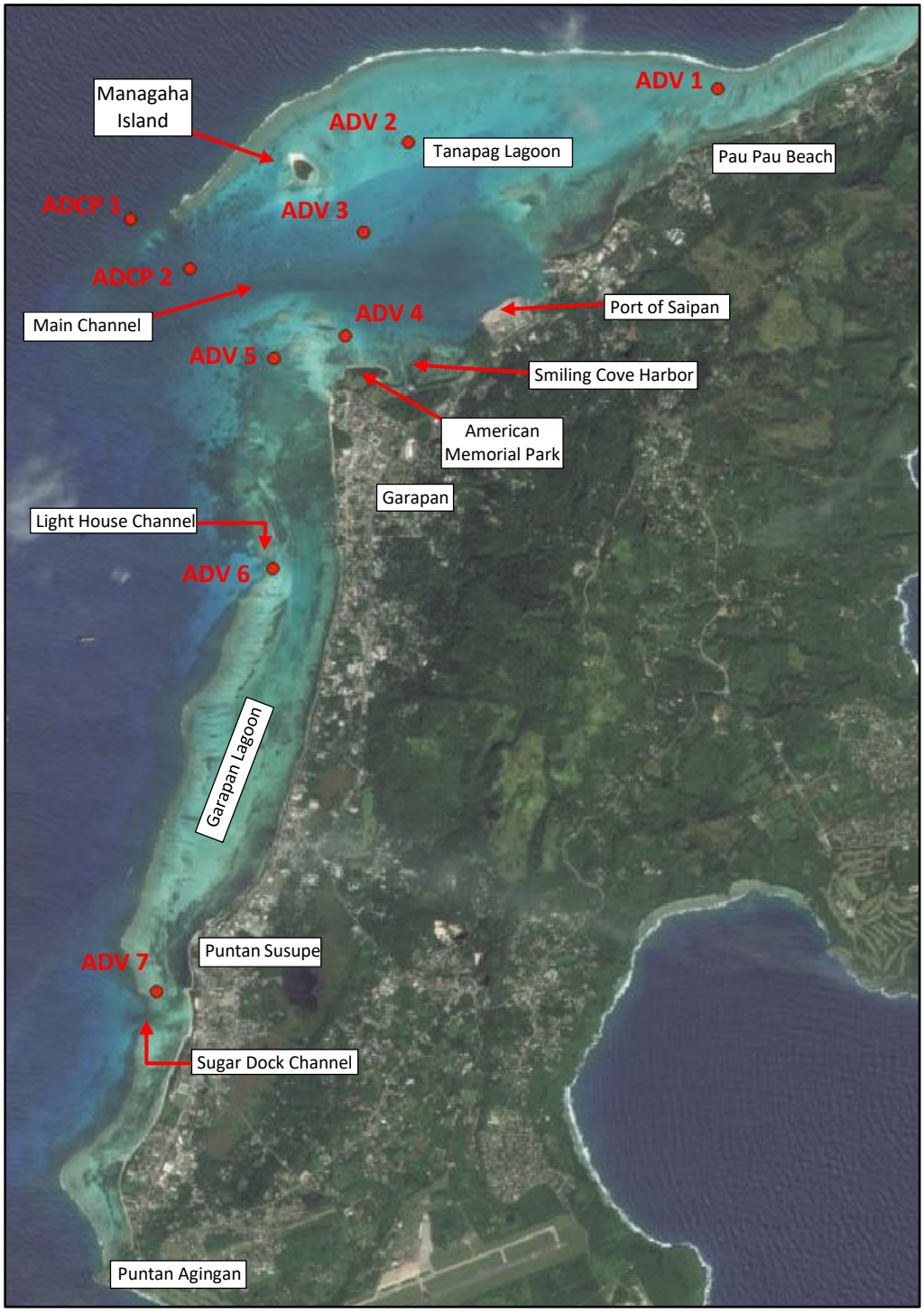

Figure 3-9. Instrument locations.

Table 3-2. Instrument Deployment Summary.

Name	Latitude	Longitude	Depth (m)	Deployed	Retrieved	Description
ADCP 1	15.23589756 N	145.69362978 E	21.77	6/29/2017	10/17/2017	North of Garapan Harbor Entrance Channel
ADCP 2	15.23045018 N	145.70013704 E	11.48	6/29/2017	10/31/2017	Garapan Harbor Entrance Channel
ADV 1	15.25019211 N	145.75808601 E	1.52	6/29/2017	10/18/2017	Pau Beach
ADV 2	15.24430711 N	145.724129 E	3.54	6/29/2017	10/18/2017	East of Managaha Island
ADV 3	15.2344492 N	145.71922906 E	7.32	6/29/2017	10/18/2017	Garapan Lagoon
ADV 4	15.22310605 N	145.71720054 E	2.88	6/30/2017	10/17/2017	American Memorial Park
ADV 5	15.22064287 N	145.70939735 E	3.45	6/30/2017	10/17/2017	Micro Beach/Hyatt
ADV 6	15.19759292 N	145.7092623 E	2.33	6/30/2017	10/17/2017	Lighthouse Channel Entrance
ADV 7	15.15119924 N	145.69648297 E	0.94	7/1/2017	10/17/2017	Sugar Dock Channel Entrance

3.3.1 Wave Model Validation

Time series plots of the model results with the CDIP 197 buoy and SEI instrument measurements are presented in Figure 3-10 through Figure 3-19. The figures show two distinct peaks in wave heights spanning July 28-30 and August 28-30, likely associated with the passage of typhoons Naru and Nesat for the first peak and typhoon Hato and severe tropical storm Pakhar for the second peak. A comparison between ADCP 1 and ADCP 2 measurements and model results (Figure 3-11 and Figure 3-12) shows excellent agreement in the deep water of ADCP 1 and in the entrance to the lagoon at ADCP 2. The ADVs are located within the lagoon, and therefore record waves that have been extensively transformed at the cross over the reef. The ADV measurements also indicate good agreement between the model and the measurements. The largest discrepancies occur at ADV 1 and ADV 3 (Figure 3-13 and Figure 3-15). At ADV 1, the model slightly over estimates wave heights, while at ADV 3 the model underestimates wave heights. The strong model agreement in deeper water with ADCP 1 and ADCP 2 indicates that the differences at the inshore

instruments (ADV 1 and ADV 3) are likely dependent on inaccuracies in the bathymetry or bottom friction, which both have a strong influence on wave heights in shallow reef environments. Bottom roughness values were assigned to the model based on aerial images and photographs from previous field efforts. Studies have shown that wave height dissipation is primarily due to bottom friction on broad reef flats after the initial wave breaking at the reef crest (Lowe 2005). The remaining ADVs show excellent agreement between the model results and field measurements.

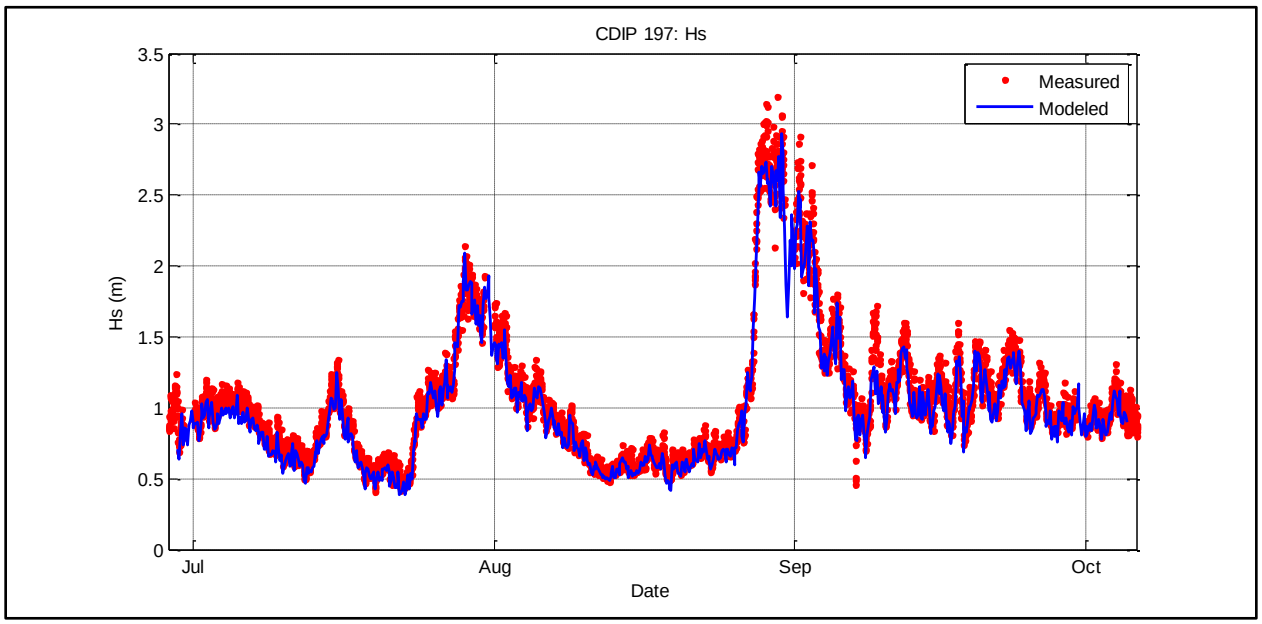

Figure 3-10.Wave height time series at CDIP 197.

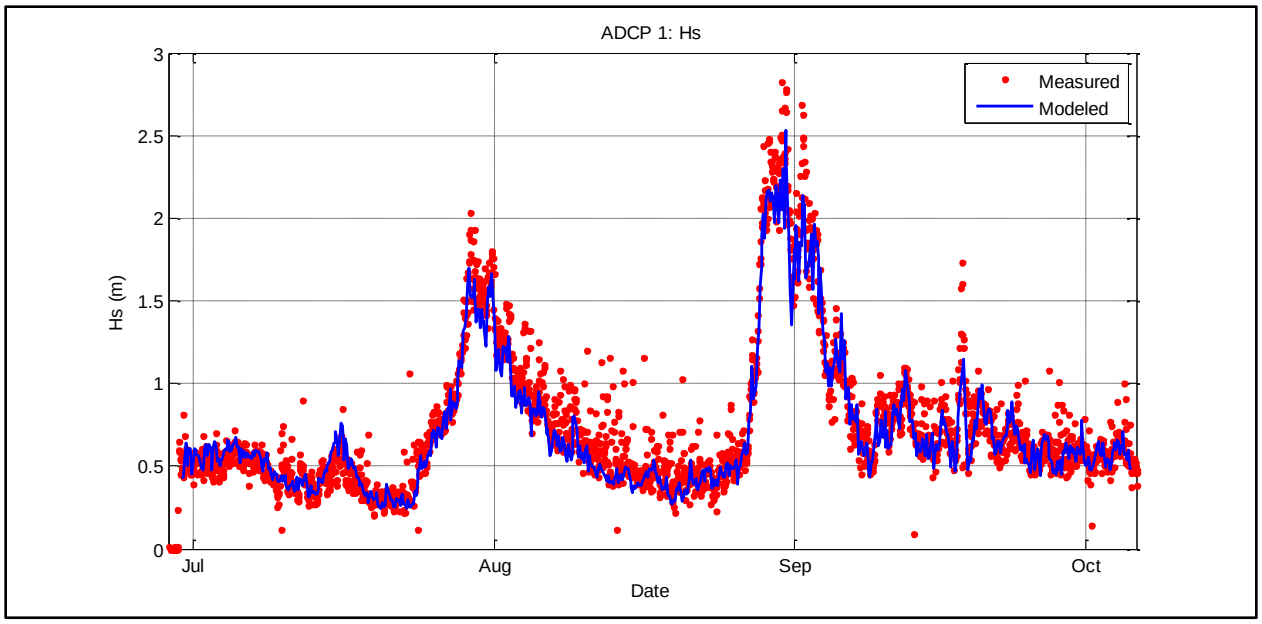

Figure 3-11. Wave height time series at ADCP 1.

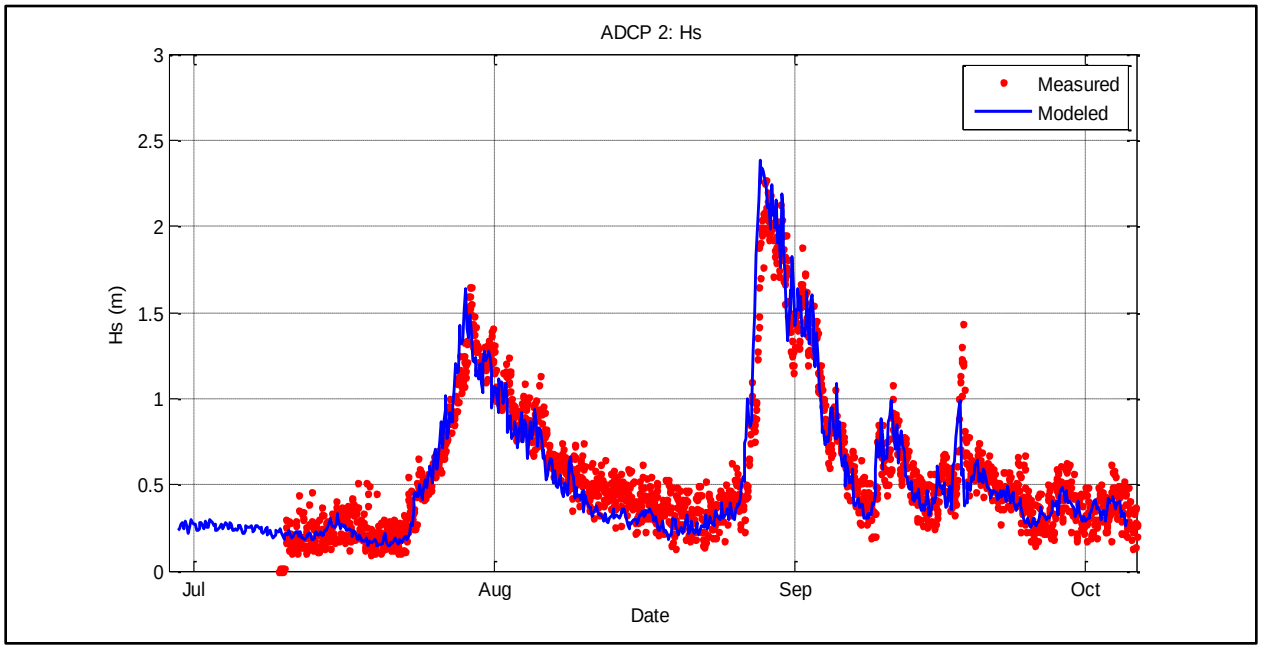

Figure 3-12. Wave height time series at ADCP 2.

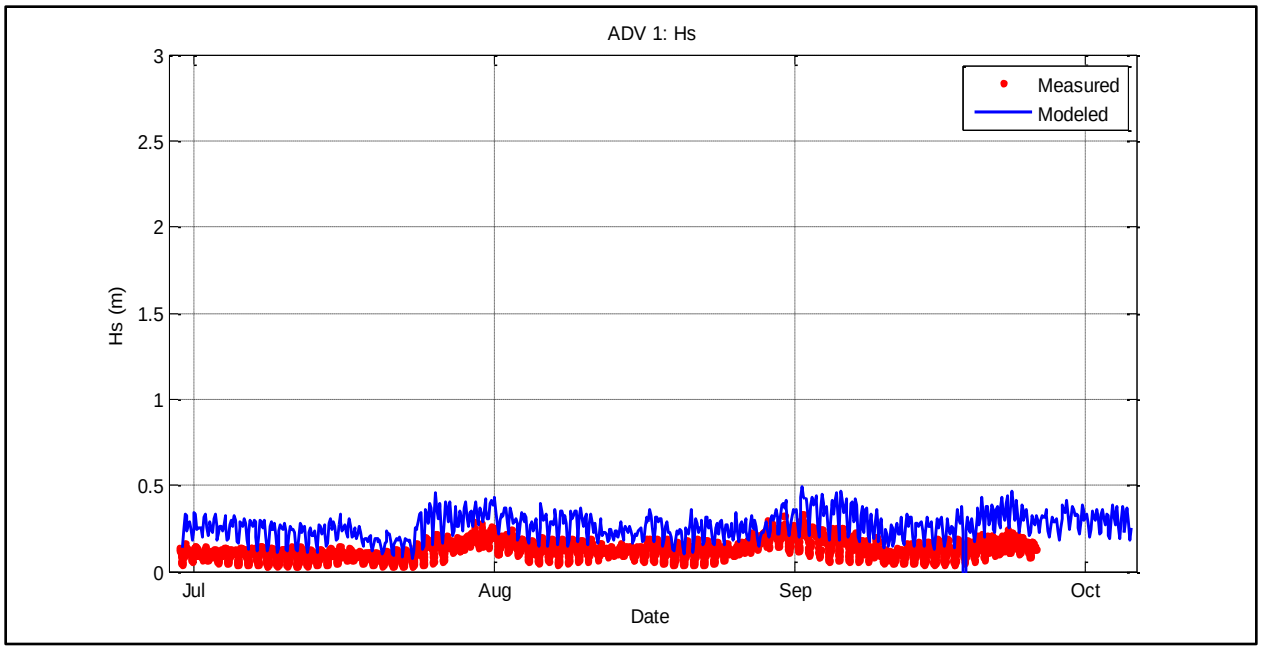

Figure 3-13. Wave height time series at ADV 1.

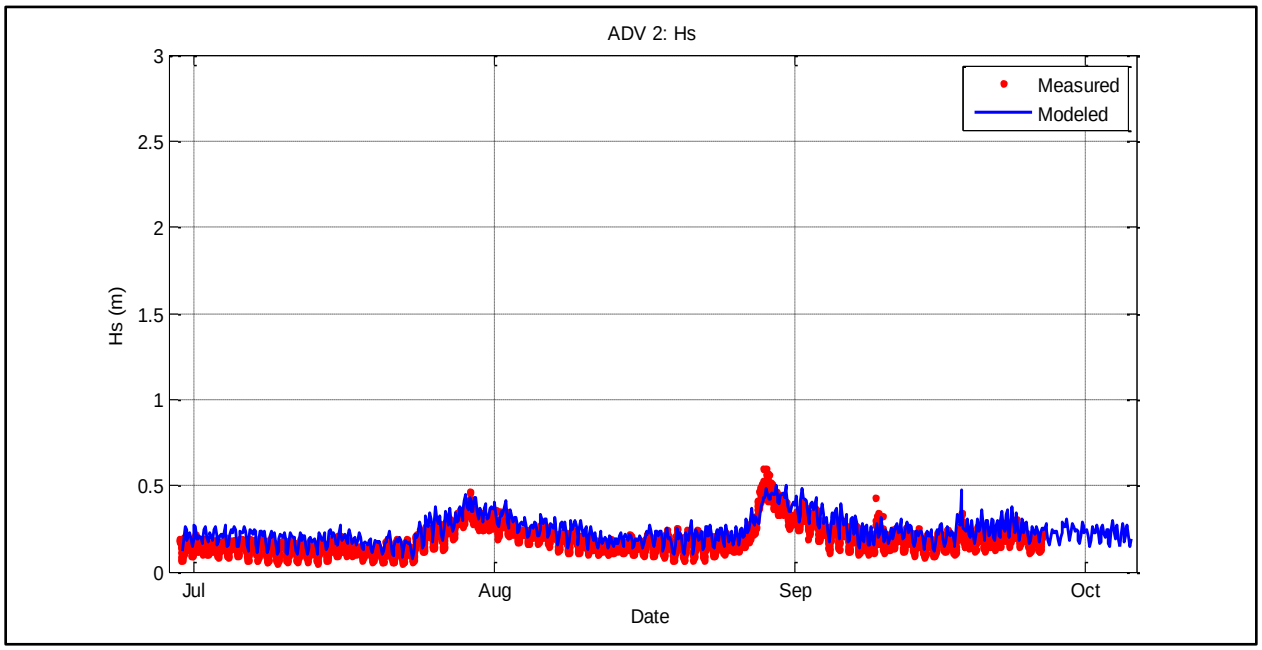

Figure 3-14. Wave height time series at ADV 2.

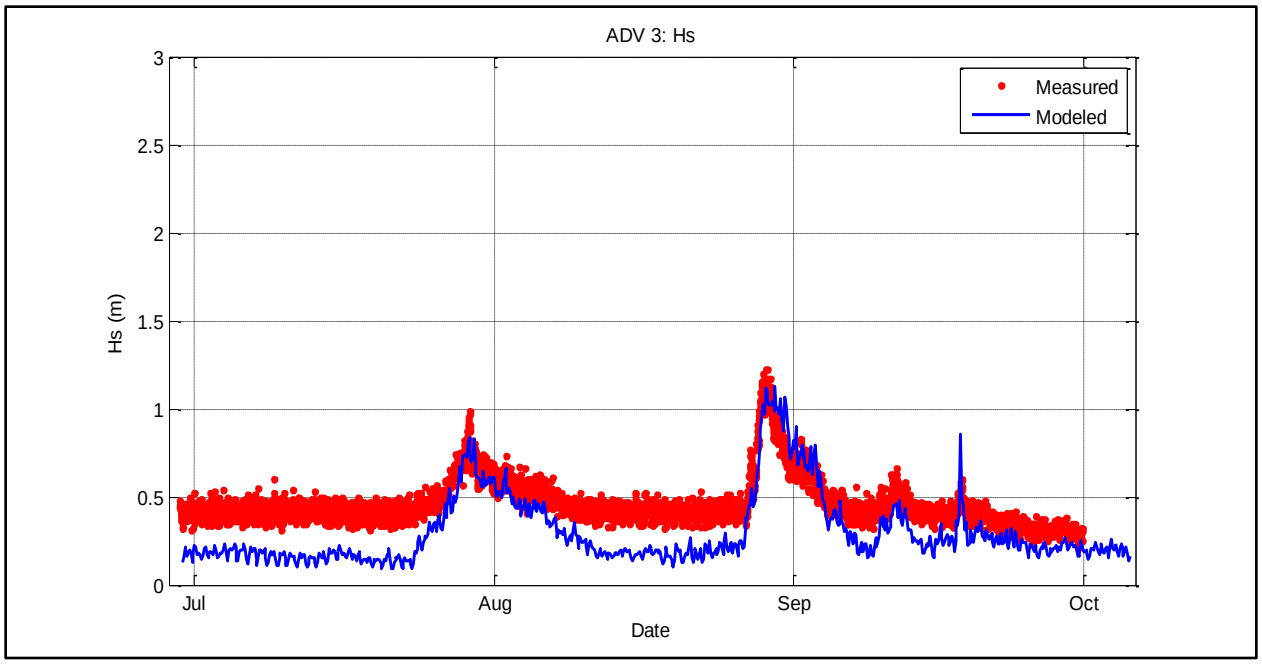

Figure 3-15. Wave height time series at ADV 3.

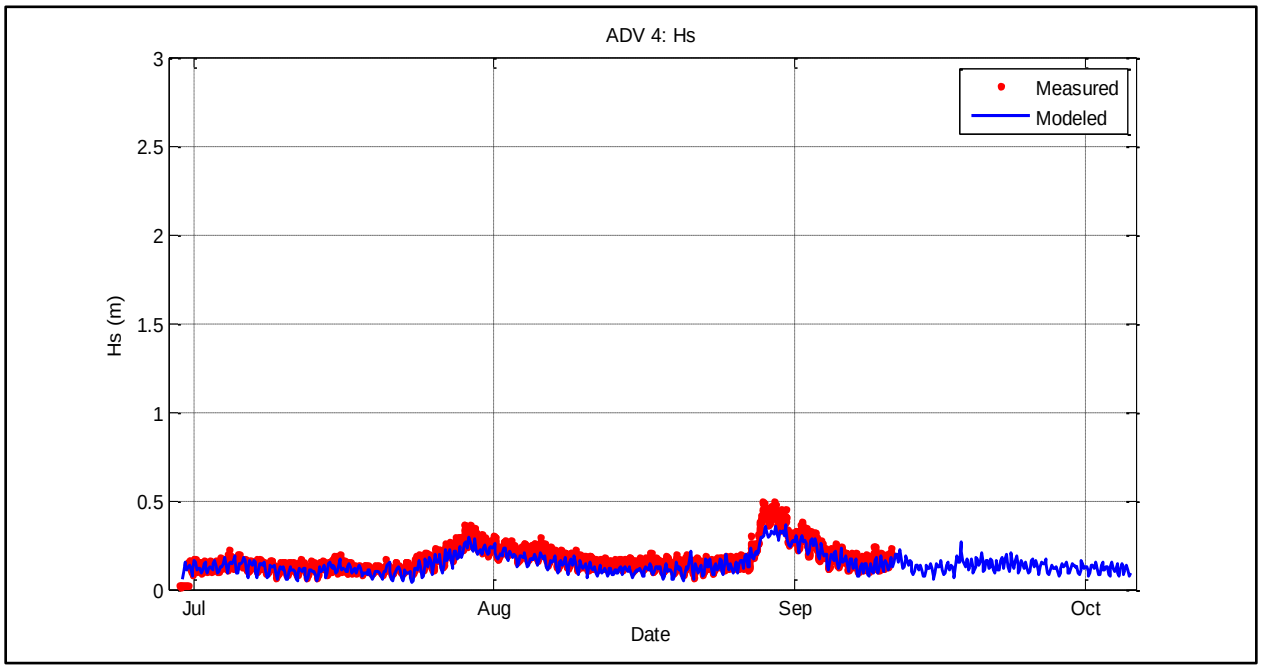

Figure 3-16. Wave height time series at ADV 4.

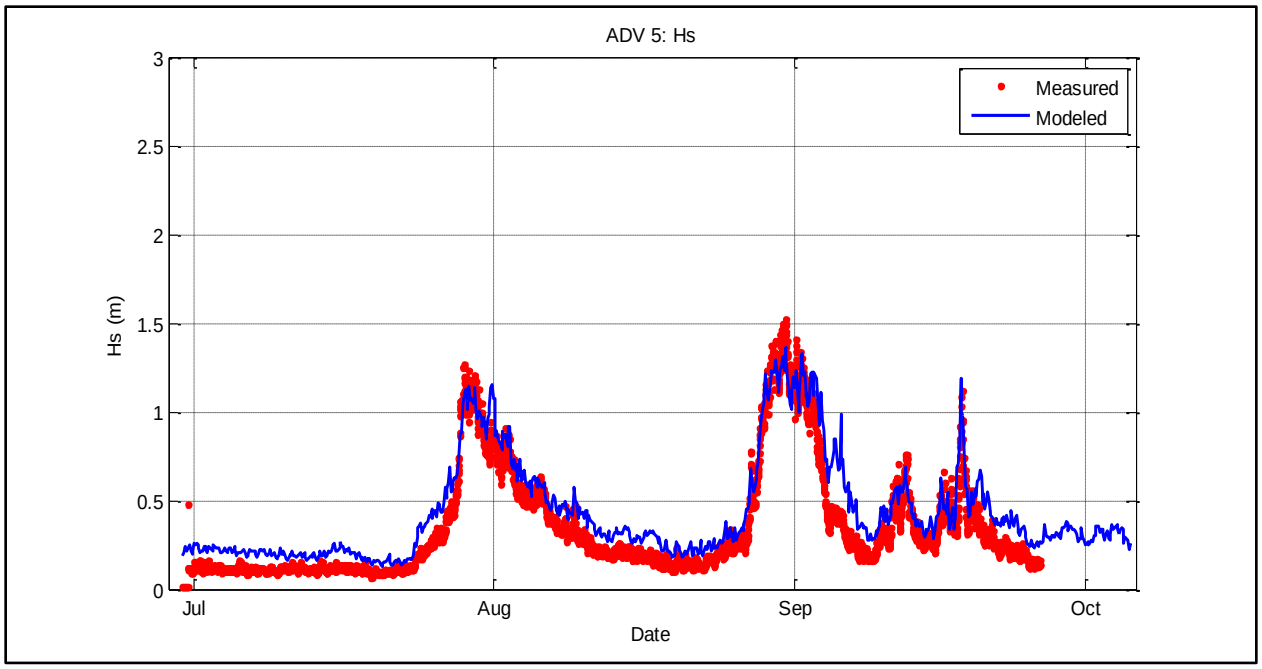

Figure 3-17. Wave height time series at ADV 5.

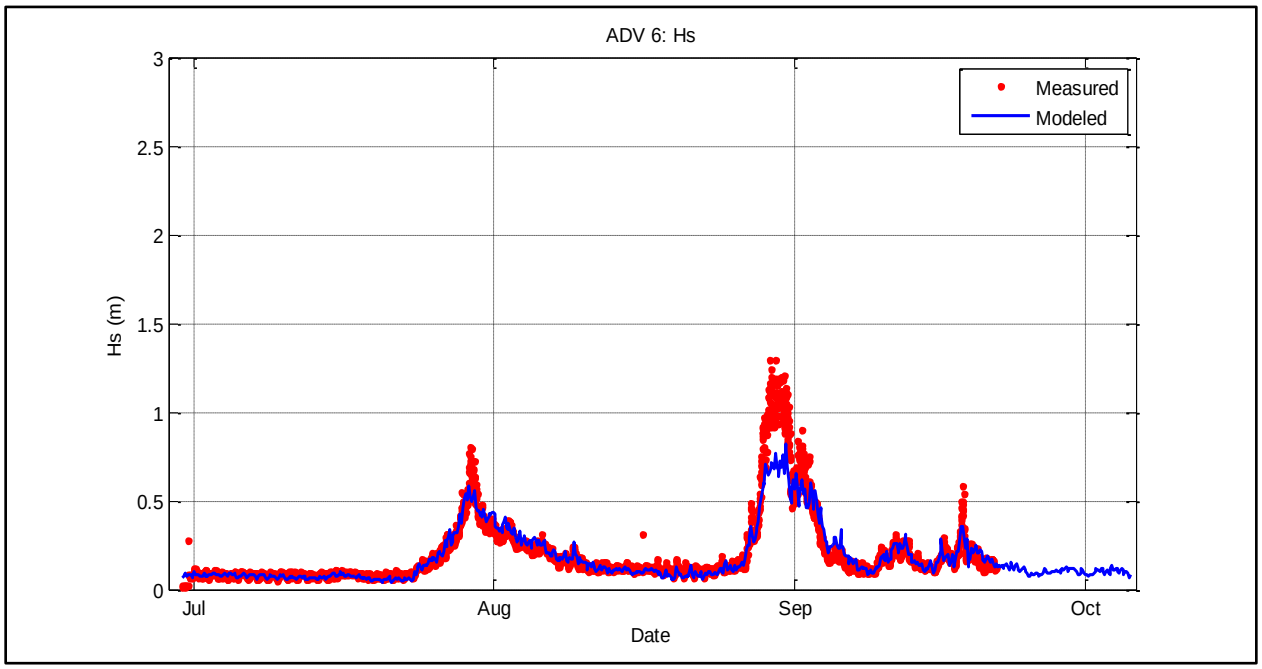

Figure 3-18. Wave height time series at ADV 6.

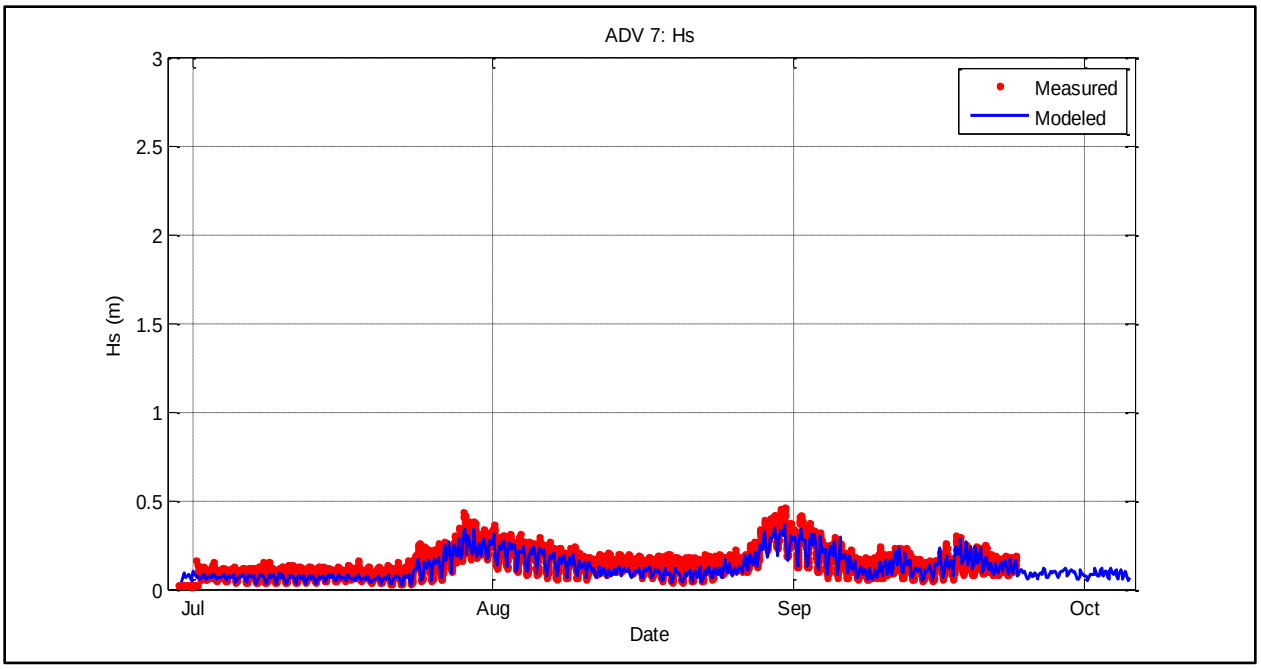

Figure 3-19. Wave height time series at ADV 7.

3.3.2 Hydrodynamic Validation

The wave model computations proceed significantly faster than the hydrodynamic model. It was therefore possible to verify the wave model for the full 3-months the instruments were deployed. The hydrodynamic model, however, requires significantly more computation and has more tunable parameters, and therefore was verified for select durations of the field deployment to capture typical tradewind wave conditions and larger westerly storm wave conditions. Since a majority of the domain consists mostly of a shallow area, the model was run in 2-dimensional mode such that all flow is depth averaged. This assumption was verified by agreement with the instrument data. Model runs were also conducted without wind forcing for two reasons: the measured field data indicated that waves and tide are the primary drivers currents in the lagoon, and wind data is incomplete and could not be accurately imposed throughout the model domain. Tidal forcing consisted of the outputs for the TPXO8 global tidal model. The water level over several tidal cycles at ADCP 1, ADV 3, and ADV 7 are plotted in Figure 3-21 through Figure 3-23. The figures illustrate that the numerical model accurately reproduces the tidal water levels measured during the field program.

During the field deployment there were distinct periods of typical tradewind waves and westerly waves from passing storms. The time period from July 11 to July 23, 2017 was used to validate the model during tradewind conditions. Two other periods were selected to validate model performance during storm wave events impacting the lagoon: July 27 to August 11, 2017 encompassing a several day period of high waves due to Typhoons Naru and Nesat which were active in the area at the time; and August 27 to September 12, 2017 encompassing a sharp

increase in wave energy believed to be from typhoon Hato and severe tropical storm Pakhar. The offshore wave conditions during the time periods listed above are presented in Figure 3-20. The figure shows that the storm wave events are marked by increased wave heights and abrupt shifts in wave direction relative to trade wind conditions. On the figure, the tradewind wave period is bounded by blue lines, while the storm wave events are bounded by green lines.

Comparison of model results with field measurements is presented in two formats: 1) time series plots of total velocity, the east directed component of current velocity (easting) , and the north directed component of current velocity (northing) at all nine instruments deployed throughout the lagoon as shown in Figure 3-24 through Figure 3-33; 2) net flow rose diagrams for the tradewind and wave event validation periods shown in Figure 3-34 and Figure 3-35.

Validation results are discussed below for each instrument location.

ADCP 1

Figure 3-24, Figure 3-34 and Figure 3-35 present model results compared with measurements at ADCP 1. The ADCP measurements indicate reversing tidal currents with peak magnitudes of 0.3 to 0.5 m/s, without notable change during storm wave events. The model calculated currents are weaker, typically less than 0.2 m/s. Figure 3-21 through Figure 3-23 illustrate that the TPXO8 tidal inputs used for the model replicate well the actual water levels measured by the current meters. This suggests that there are strong regional tidal currents offshore of the lagoon that were measured at ADCP 1 that are not produced in the model using local water levels. These regional oceanic currents, however, appear to have a minimal impact on the flow patterns in the Tanapag and Garapan lagoon, which are sheltered by the shallow reef along the offshore perimeter, and largely driven by waves.

ADCP 2

Figure 3-25, Figure 3-34 and Figure 3-35 present the comparison between the measured and modeled currents at ADCP 2. The model results match well the measurements showing current predominantly flowing west-southwestward out of the lagoon. The measurements also indicate a tidal oscillation in the north-south direction that would tend to shift the overall west-southwestward current slightly to the north or south. The model does not capture well this north-south oscillation. This could also be due to the influence of the regional oceanic currents near the mouth of the lagoon. During pronounced wave events at the end of July and August, the model reproduces well the stronger west-southwest current out of the lagoon.

ADV 1

The comparison of measured and model currents at ADV 1 are plotted in Figure 3-26, Figure 3-34 and Figure 3-35. Measured currents oscillate east to west with the tides, with a strong predominance of flow to the west at speeds typically less than 0.25 m/s. During the storm wave events, flow to the west toward the lagoon strengthens to speeds of 0.3 to 0.5 m/s. The model reproduces well the predominance of flow to the west, weak net flow during prevailing tradewinds, and strong flow to the west during the wave events. The model does not reproduce well the tidal oscillations during prevailing trade wind conditions. Currents at ADV 1 are heavily dependent on the morphology and bathymetry of the reef in this area and the reef flat extending

4,000 meters to the northeast. As discussed in Section 5.2.2, bathymetry in this region is poorly characterized by IKONOS data, and required significant interpolation, smoothing and estimation. Incorrect reef crest elevations or reef channels could result in not resolving the magnitude of the tidal oscillations.

ADV 2

Figure 3-27, Figure 3-34 and Figure 3-35 present the comparison between the measured and modeled currents at ADV 2. Currents at ADV 2 relatively weak, averaging 0.12 m/s, and predominantly to the south-southwest into the lagoon channel. During wave events, the flow increases to 0.3 to 0.5 m/s, and veers slightly toward the southwest. The model reproduces this flow pattern accurately, with the exception of the slight veer to the southwest during the large wave events. This is likely due to details in bathymetry than are not resolved by the bathymetric data or model grid.

ADV 3

Figure 3-28, Figure 3-34 and Figure 3-35 present the comparison between the measured and modeled currents at ADV 3. Currents at ADV 3 are similar to ADV 2 – weak, averaging 0.08 m/s, and almost entirely to the south toward the lagoon channel. During large wave events, flow to the south strengthens to 0.2 to 0.3 m/s. The model accurately reproduces the measurements at ADV 3.

ADV 4

Figure 3-29, Figure 3-34 and Figure 3-35 present the comparison between the measured and modeled currents at ADV 4. ADV 4 is notable because it is in shallow, sheltered water approximately 400 meters north of American Memorial Park, and the currents are weak. The average measured current is 0.05 m/s, and the maximum measured current was 0.2 m/s during the large wave event at the end of August. The model accurately reproduces the typical weak magnitude of the currents, and the stronger flow and flow direction during the wave events. During the wave events, flow is to the northeast, toward the lagoon channel.

ADV 5

Figure 3-30, Figure 3-34 and Figure 3-35 present model results compared with measurements at ADV 5. Measured currents at ADV 5 were extremely weak, averaging 0.03 m/s, with no predominant direction. Even during the large wave events, currents remained weak. The model accurately reproduces the weak currents during typical trade wind and low energy conditions. However, the model results showed a notable current up to 0.2 m/s to the east during the occurrence of large waves from the west that were not measured. This is likely due to small scale bathymetric features sheltering ADV 5 that are not adequately resolved in the model bathymetry.

ADV 6

Figure 3-31, Figure 3-32, Figure 3-34, and Figure 3-35 present the comparison between the measured and modeled currents at ADV 6. ADV 6 is located on the south margin of the Light House channel within Garapan Lagoon. This area is characterized by irregular channel and reef bathymetry and marks the transition from a well-defined reef crest and shallow lagoon to the south, and a more gradually sloping reef to the north to the harbor channel. Measured currents

at this location are bimodal. During prevailing tradewind and small wave conditions, the current is east-west, reversing with the tides, and with a net flow to the east into Garapan Lagoon. During the wave events, flow speed increase markedly to 0.5 to 0.7 m/s, directed to the north-west into Lighthouse Channel. The model reproduces the east-west reversing tides during the prevailing, low wave conditions, with greater magnitude and slight net flow to the west. The model also reproduces well the strong flow to the northwest out of the channel during wave events, with slightly smaller magnitudes.

ADV 7

Figure 3-33, Figure 3-34 and Figure 3-35 present model results compared with measurements at ADV 7. This site is on the north margin of Sugar Dock Channel. The seafloor is characterized by sand patches with numerous coral heads that could deflect flow. Measured currents during prevailing, small wave conditions are weak, typically less than 0.1 m/s, with little net flow. The model accurately reproduces this pattern. During large wave events, measured currents flow to the southwest into Sugar Dock Channel with speeds up to 0.4 m/s. The model replicates the magnitude of the wave driven flow, but the flow is directed to the southeast, rather than the southwest (Figure 3-35). Again, this is likely due to the model not being able to accurately represent the small-scale bathymetric features such as coral patches that are present in the area and which can channelize flow. The model also generates larger magnitude north-south tidal oscillations than were recorded by the instrument. The main flow features of weak currents during prevailing, small wave conditions, and flow toward the south into the channel during the large wave events are captured by the model.

In summary, comparison of model calculated waves and currents within the lagoon with field measurements indicates that the coupled nearshore wave and flow model is able to replicate well the wave conditions and basic flow patterns within the lagoon over the range of prevailing to large typhoon wave conditions that the lagoon experiences. Minor discrepancies are evident at some locations during some conditions. Outside of the lagoon, the model does not capture well the magnitude of the reversing tidal currents. These currents are the result of regional oceanic tidal currents that are not included in the model. For the present study, this is not a concern because the regional tidal currents have little effect on currents within the lagoon.

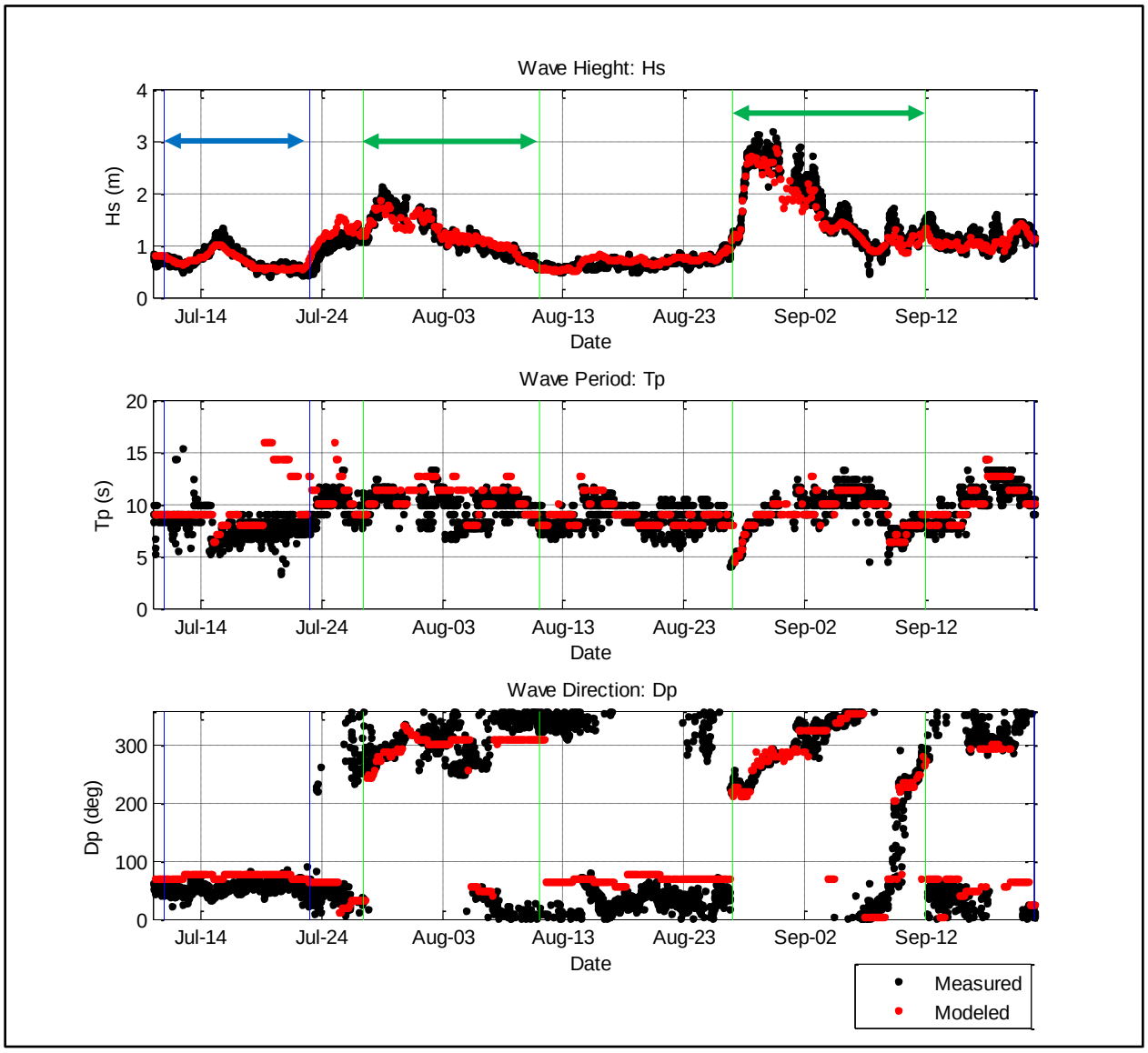

Figure 3-20 Measured and modeled deepwater wave conditions used for model validation.

The blue boundaries mark the tradewind period and green boundaries mark the larger wave event periods.

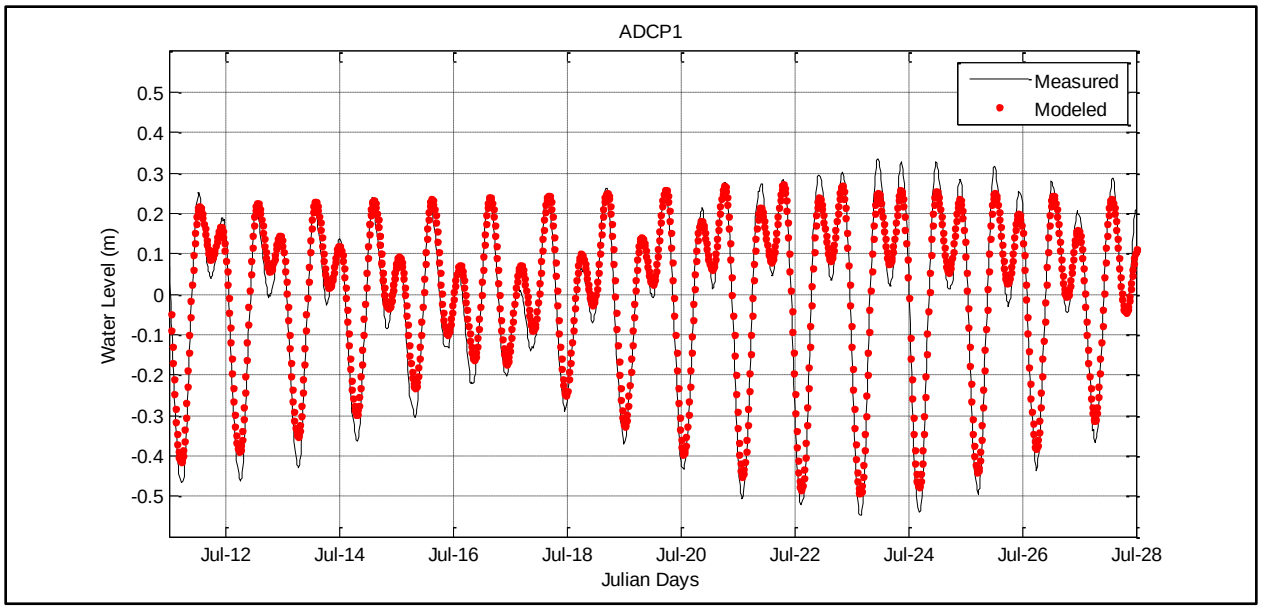

Figure 3-21. Measured and modeled water level relative to mean sea level at ADCP 1.

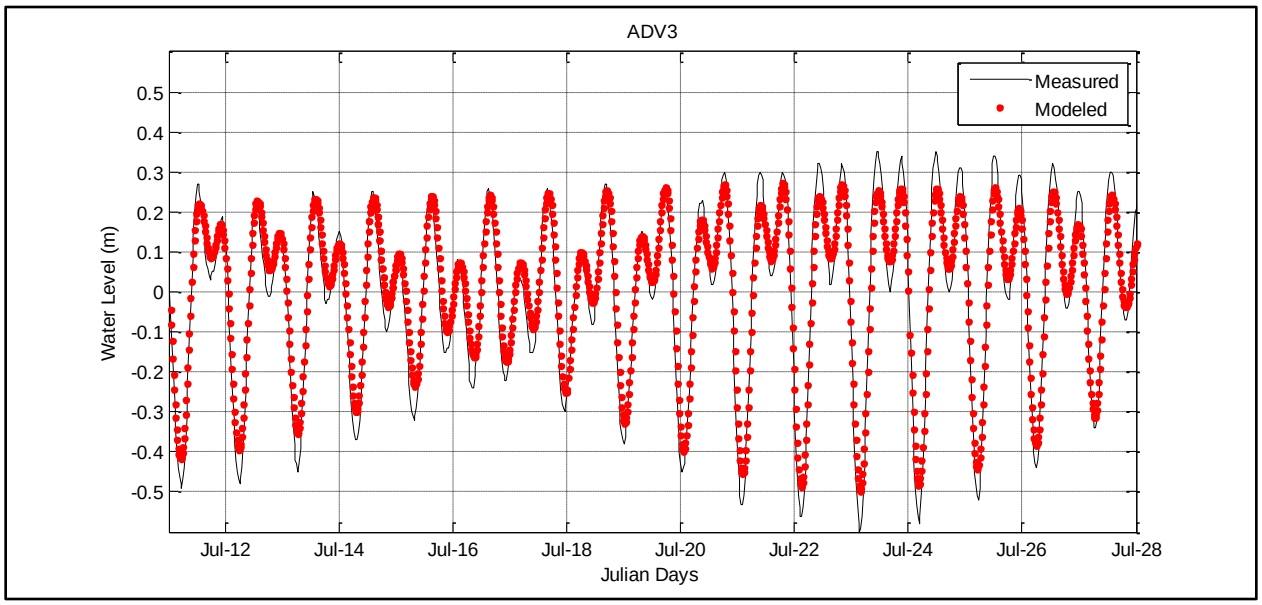

Figure 3-22 Measured and modeled water level relative to mean sea level at ADV 3.

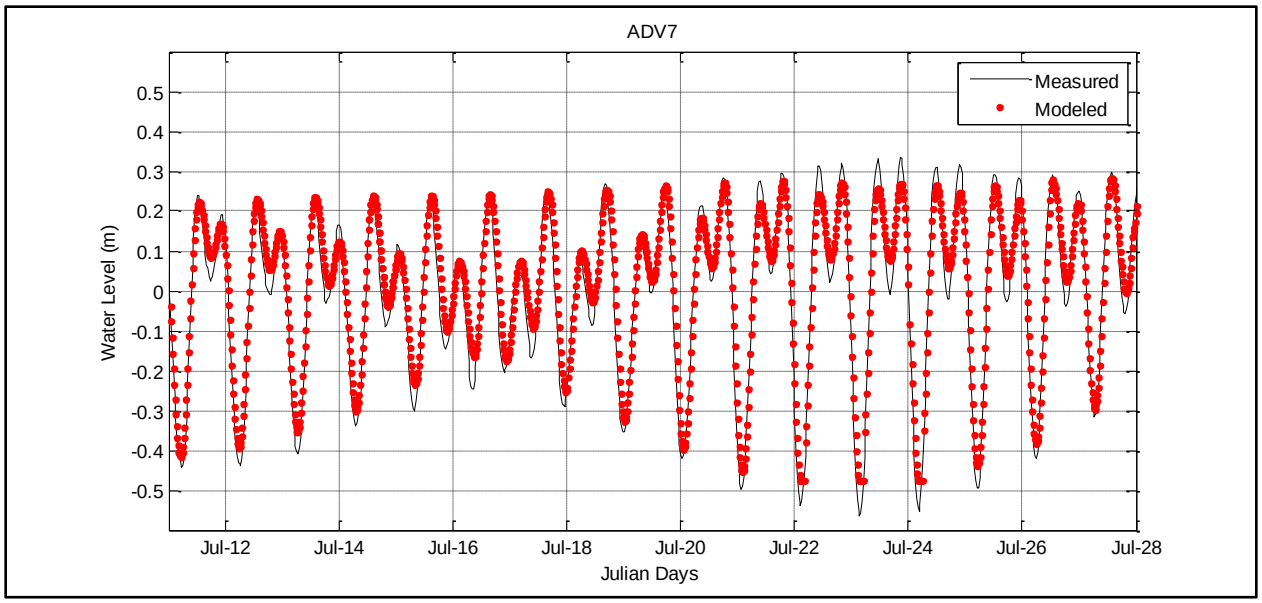

Figure 3-23. Measured and modeled water level relative to mean sea level at ADV 7.

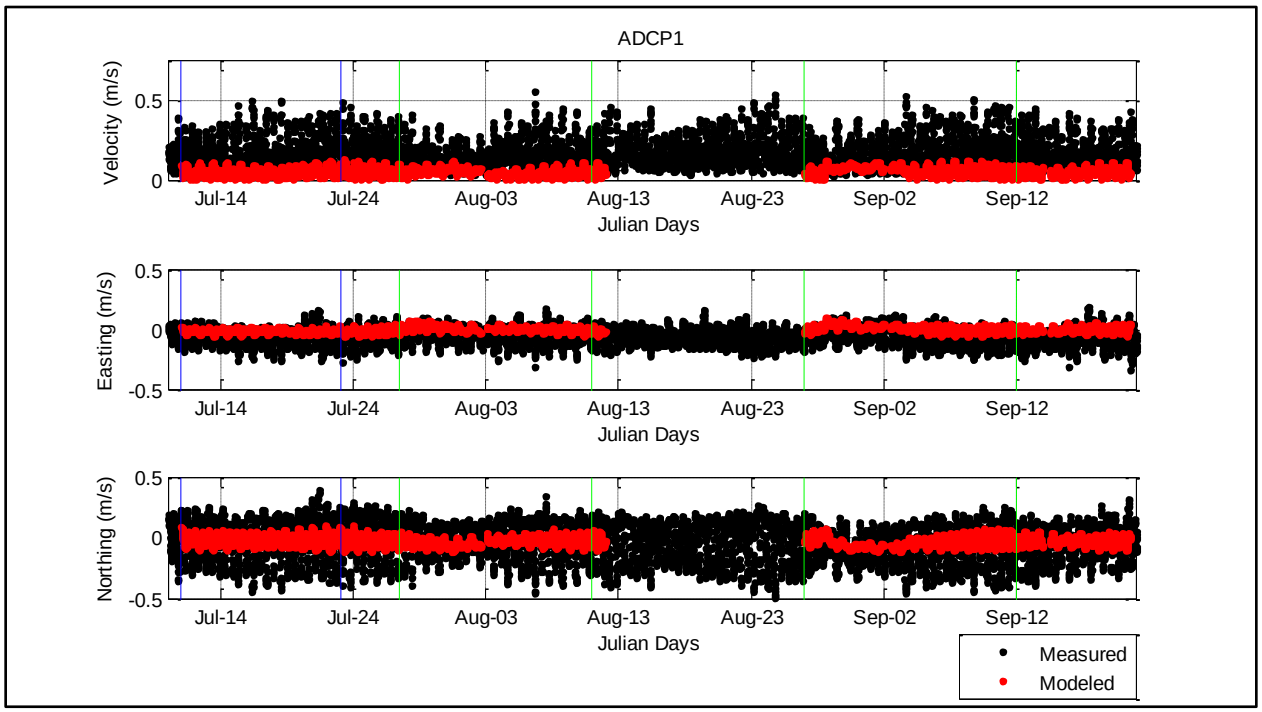

Figure 3-24. Measured and modeled currents at ADCP 1.

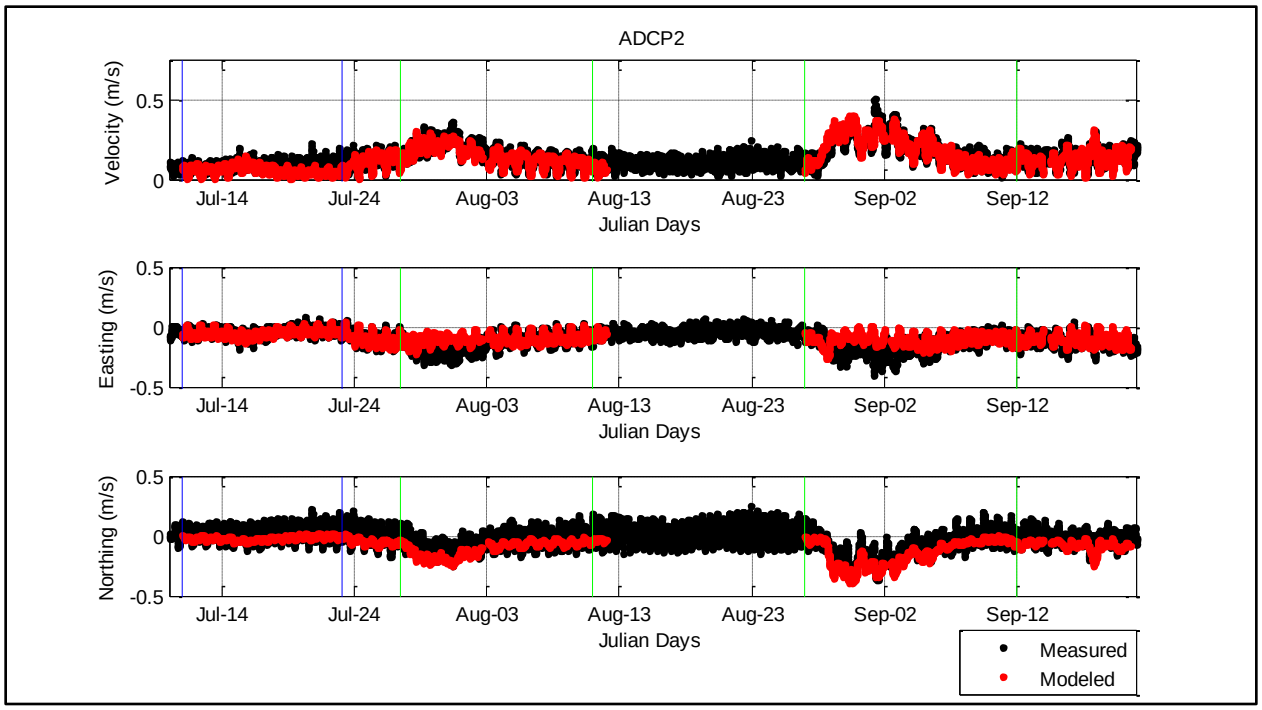

Figure 3-25. Measured and modeled currents at ADCP 2.

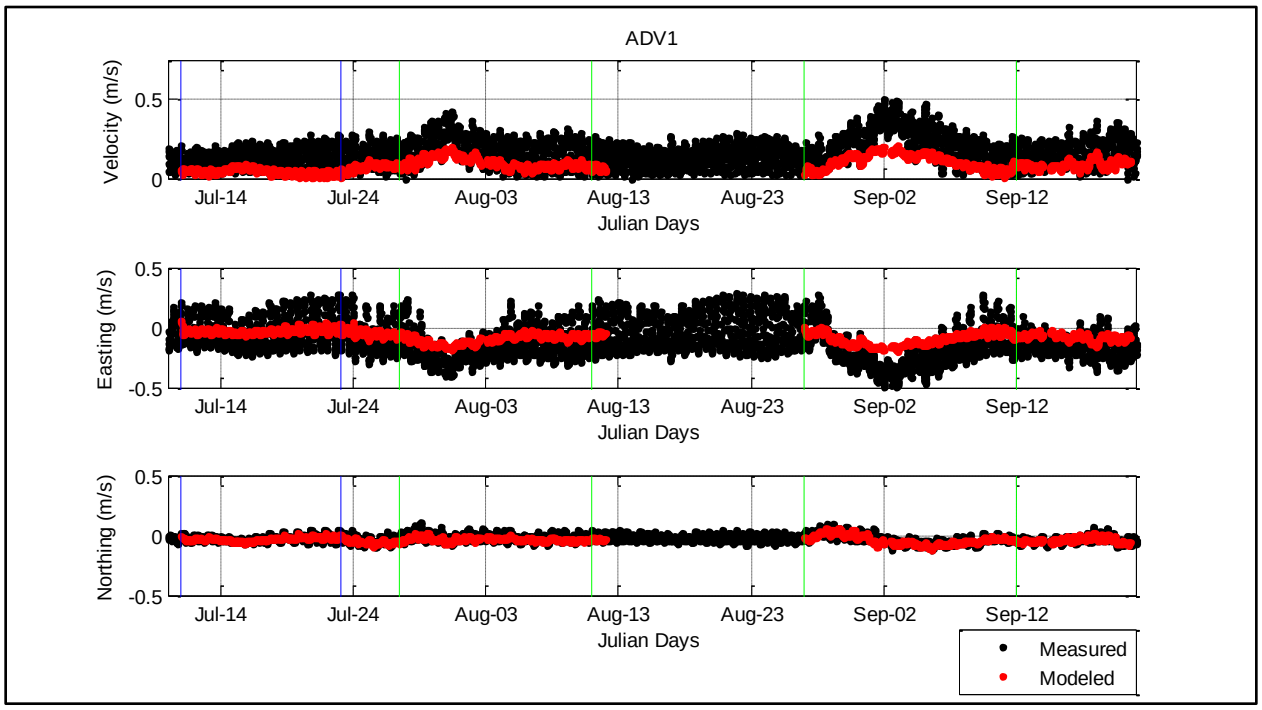

Figure 3-26. Measured and modeled currents at ADV 1.

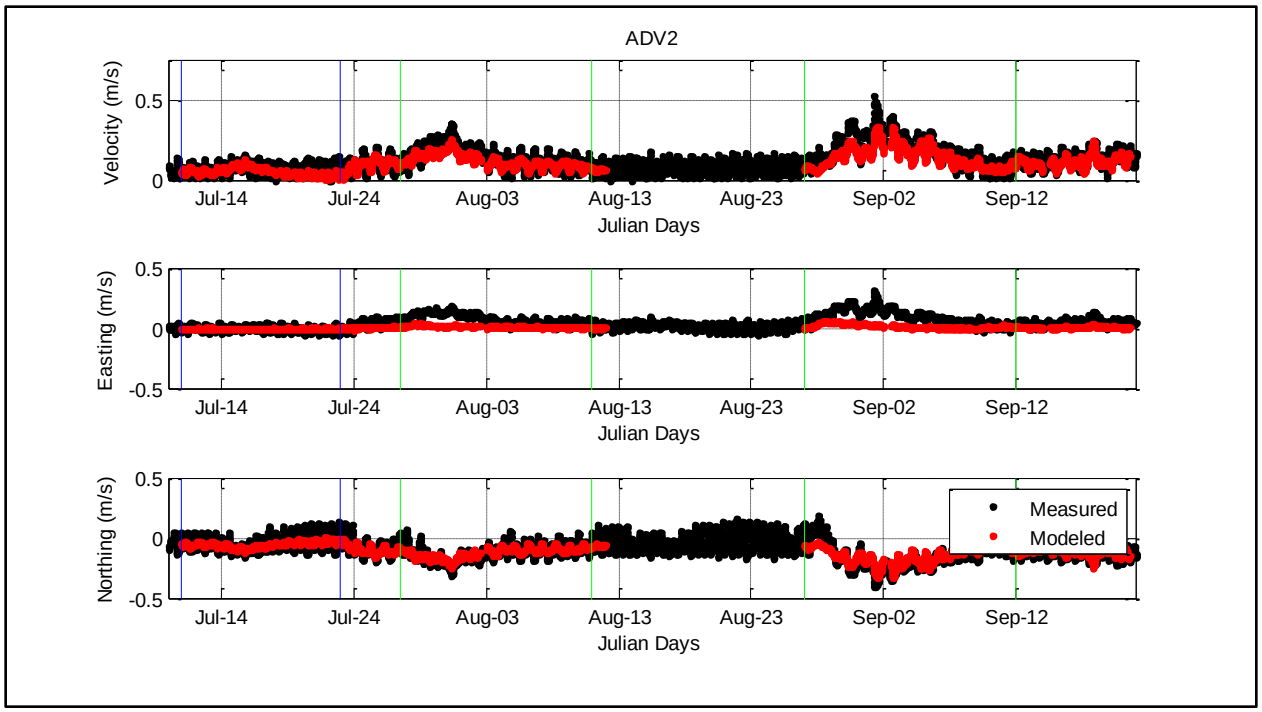

Figure 3-27. Measured and modeled currents at ADV 2.

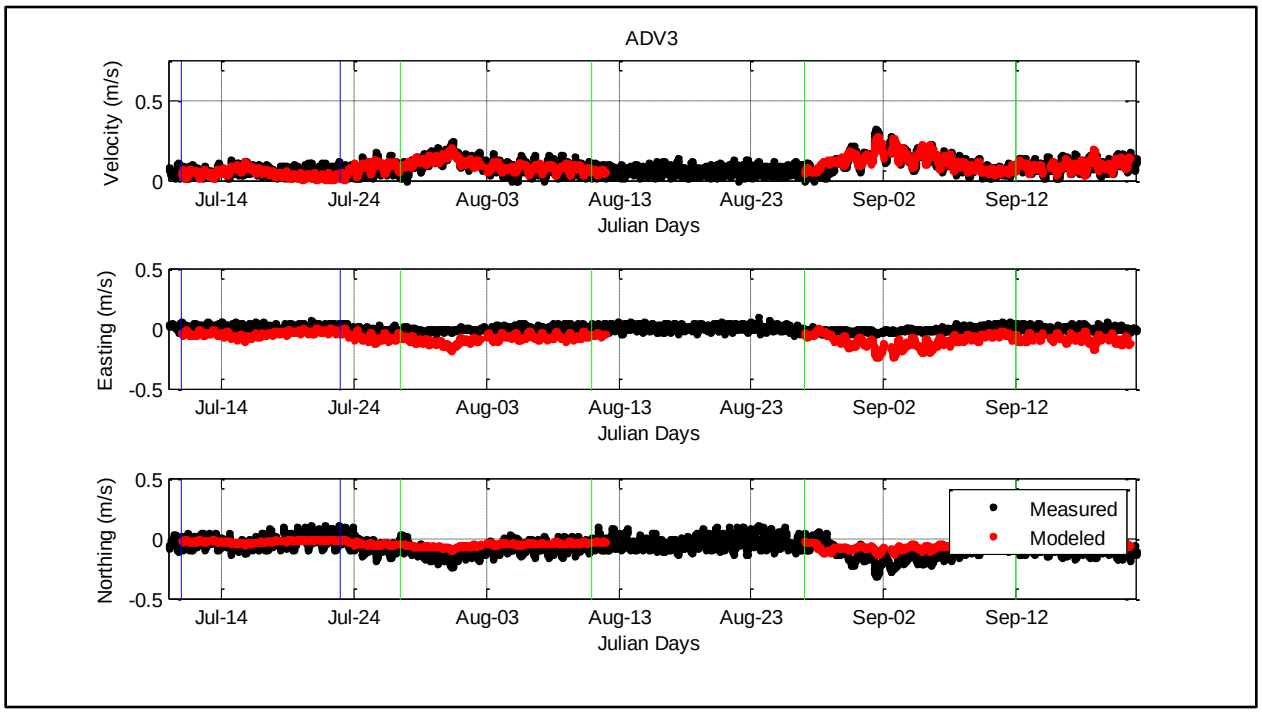

Figure 3-28. Measured and modeled currents at ADV 3.

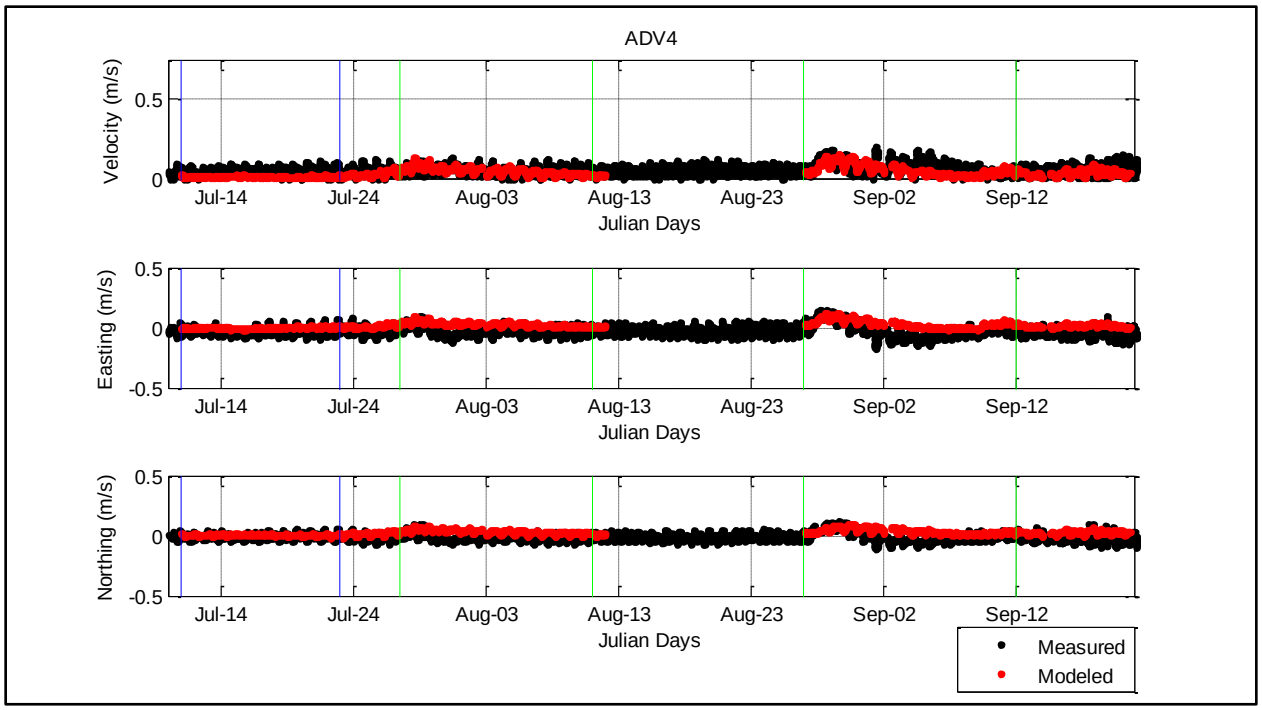

Figure 3-29. Measured and modeled currents at ADV 4.

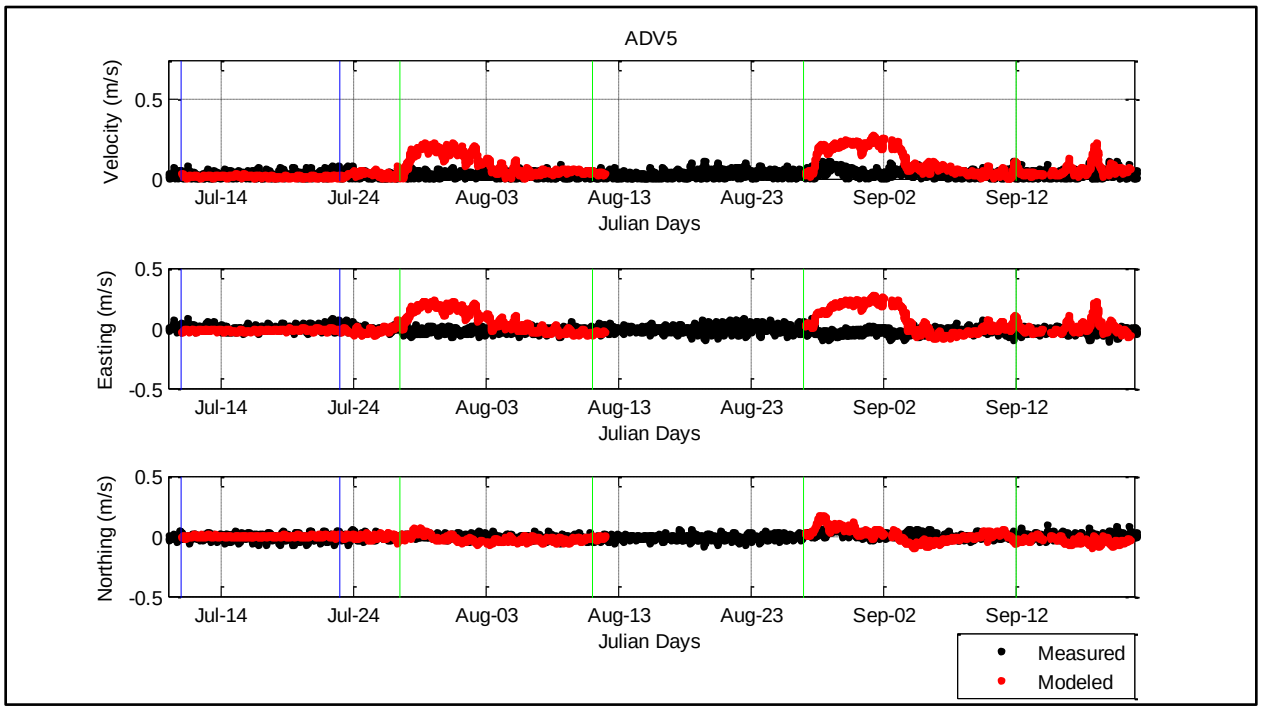

Figure 3-30. Measured and modeled currents at ADV 5.

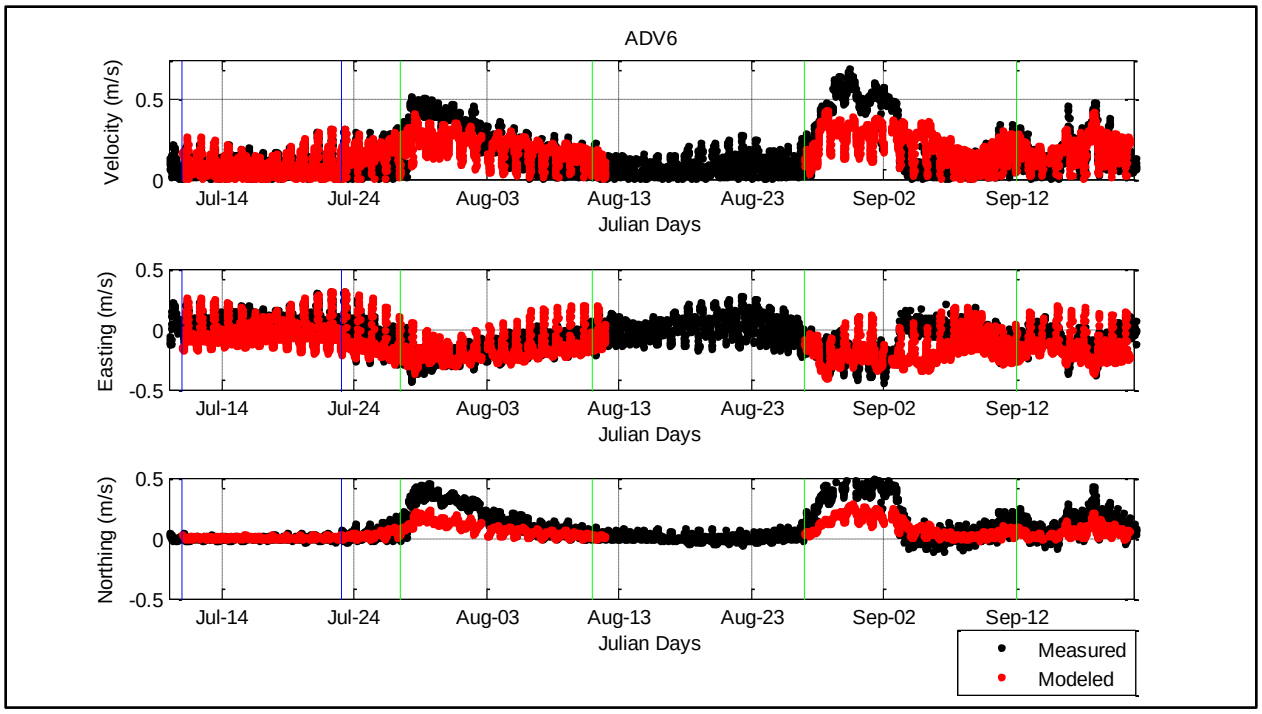

Figure 3-31. Measured and modeled currents at ADV 6.

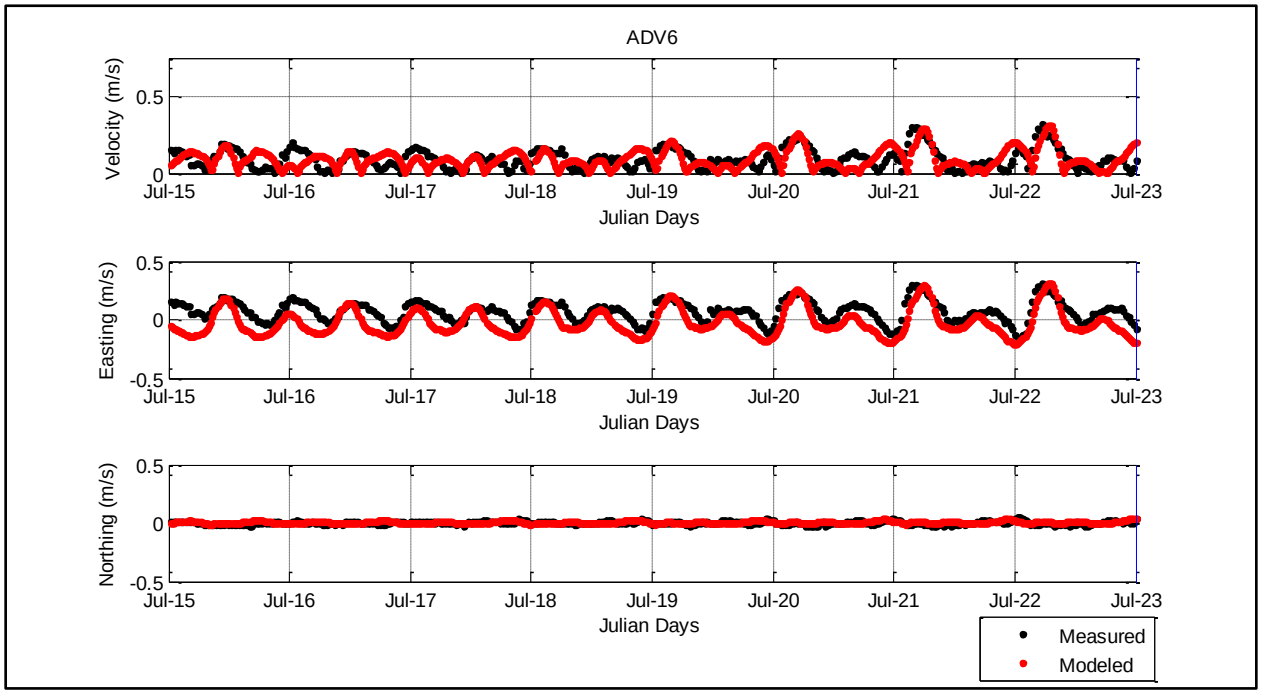

Figure 3-32. Currents at ADV 6 during light tradewind wave conditions.

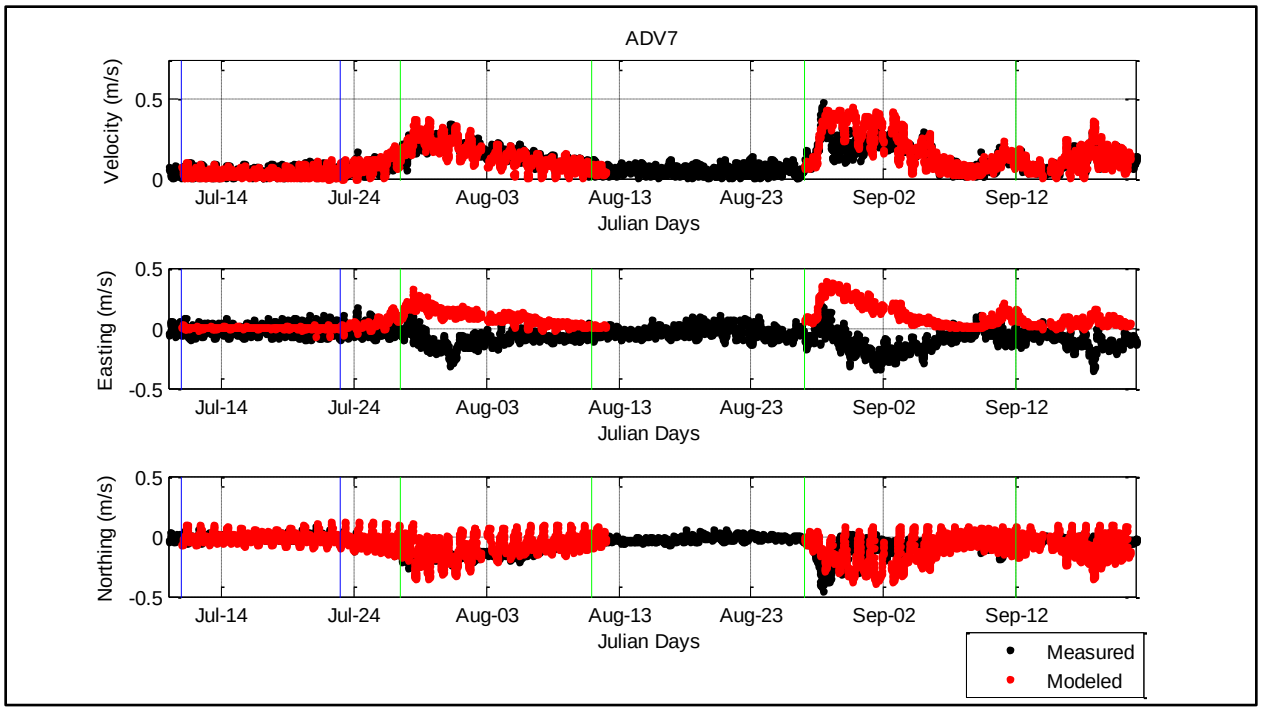

Figure 3-33. Measured and modeled currents at ADV 7.

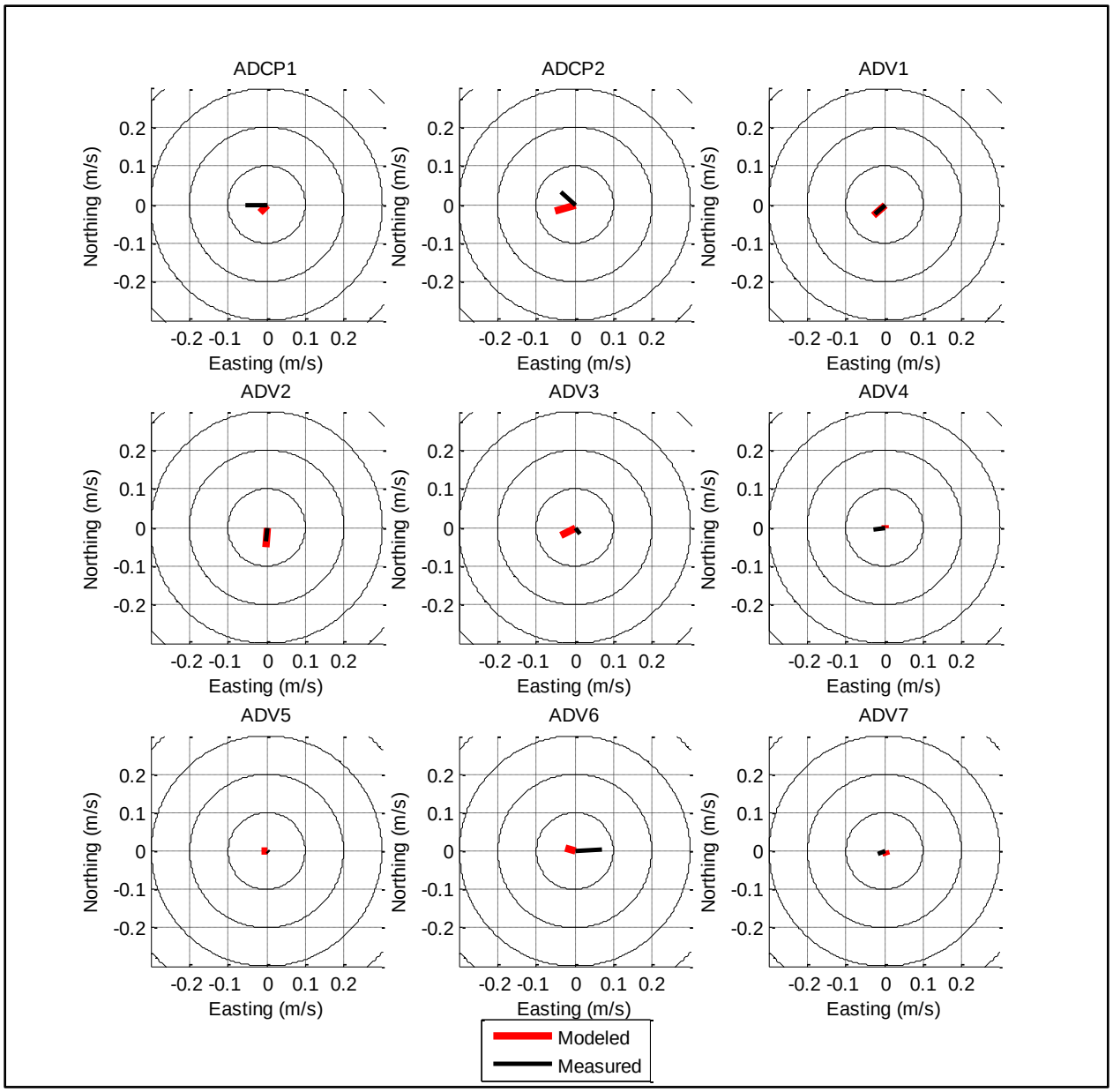

Figure 3-34. Average velocities during tradewind wave conditions.

The data is averaged over the time period from July 11 to July 23, 2017.

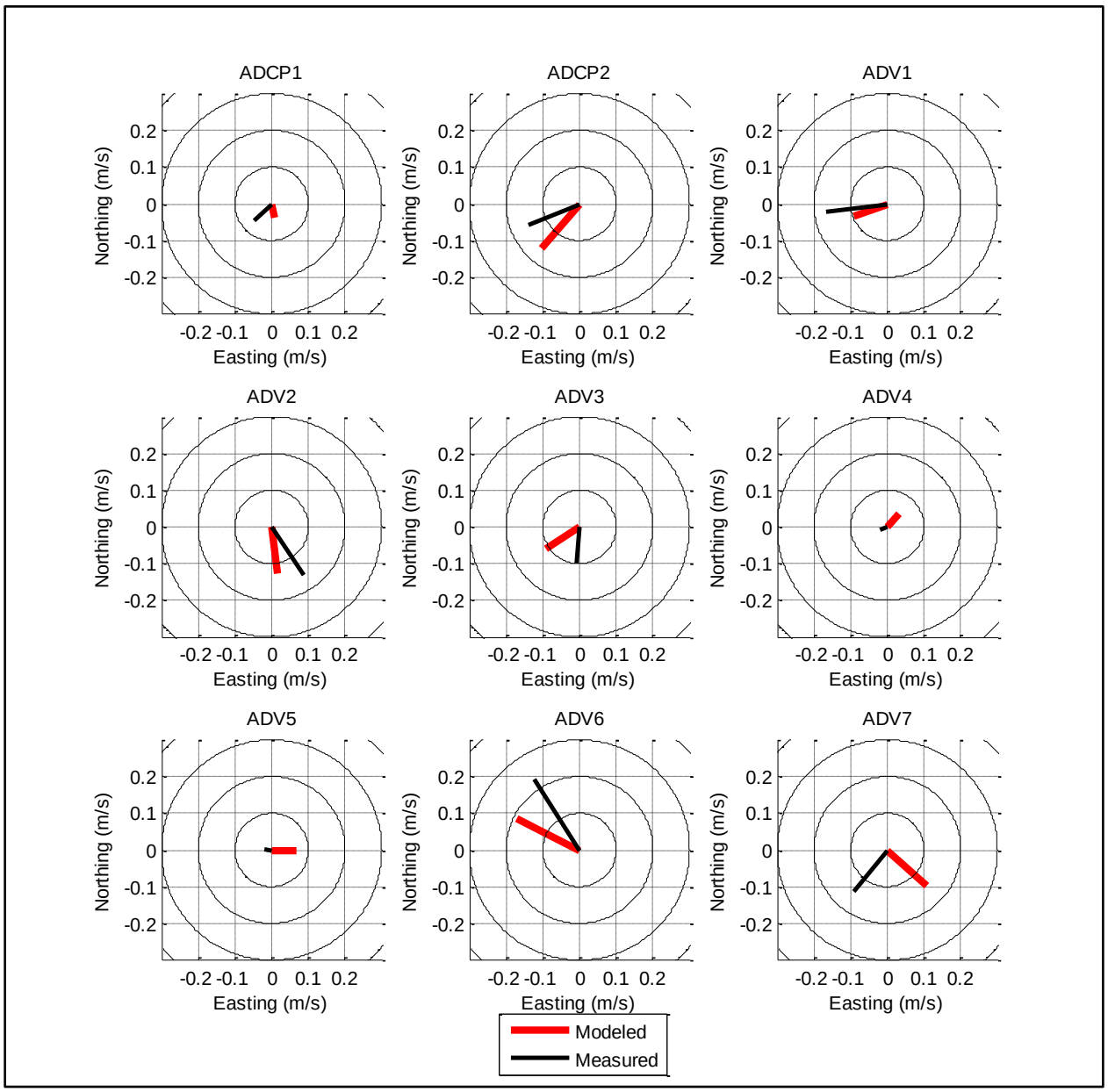

Figure 3-35. Average velocities during westerly wave conditions.

The data is the average from the time spans of July 27 to August 11, 2017, August 27 to September 12, 2017.

3.4 Case Studies

Five flow cases were selected for modeling to represent the range conditions that most typically occur in the lagoon. The current measurement program and model validation indicate that currents in the lagoon are primarily driven by waves. Five cases were therefore selected to encompass the range of wave conditions most typically impacting the lagoon: typical winter tradewind wave conditions, typical summer tradewind wave conditions, typical summer westerly wave conditions, a 1-year return period typhoon wave from the southwest, and a 1-year return period typhoon wave from the north-northwest. A summary of the deepwater wave condition for each case is listed in

Table 3-3. The cases were selected based on results of the deepwater wave climate discussed in Section 2.5. Tidal input was an intermediate tide between a spring tide and a neap tide. The case studies results are presented by figures showing the average net currents in the lagoon along with two snap shots during a rising and falling tide to show flow variation over the course of the day. To allow presentation of greater detail, separate figures are provided for each of the Garapan and Tanapag Lagoon areas. Figure 3-36 and Figure 3-37 show these two areas. In addition, figures are presented showing the transport paths followed by tracers placed at select locations within the lagoon and along the shoreline. The tracer paths allow visualization of overall circulation patterns throughout the lagoon and how pollutants or other items of interest released into the water are likely to move.

Table 3-3. Model Cases.

Case	Description	Hs (ft)	Hs (m)	Tp (s)	Dp (deg)
1	Typical Winter Tradewind Waves	5	1.52	10	55
2	Typical Summer Tradewind Waves	3.5	1.07	9	67.5
3	Typical Summer Westerly Waves	5	1.52	9	260
4	1-year Typhoon Wave from SW	14.2	4.33	12	240
5	1-year Typhoon Wave from NNW	14.2	4.33	12	345

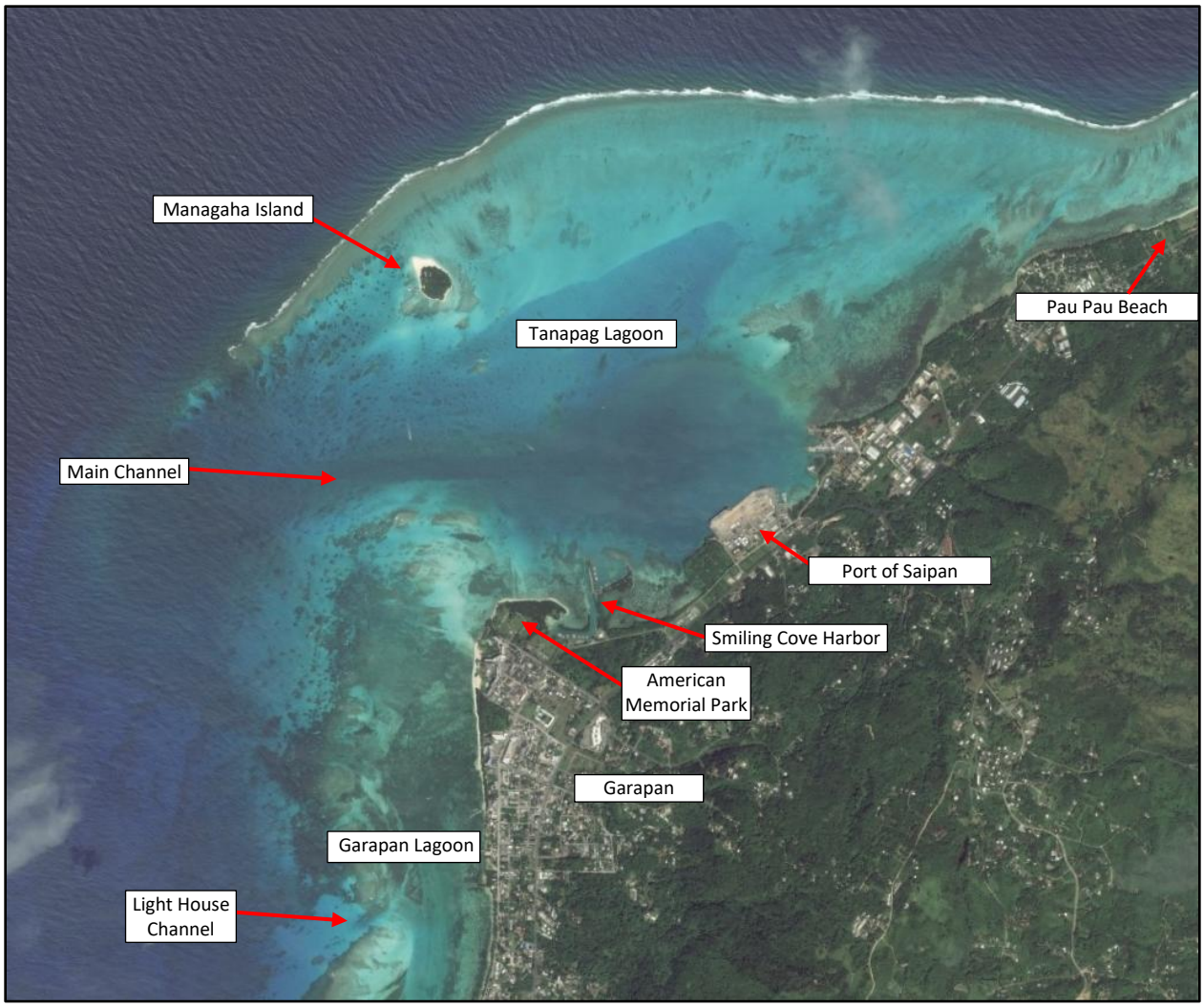

Figure 3-36. Reference map for Tanapag Lagoon.

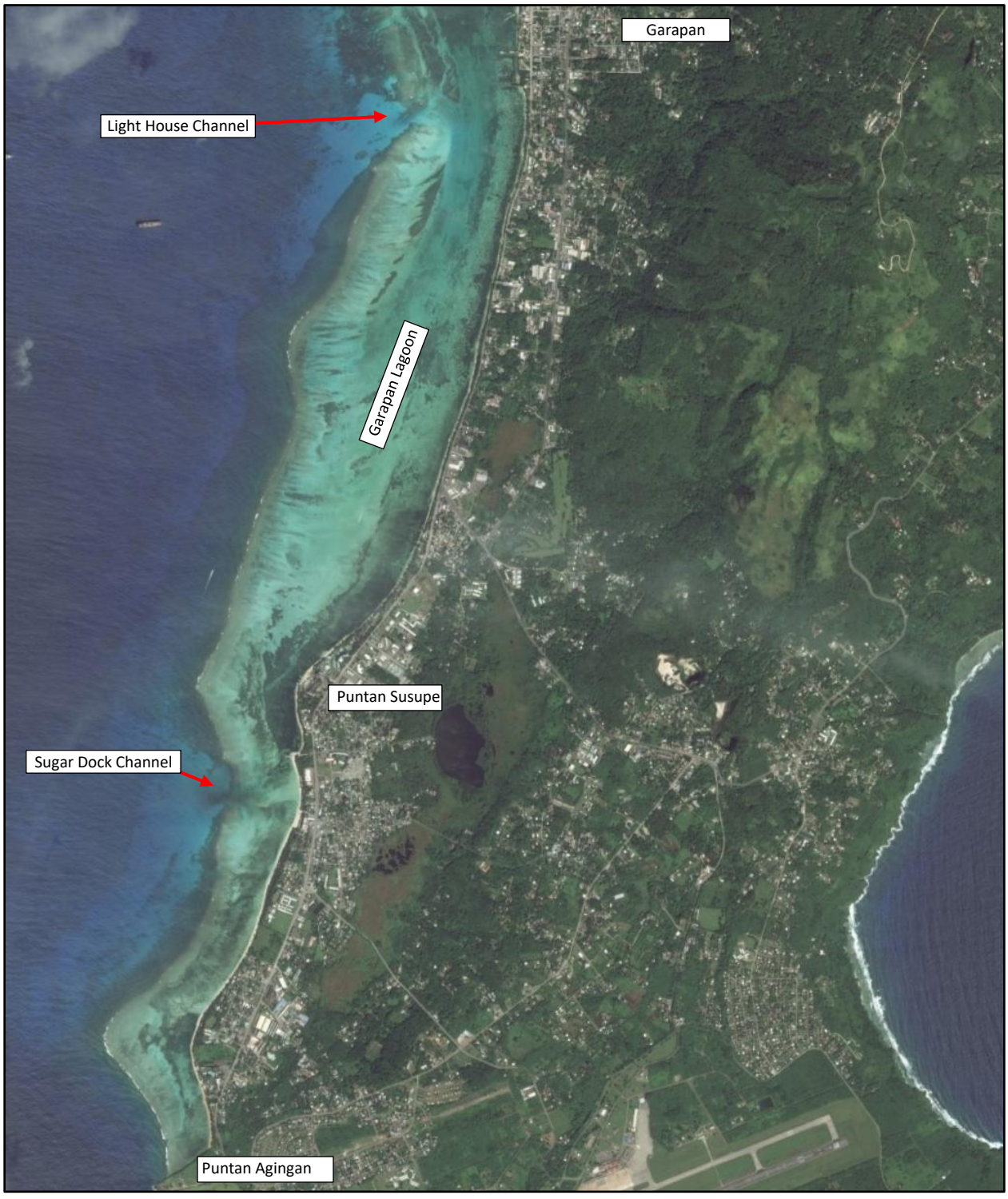

Figure 3-37. Reference map for Garapan Lagoon.

3.4.1 Case 1: Winter Season Tradewinds Waves

Typical winter season deepwater tradewind waves approach Saipan from 55 degrees with a height of 1.52 meters and period of 10 seconds. This wave pattern is presented in Figure 3-38. The waves approach from the northeast and wrap around to the west side of the island. As seen in the figure, the reef along the edge of the Tanapag lagoon that runs east to west receives more wave energy compared to the reef along the edge of the Garapan lagoon. The depth-averaged current flow patterns in Tanapag Lagoon are shown in Figure 3-39 and Garapan Lagoon in Figure 3-40. Figure 3-39 illustrates that waves drive flow over the reef, into the Tanapag lagoon, and out the main channel. Velocities over the reef are greatest at sections of reef with direct exposure to the north and have speeds of 0.3-0.5 m/s. The current speeds dissipate as depths increase to maintain conservation of mass. The main flow moves southwest into the deeper water of the Tanapag Lagoon and heads out main the channel with speeds on the order of magnitude from 0.1 to 0.2 m/s. The average flow in the inner basin in the vicinity of the port are near zero. Currents in the patch reef area offshore of American Memorial Park and to the west of Garapan are weak and generally drain out adjacent channels with no distinct pattern. Figure 3-40 illustrates that with the exception of the Sugar Dock and Lighthouse Channels, average flow in Garapan Lagoon is extremely weak. Averaged over a tide cycle, the average current for most of the Garapan Lagoon is less than 0.01 m/s. The model calculates a weak average flow out of the Light House channel with a maximum speed of approximately 0.1 m/s and a net flow out of the Sugar Dock channel of approximately 0.04 m/s.

The flow patterns in the middle of a rising tide are shown in Figure 3-41 and Figure 3-42. In Tanapag Lagoon (Figure 3-41) the same flow pattern is evident as for the time averaged flow but with weaker currents flowing from the deeper sections of the lagoon and out of the main channel. The peak flow out of the main channel is approximately 0.17 m/s. To the southwest of American Memorial Park, the current floods in strongly through Light House channel with a velocity of approximately 0.25 m/s and flows from north to south into the Garapan Lagoon with velocities of up to 0.15 m/s. As seen in Figure 3-42, flow velocities weaken toward Puntan Susupe. The current also floods in the Sugar Dock channel with a speed of approximately 0.15 m/s. The incoming flow splits and continues up towards Puntan Susupe and south towards Puntan Agingan dropping in speed as it travels away from the Sugar Dock channel.

The flow patterns in the middle of a falling tide are shown in Figure 3-43 and Figure 3-44. In Tanapag Lagoon (Figure 3-43) the same pattern is evident as with the time averaged flow but with stronger currents flowing from the deeper sections of the lagoon and out of the main channel. The peak speeds flowing out of the main channel are approximately 0.25 m/s. Currents generally reverse in Garapan Lagoon (Figure 3-44), flowing to the north from Puntan Susupe to Garapan at speeds up to approximately 0.15 m/s. A portion of the ebbing tide flows out of the Light House Channel with a maximum speed of approximately 0.36 m/s and portion continues north and out of the main channel. To the south of Puntan Susupe, flow travels along the coast and converges to flow out of the Sugar Dock channel with a maximum speed of approximately 0.21 m/s.

Figure 3-45 presents the model calculated transport paths followed over 6 and 23.5 hours of tracers released into the water at select locations within the lagoon and along the shoreline during typical winter tradewind wave conditions. The tracers are released at 00:00 on a day – August 16, 2017 - with an intermediate tide between a neap and spring tide. Black circles on the figure mark the starting locations. The tide for August 16, 2017 is plotted in Figure 3-46. A tracer's instantaneous position is marked with a black dot and its path marked with a red line. Figure 3-45 shows the following:

- Tracers released in the Tanapag lagoon are transported out of the main channel by wave driven flow
- Tracers released near the port travel a minimal distance in weak currents
- Tracers released in the Garapan Lagoon north of Puntan Susupe flow up and down the coast with minimal net transport.
- Tracers released in the Garapan Lagoon south of Puntan Susupe flow towards and out of the Sugar Dock channel.

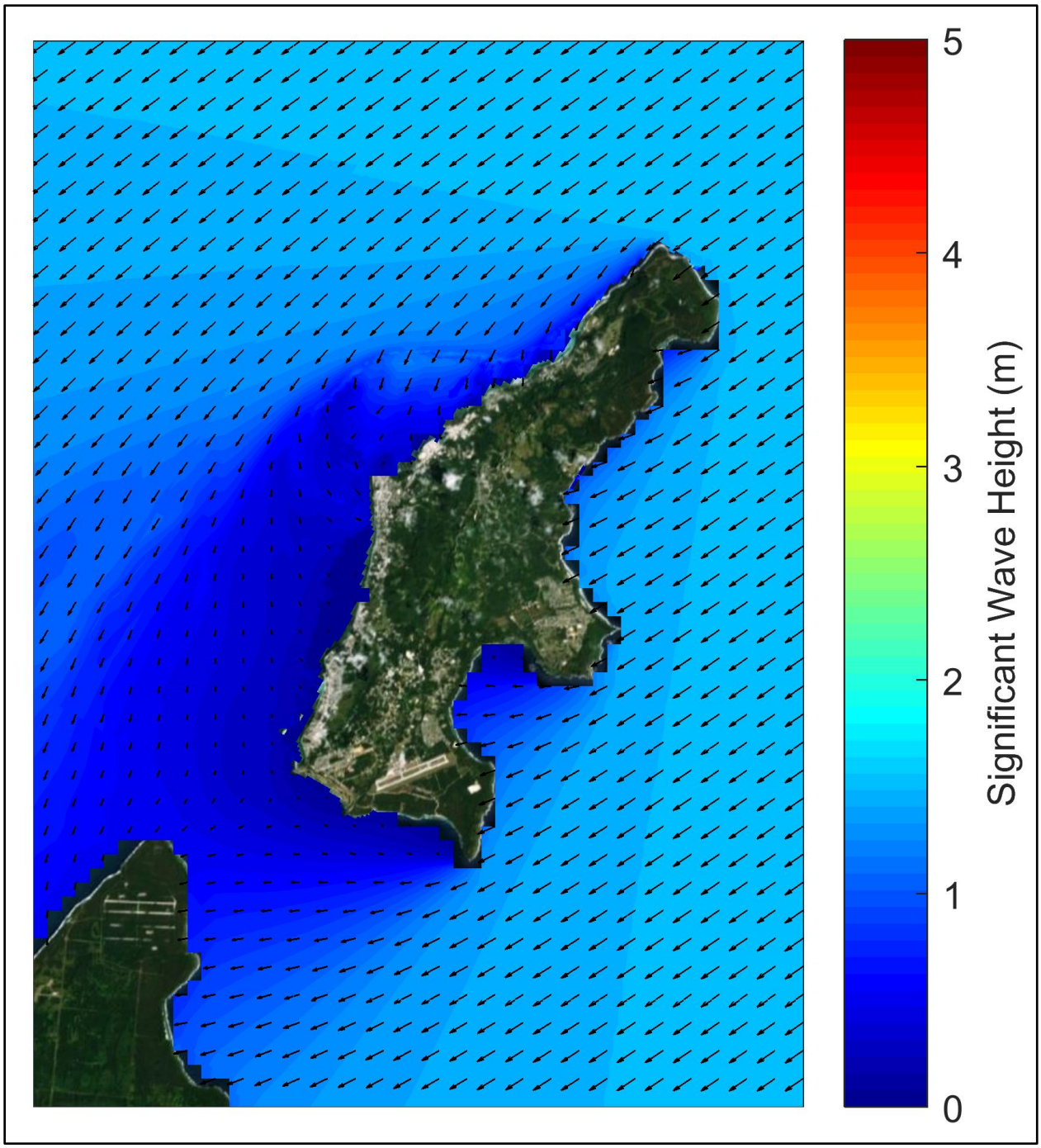

Figure 3-38. Typical winter tradewind wave patterns.

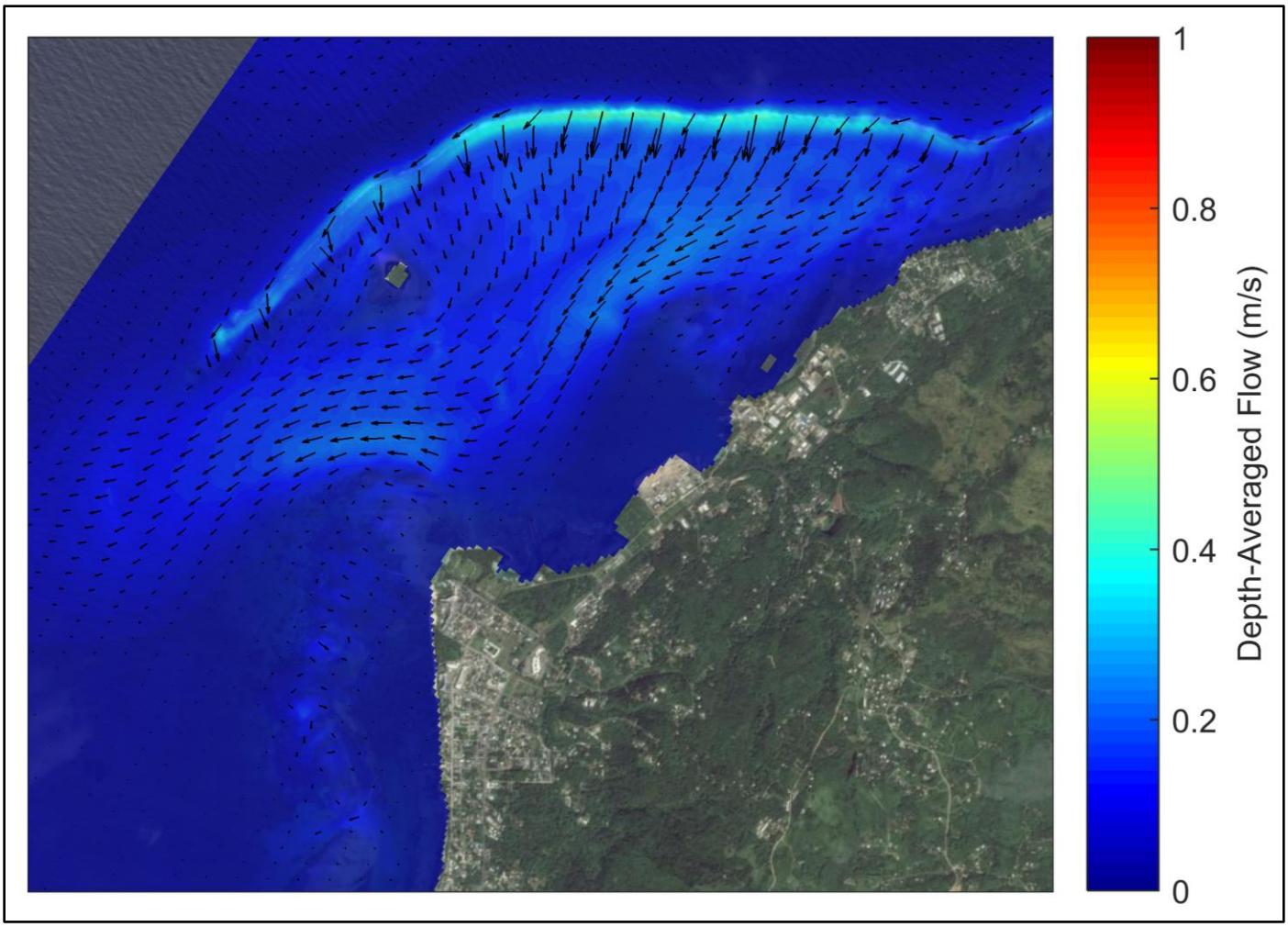

Figure 3-39. Average flow generated by winter tradewind waves in Tanapag Lagoon.

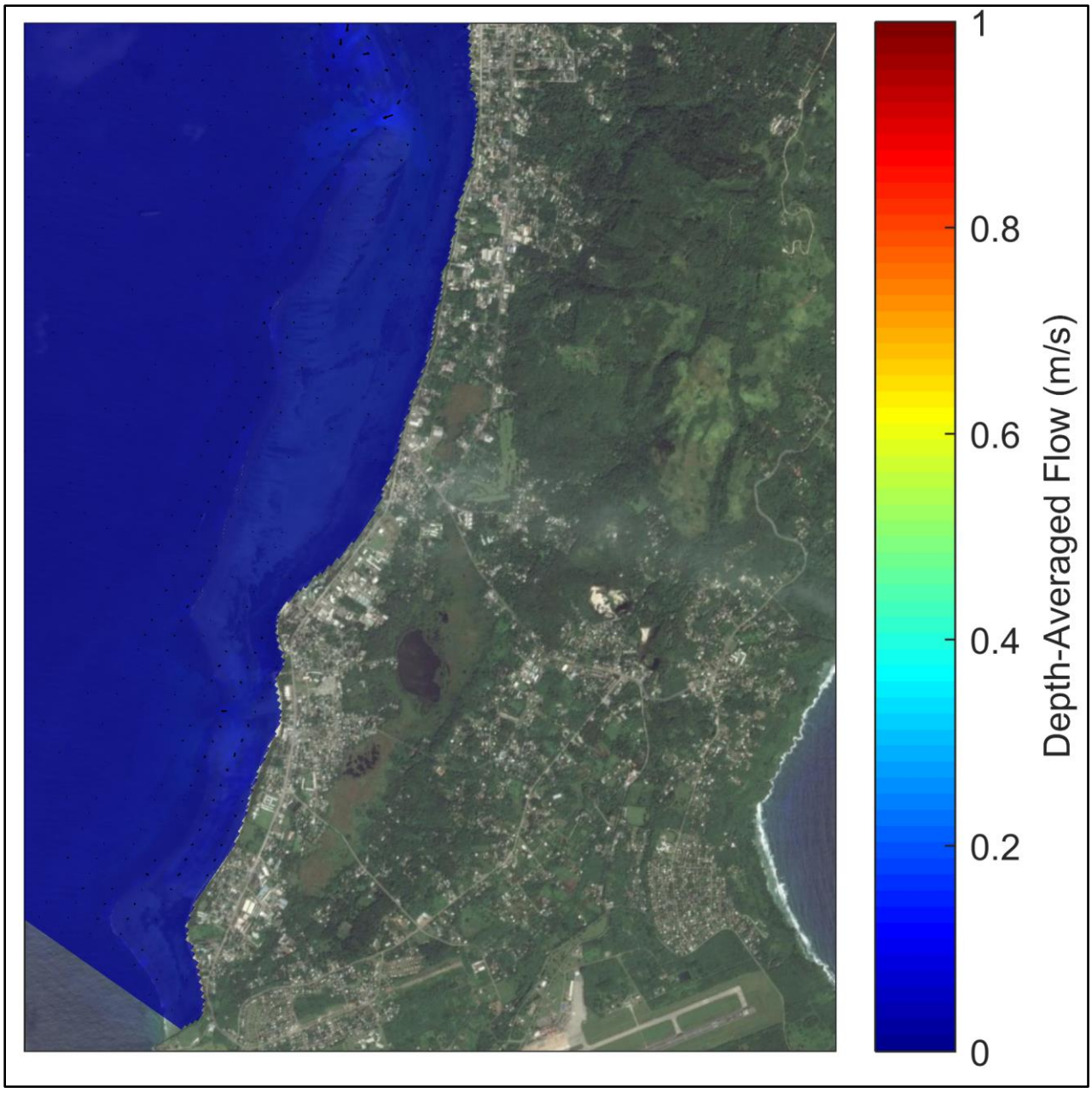

Figure 3-40. Average flow generated by winter tradewind waves in Garapan Lagoon.

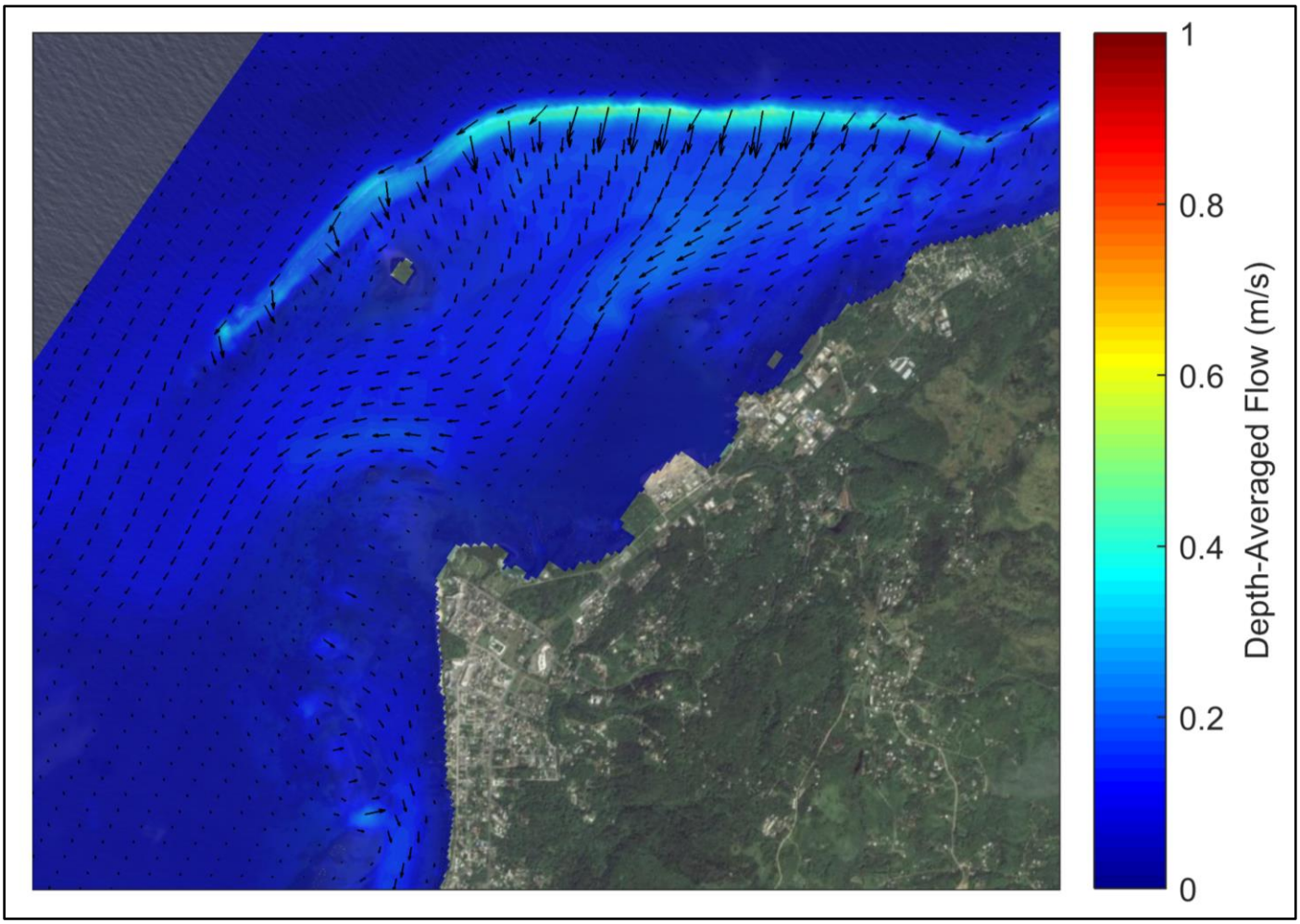

Figure 3-41. Currents during a rising tide - winter tradewind waves conditions, Tanapag Lagoon.

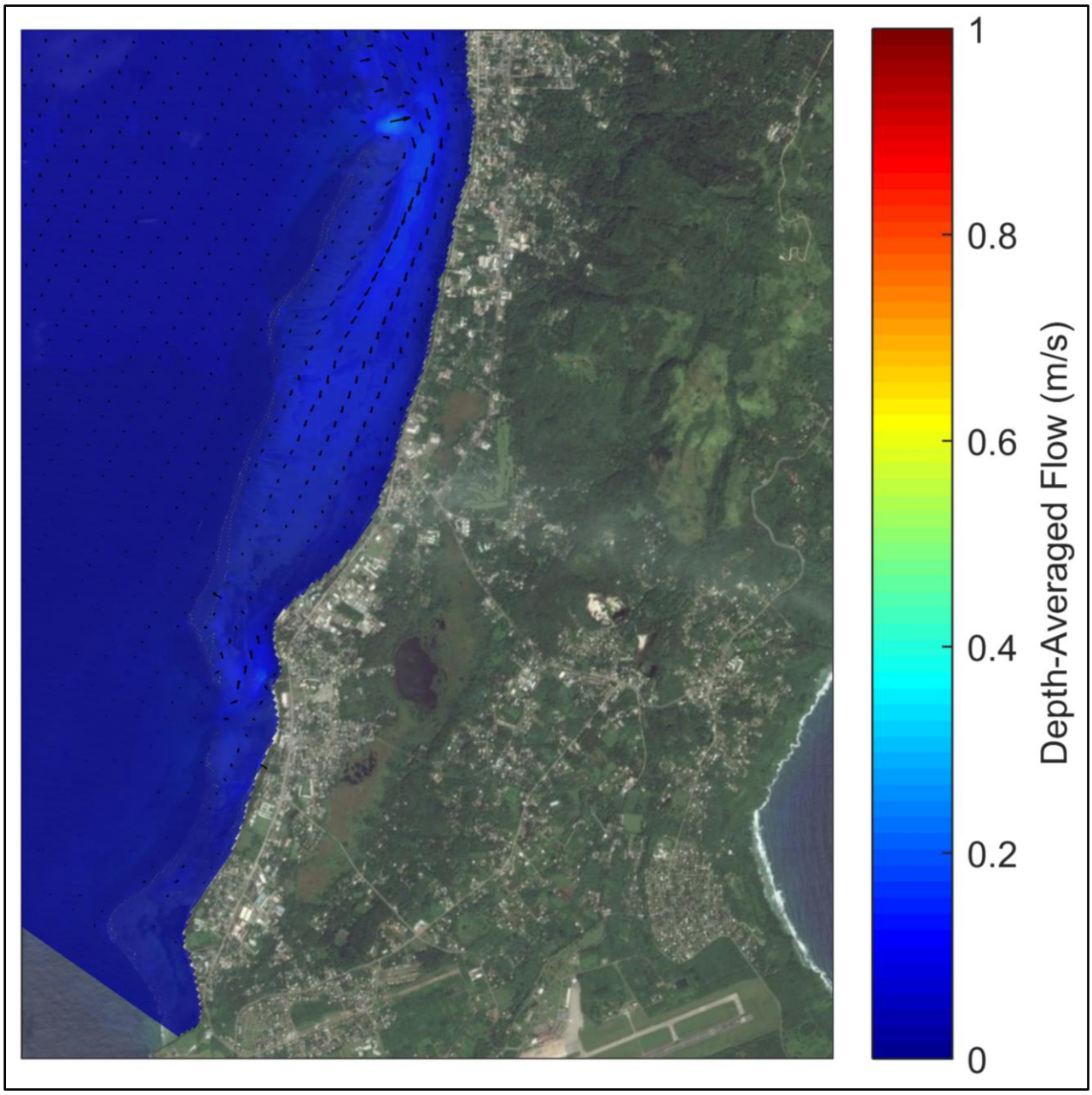

Figure 3-42. Currents during a rising tide - winter tradewind waves conditions, Garapan Lagoon.

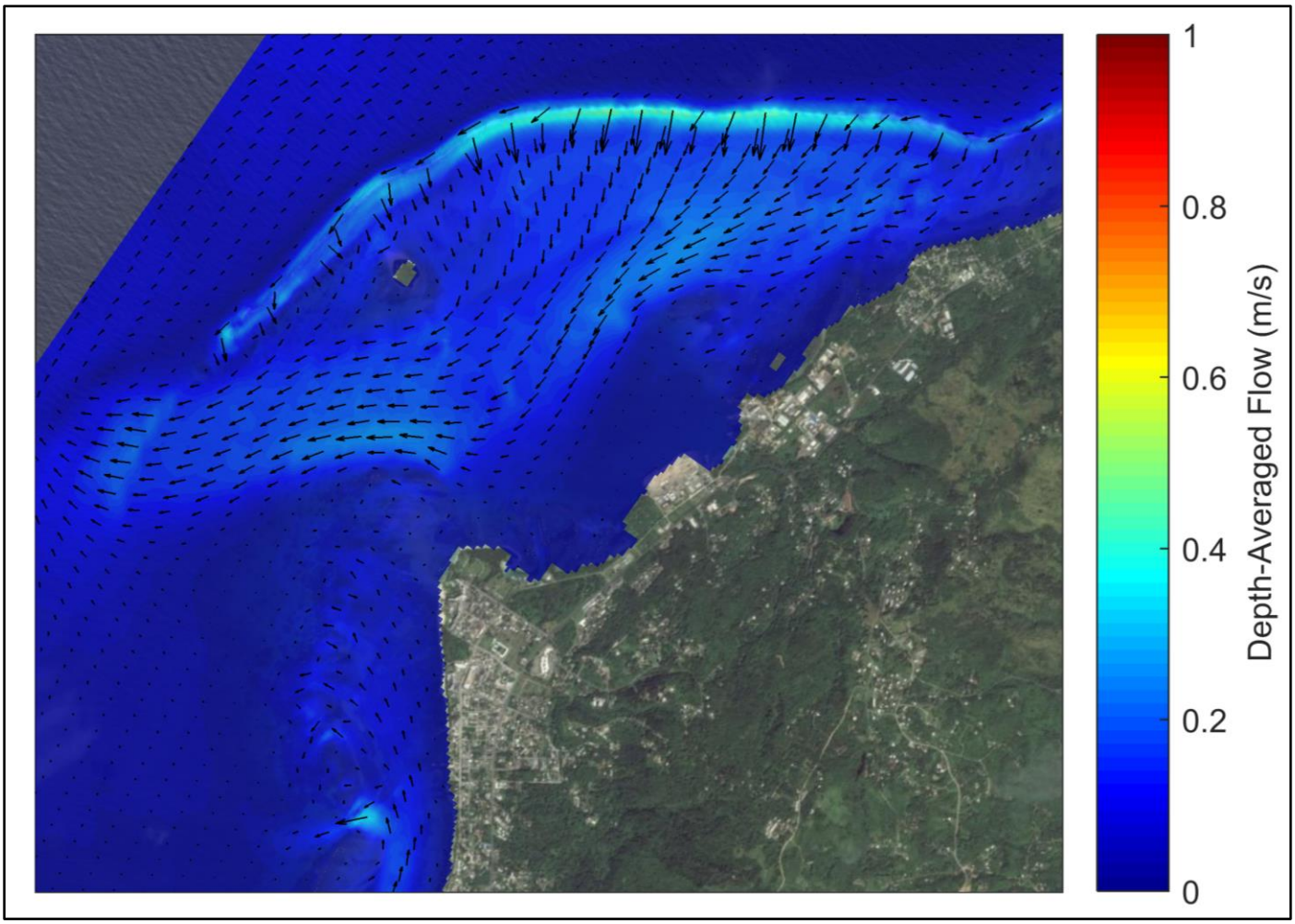

Figure 3-43. Currents during a falling tide - winter tradewind waves conditions, Tanapag Lagoon.

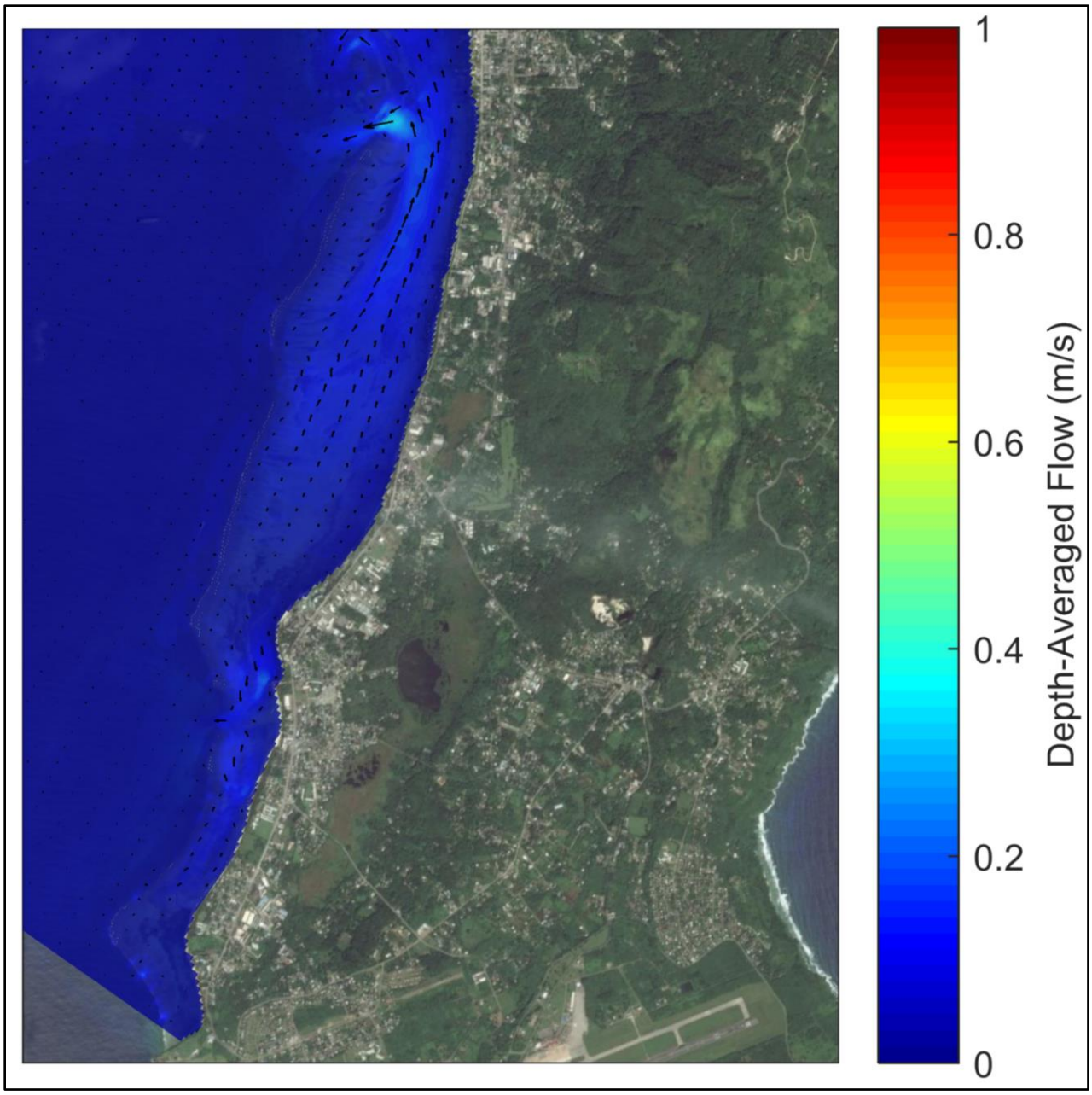

Figure 3-44 Currents during a falling tide - winter tradewind waves conditions, Garapan Lagoon.

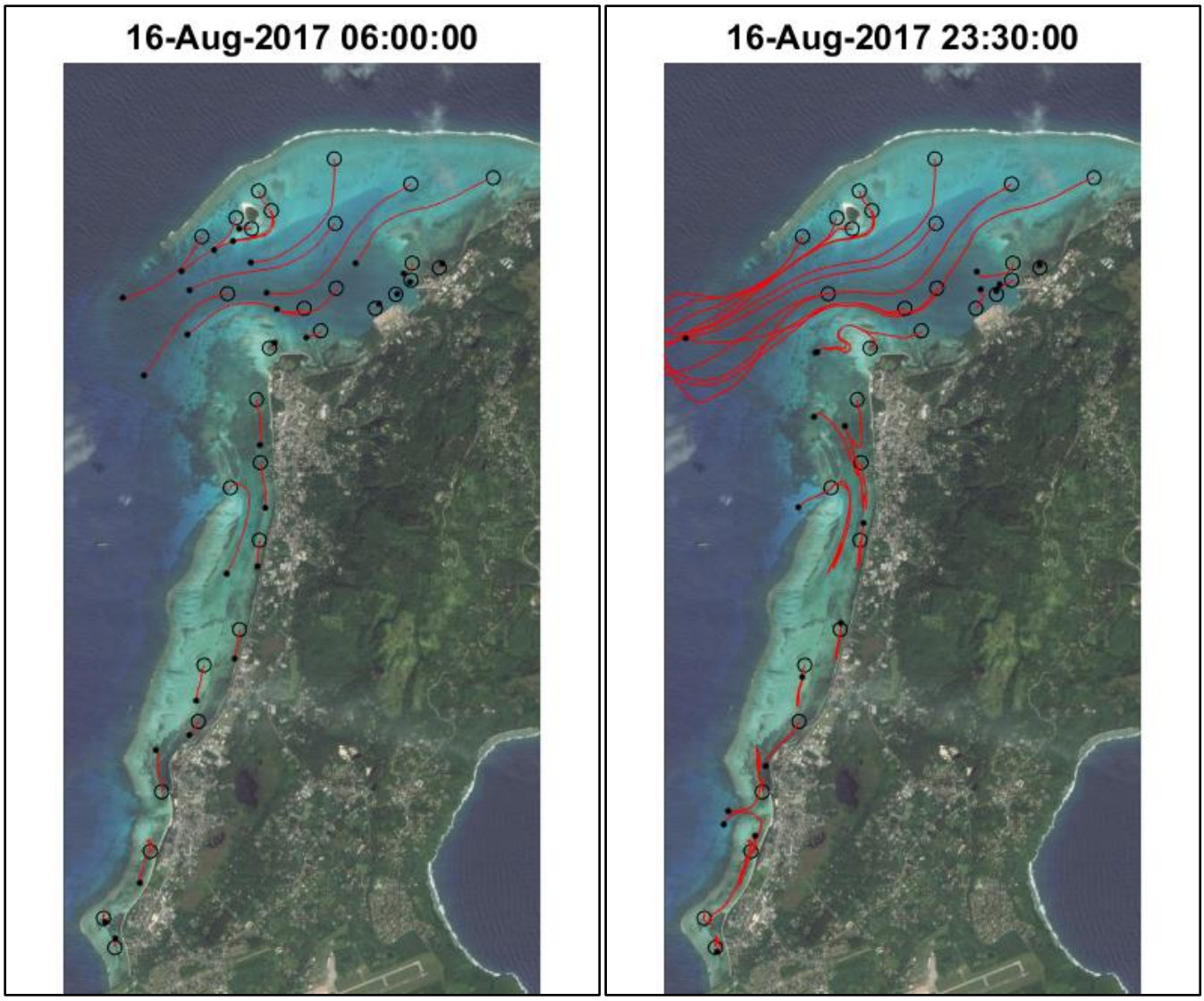

Figure 3-45. Tracer paths during typical winter tradewinds wave conditions.

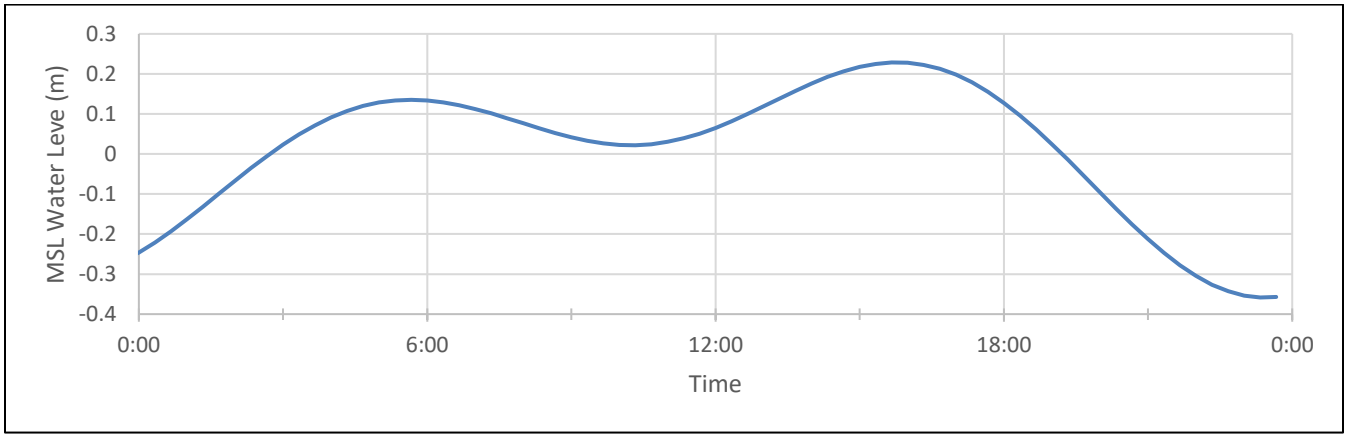

Figure 3-46. Tide level during tracer interval.

3.4.2 Case 2: Summer/Typhoon Season Tradewind Waves

Typical summer tradewind waves approach Saipan from 67 degrees, with deepwater wave heights of 1.07 meters and periods of 9 seconds. This wave pattern is illustrated in Figure 3-47. The waves approach from the east-northeast and wrap around to the west side of the island. As seen in the figure, the reef along the edge of the Tanapag Lagoon that runs east to west receives more wave energy compared to the reef along the edge of the Garapan Lagoon. The depth-averaged current flow patterns in Tanapag Lagoon are shown in Figure 3-48 and Garapan Lagoon in Figure 3-49, and are very similar to Case 1, with slightly weaker speeds. Figure 3-48 illustrates that waves drive flow over the reef, into the Tanapag Lagoon, and out the main channel. Velocities over the reef are greatest at sections of reef with direct exposure to the north and have speeds of approximately 0.15-0.25 m/s. The current speeds dissipate as depths increase. The main flow moves southwest into the deeper water of the Tanapag Lagoon and heads out the main channel with speeds of 0.05 to 0.11 m/s. The average flow in the inner basin in the vicinity of the port are near zero. Currents in the patch reef area offshore of American Memorial Park and to the west of Garapan are weak and generally drain out adjacent channels with no distinct pattern. Figure 3-49 illustrates average flow in Garapan Lagoon is extremely weak. Averaged over a tide cycle, the current for most of Garapan Lagoon is less than 0.01 m/s. The model calculates a weak average flow out of the Light House channel with a maximum speed of approximately 0.03 m/s and a net flow out of the Sugar Dock channel of approximately 0.02 m/s.

The flow patterns in the middle of a rising tide are shown in Figure 3-50 and Figure 3-51, and are similar to Case 1. In Tanapag Lagoon (Figure 3-50) the same flow pattern is evident as for the time averaged flow but with weaker currents flowing from the deeper sections of the lagoon and out of the main channel. The peak flow out of the main channel is approximately 0.06 m/s. To the southwest of American Memorial Park, the current floods in strongly through Light House channel with a velocity of approximately 0.26 m/s and flows from north to south into the Garapan Lagoon with velocities building up to 0.16 m/s. As seen in Figure 3-51, flow velocities weaken toward Puntan Susupe. The current also floods in the Sugar Dock channel with a speed of approximately 0.12 m/s. The incoming flow splits and continues north towards Puntan Susupe and south towards Puntan Agingan dropping in speed as it travels away from the Sugar Dock channel.

The flow patterns in the middle of a falling tide are shown in Figure 3-52 and Figure 3-53. In Tanapag Lagoon (Figure 3-52), the same pattern is evident as with the time averaged flow but with stronger currents flowing from the deeper sections of the lagoon and out of the main channel. The peak speeds flowing out of the main channel are 0.16 m/s. Currents generally reverse in Garapan Lagoon (Figure 3-53), flowing to the north from Puntan Susupe to Garapan at speeds up to approximately 0.16 m/s. A portion of the ebbing tide flows out of the Light House Channel with a maximum speed of approximately 0.30 m/s and portion continues north and out of the main channel. To the south of Puntan Susupe, flow travels along the coast and converges to flow out of the Sugar Dock channel with a maximum speed of approximately 0.14 m/s.

Figure 3-54 presents the model calculated transport paths followed over 6 and 23.5 hours of tracers released into the water at select locations within the lagoon and along the shoreline

during typical summer tradewind wave conditions. The tracers are released at 00:00 on a day – August 16, 2017 - with an intermediate tide between a neap and spring tide. Black circles on the figure mark the starting locations. The tide for August 16, 2017 is plotted in Figure 3-55. A tracer's instantaneous position is marked with a black dot and its path marked with a red line. Figure 3-54 shows similar transport paths as Case 1:

- Tracers released in the Tanapag Lagoon are transported out of the main channel by wave driven flow
- Tracers released near the port travel a minimal distance in weak currents
- Tracers released in the Garapan Lagoon north of Puntan Susupe flow up and down the coast with minimal net transport.
- Tracers released in the Garapan Lagoon south of Puntan Susupe flow up and down the coast with a net transport towards and out of the Sugar Dock channel.

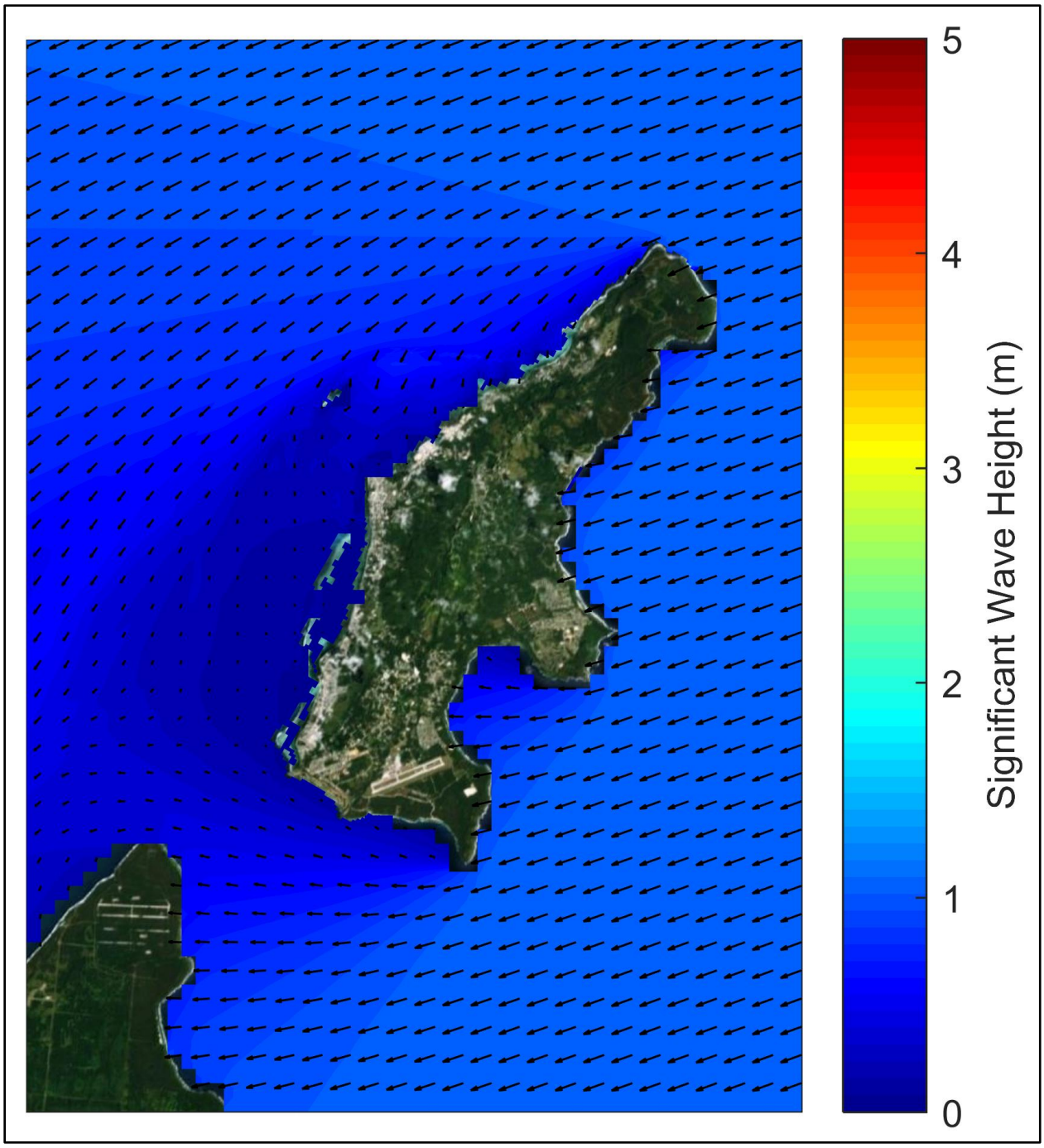

Figure 3-47 Typical summer tradewind wave patterns.

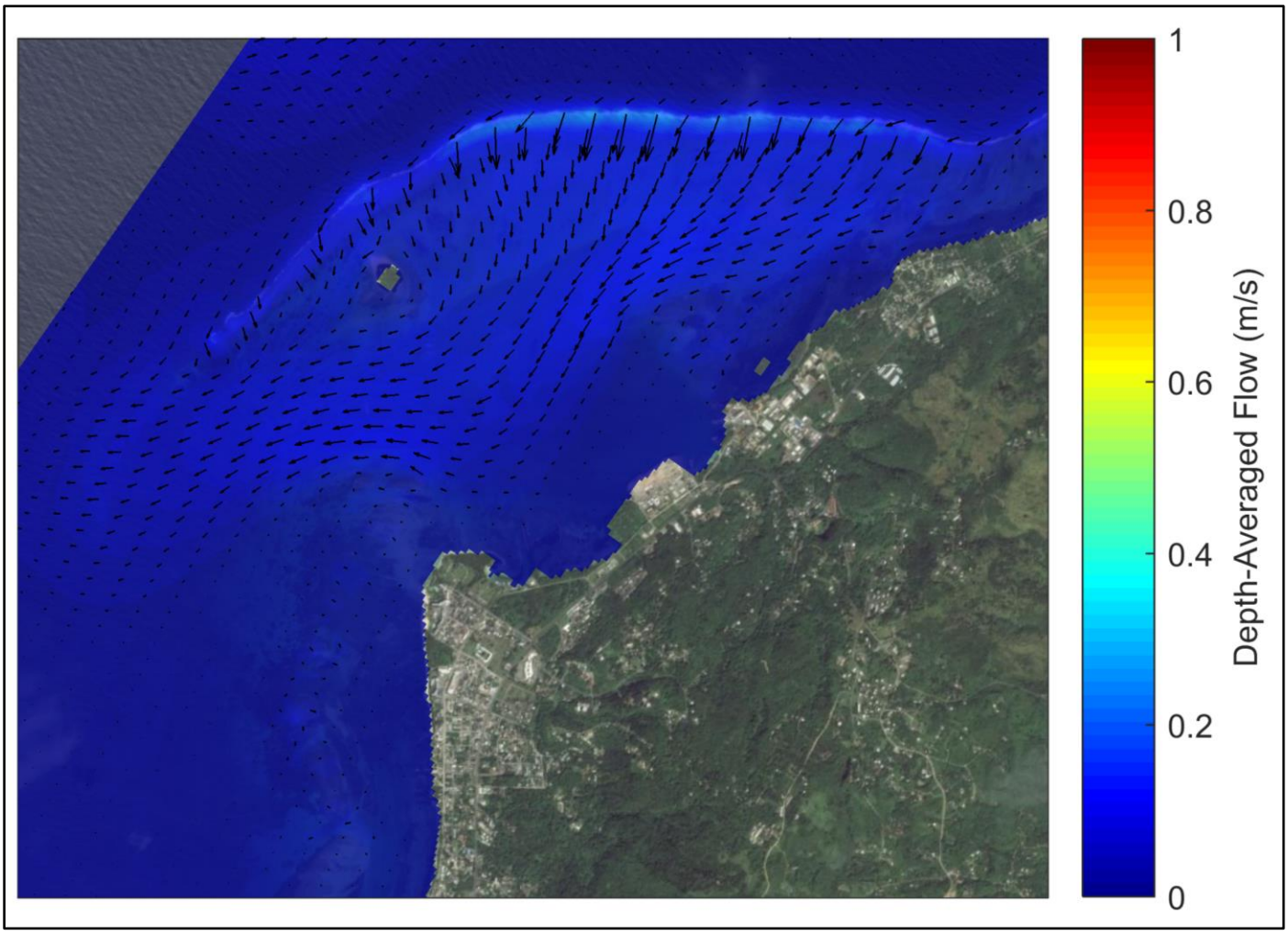

Figure 3-48. Average flows generated by summer tradewind waves in Tanapag Lagoon.

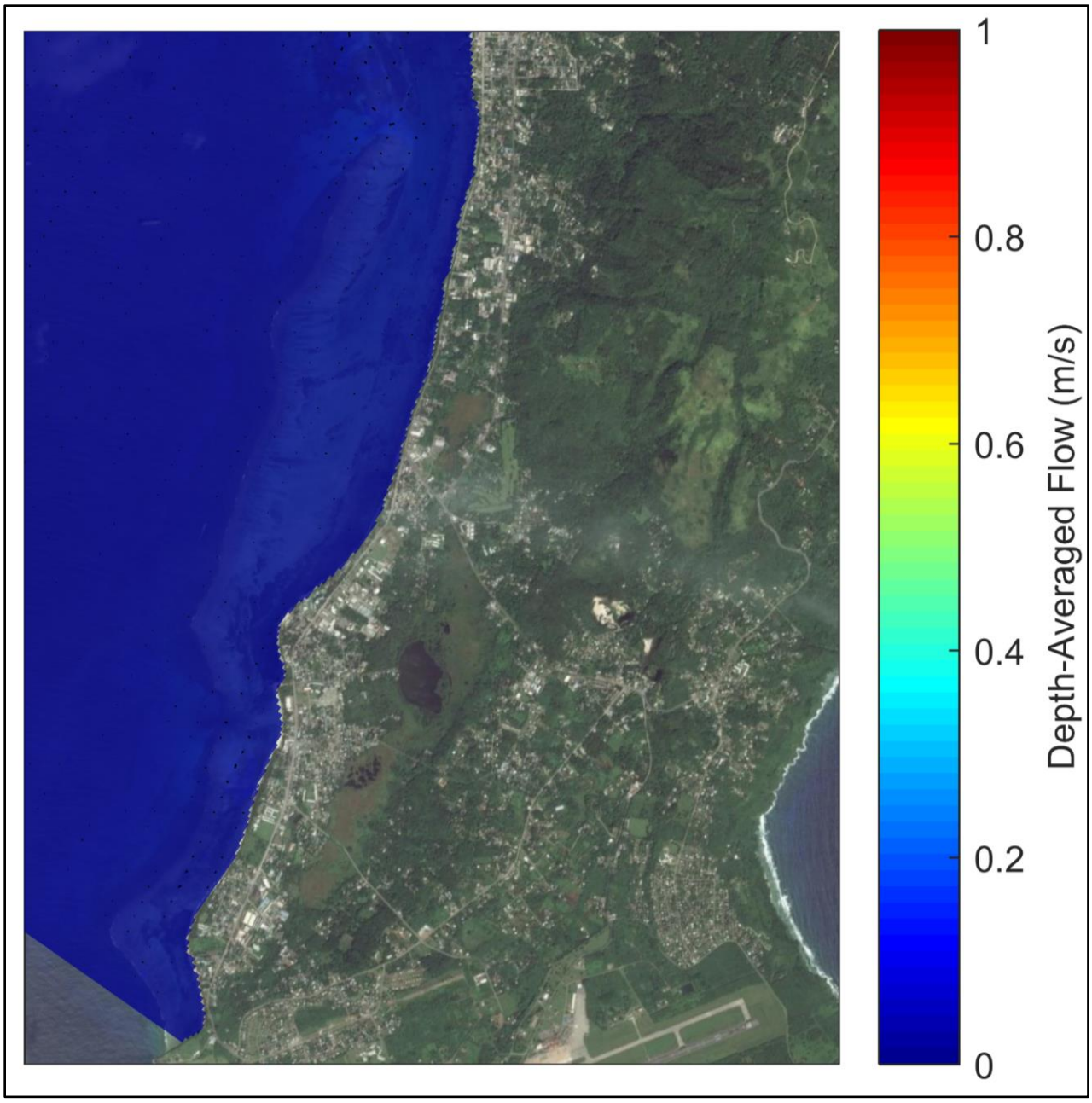

Figure 3-49. Average flows generated by summer tradewind waves in Garapan Lagoon.

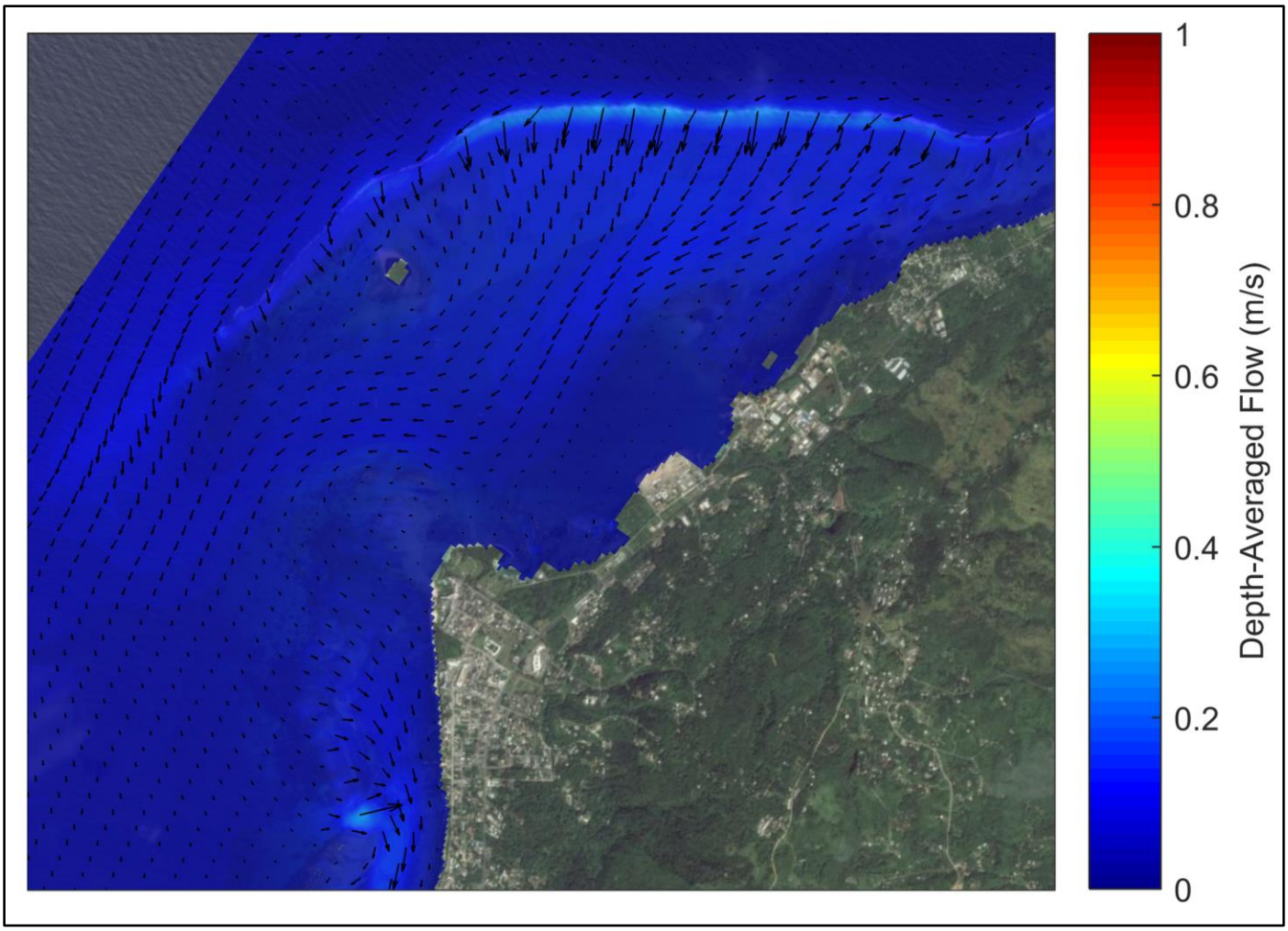

Figure 3-50. Currents during a rising tide - summer tradewind wave conditions, Tanapag Lagoon.

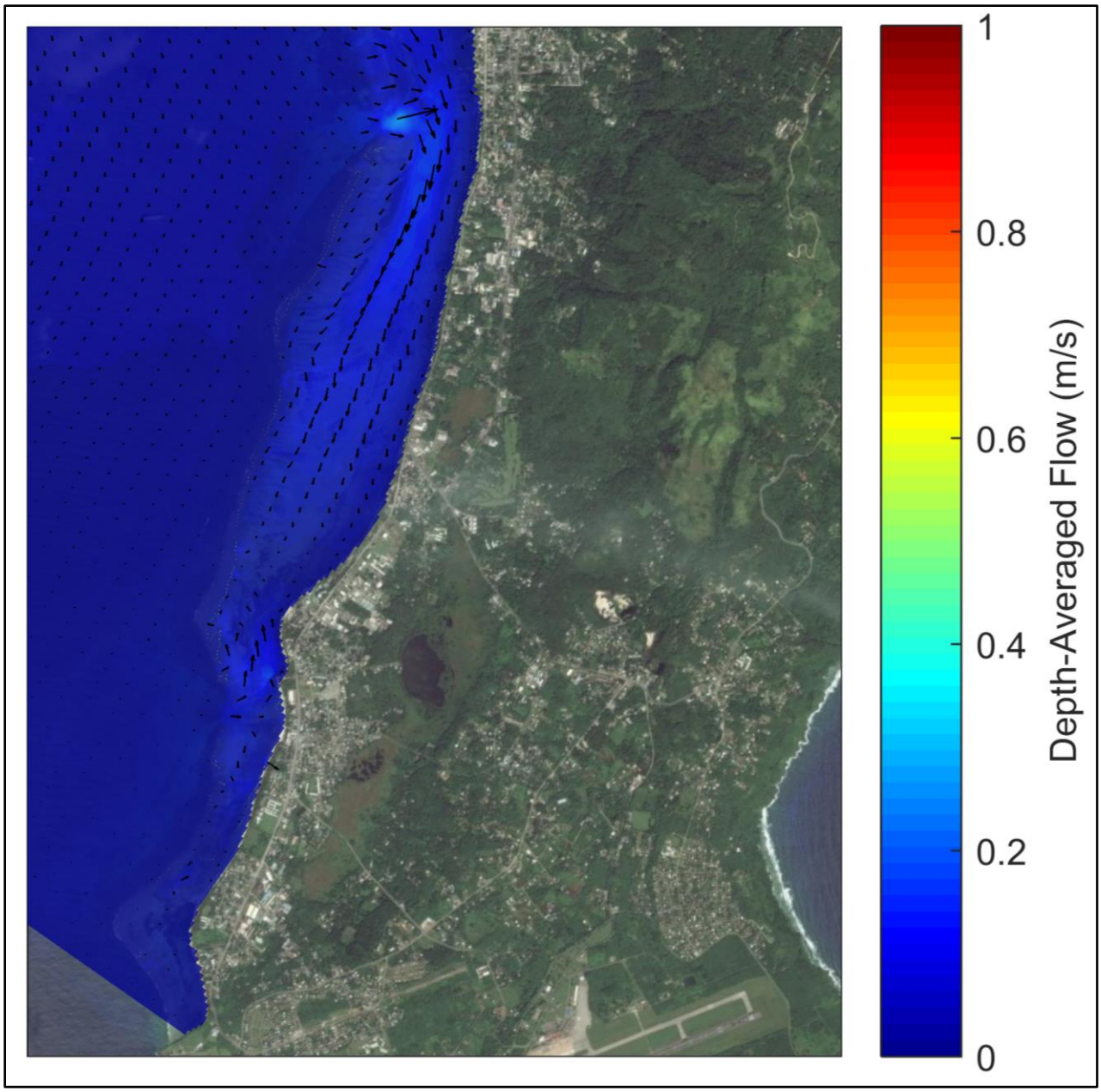

Figure 3-51. Currents during a rising tide - summer tradewind wave conditions, Garapan Lagoon.

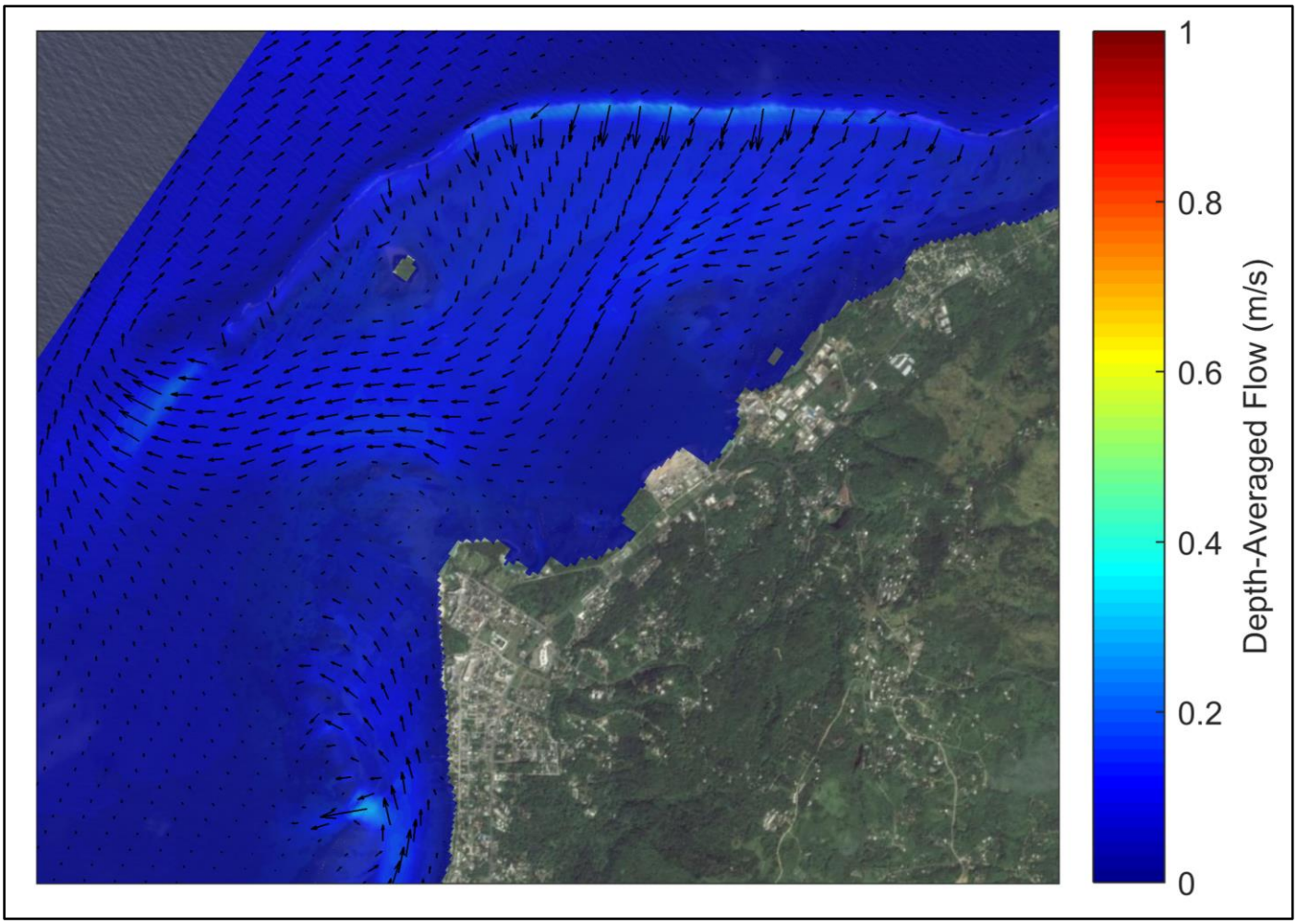

Figure 3-52. Currents during a falling tide - summer tradewind wave conditions, Tanapag Lagoon.

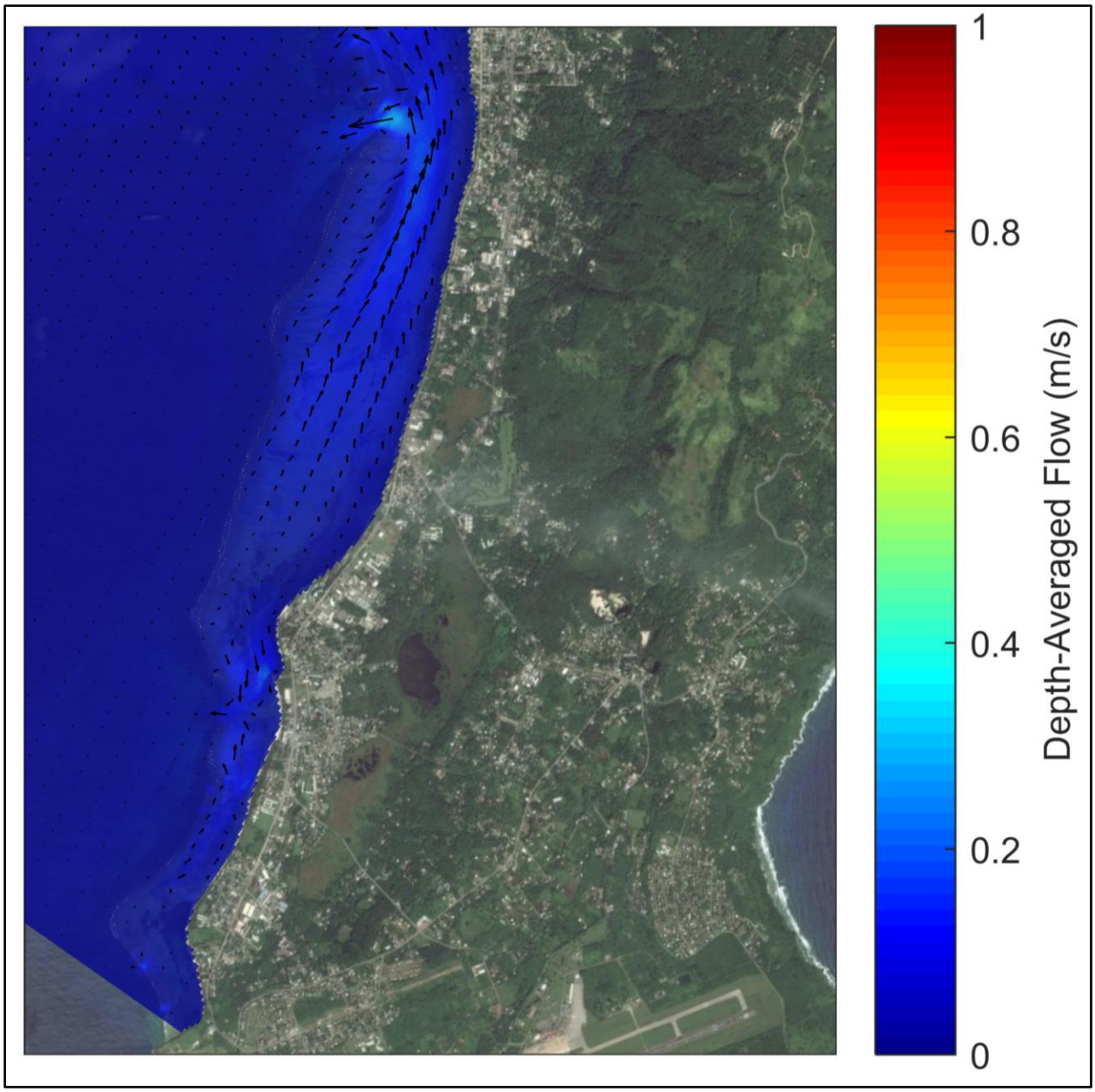

Figure 3-53. Currents during a Falling tide - summer tradewind wave conditions, Garapan Lagoon.

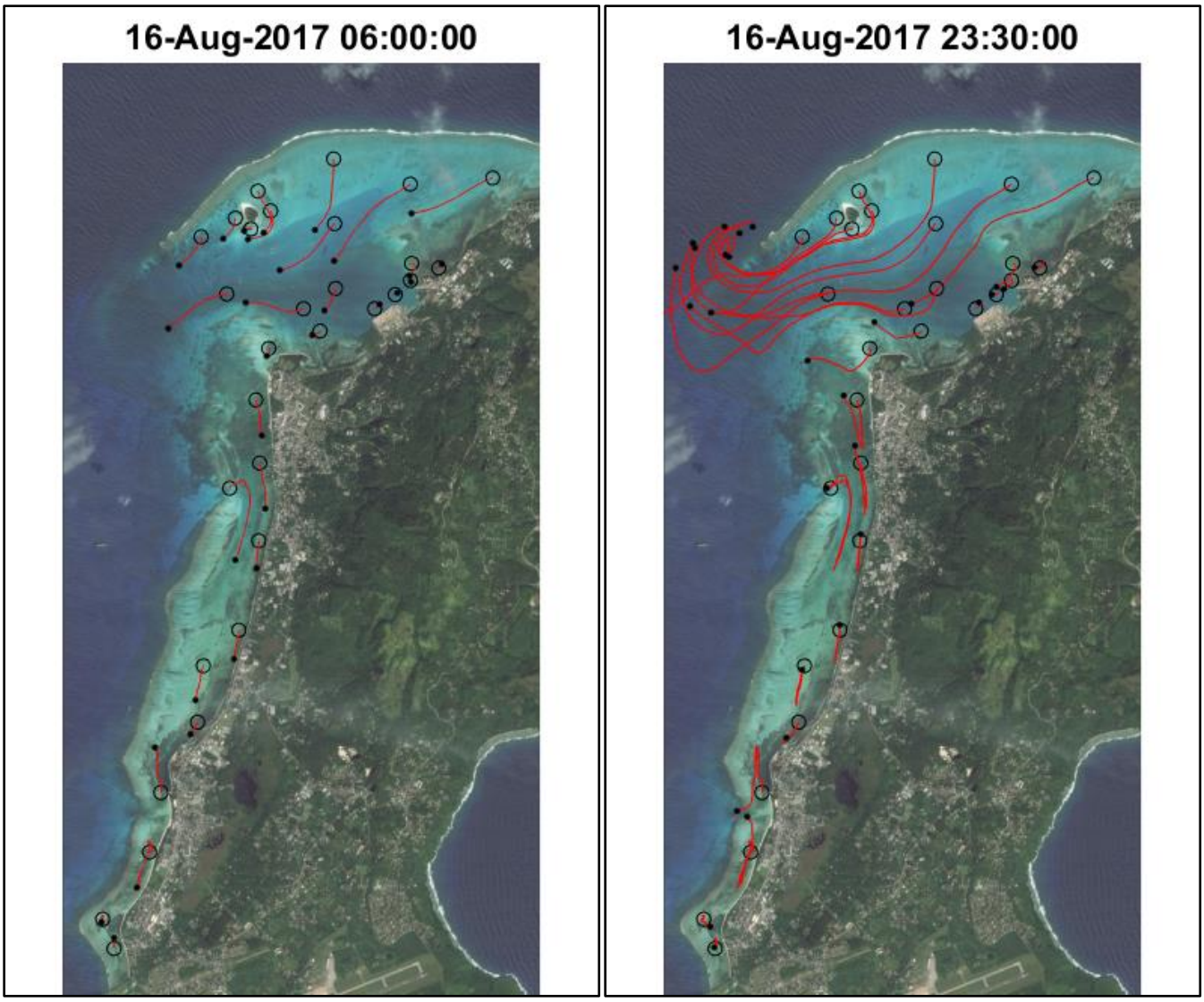

Figure 3-54. Tracer paths during typical summer tradewinds wave conditions.

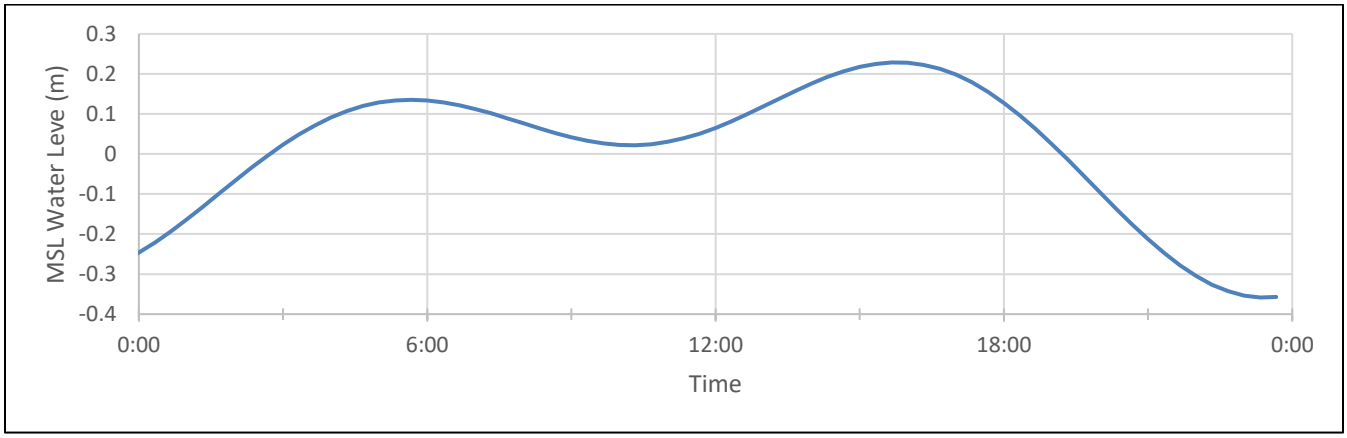

Figure 3-55. Tide level during tracer interval.

3.4.3 Case 3: Summer/Typhoon Season Westerly Waves

Typical summer westerly waves approach Saipan from 260 degrees, with deepwater wave heights of 1.52 m, and periods of 9 seconds. This wave approach is Figure 3-56. As seen in the figure, the reefs along Garapan Lagoon and the southern part of Tanapag Lagoon that are oriented north-south are exposed to the most wave energy. The depth-averaged flow patterns in Tanapag Lagoon are shown in Figure 3-57 and Garapan Lagoon in Figure 3-58. Figure 3-57 illustrates that the waves drive flow over the reef, into the Tanapag lagoon, and out the main channel. Velocities over the reef are greatest at sections of reef with direct exposure to the west and have speeds of approximately 0.25-0.43 m/s. Portions of the flow are also driven to the northeast along the reef edge before turning into Tanapag Lagoon where speeds dissipate as depths increase. There are some areas such as the south side on Managaha Island where breaking waves generate flow into the lagoon that eventually turn toward deeper water and flow out the main channel. Average currents in the northeast part of the lagoon in the vicinity of ADV 1 are weaker than for Cases 1 and 2 because this portion of the reef is partially sheltered from waves from the west. To the south of the main channel and to the northwest of American Memorial Park, wave driven flow from breaking on the reef has a peak velocity of 0.6 m/s before it turns and flows out the main channel or other smaller adjacent channels in the reef. The return flow out of the main channel has maximum speed on the order of 0.25 m/s. The average flow speeds in the inner basin in the vicinity of the port are near zero. The patch reef area to the west of Garapan shows chaotic currents in wave breaking areas.

Figure 3-58 illustrates that net flow within Garapan Lagoon during westerly waves is uniformly to the north from Puntan Susupe at speeds up to 0.2 m/s, and then seaward out of Light House channel at speeds of up to 0.6 m/s. A portion of the northward flow continues past Light House channel, and out the main channel. The section of the Garapan Lagoon south of Puntan Susupe drains toward the Sugar Dock channel where flow exists the Lagoon with a maximum velocity of 0.7 m/s.

The flow patterns in the middle of a rising tide are shown in Figure 3-59 and Figure 3-60. In Tanapag Lagoon (Figure 3-59) the same flow pattern is evident as for the time averaged flow, but with slightly weaker currents in the deeper sections of the lagoon and out of the main channel. The peak flow out of the main channel is still approximately 0.20 m/s. As seen in Figure 3-60, during a flooding tide, currents flow into Light House channel and to the south toward Puntan Susupe – a reversal of the net flow pattern shown in Figure 3-58. Velocities are generally weaker (0.13 m/s) as the southward tidal currents are flowing against wave driven flow to the north. The model calculates a narrow band of strong currents on the outside of the reef that continues to flow to the north from Susupe to the Light House Channel, where there is a mix of flow in and out of the channel. The model also predicts a mix of flow into and out of the Sugar Dock channel during a rising tide and westerly waves.

The flow patterns during the middle of a falling tide are shown in Figure 3-61 and Figure 3-62. In Tanapag Lagoon (Figure 3-61) the same flow pattern is evident as with the time averaged flow but with stronger currents flowing from the deeper sections of the lagoon and out of the main channel. The peak speeds flowing out of the main channel are calculated to be 0.27 m/s. To the

west of Garapan, flow is to the north, and then to the northwest and west out of the main channel. Figure 3-62 illustrates that during the falling tide, flow within Garapan Lagoon is strongly to the north at speeds up to 0.25 m/s. There is strong flow up to 0.7 m/s out of the Light House channel, as well as continued northward flow past Light House channel and out the main channel. To the south of Puntan Susupe, flow travels along the coast and converges to flow out of the Sugar Dock channel with a maximum speed of approximately 0.64 m/s.

Figure 3-63 presents the model calculated transport paths followed over 6 and 12 hours of tracers released into the water at select locations within the lagoon and along the shoreline during typical summer westerly wave conditions. The tracers are released at 00:00 on a day – August 16, 2017 - with an intermediate tide between a neap and spring tide. Black circles on the figure mark the starting locations. The tide for August 16, 2017 is plotted in Figure 3-64. A tracer's instantaneous position is marked with a black dot and its path marked with a red line. Figure 3-63 shows the following:

- Tracers released in the Tanapag Lagoon are transported out of the main channel by wave driven flow. Currents are greater than during the tradewind cases, resulting in more rapid and further transport of the tracers.
- Tracers released near the port travel a small distance to the southwest along the coast in weak currents.
- Tracers released in the Garapan Lagoon north of Puntan Susupe flow to the north. Wave driven flow dominates of small oscillations in the tidal flow. This is in contrast to Cases 1 and 2, where there was little net transport.
- There is net transport out of Light House Channel and the Sugar Dock Channel.

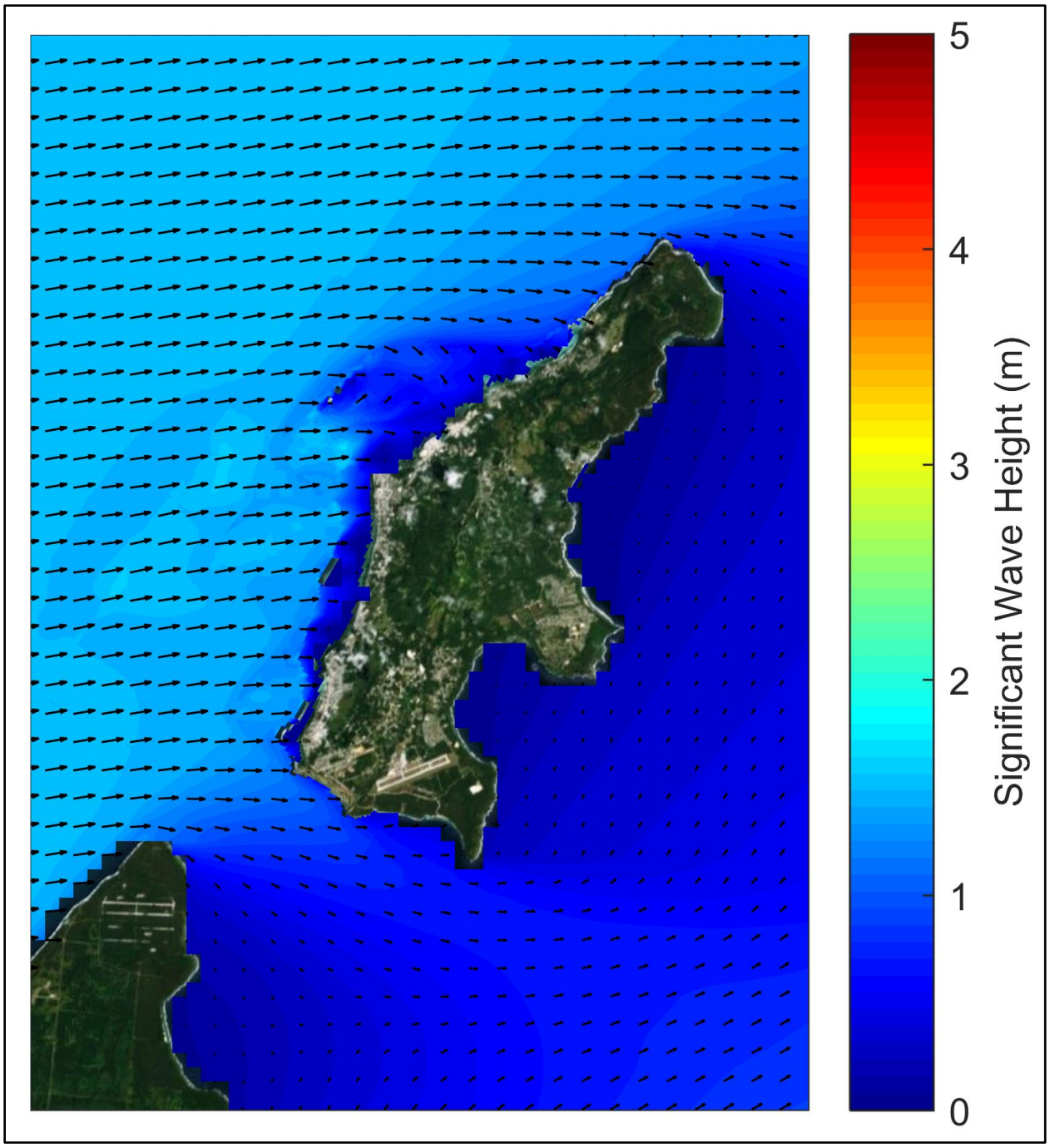

Figure 3-56. Typical westerly wave patterns during summer/typhoon season.

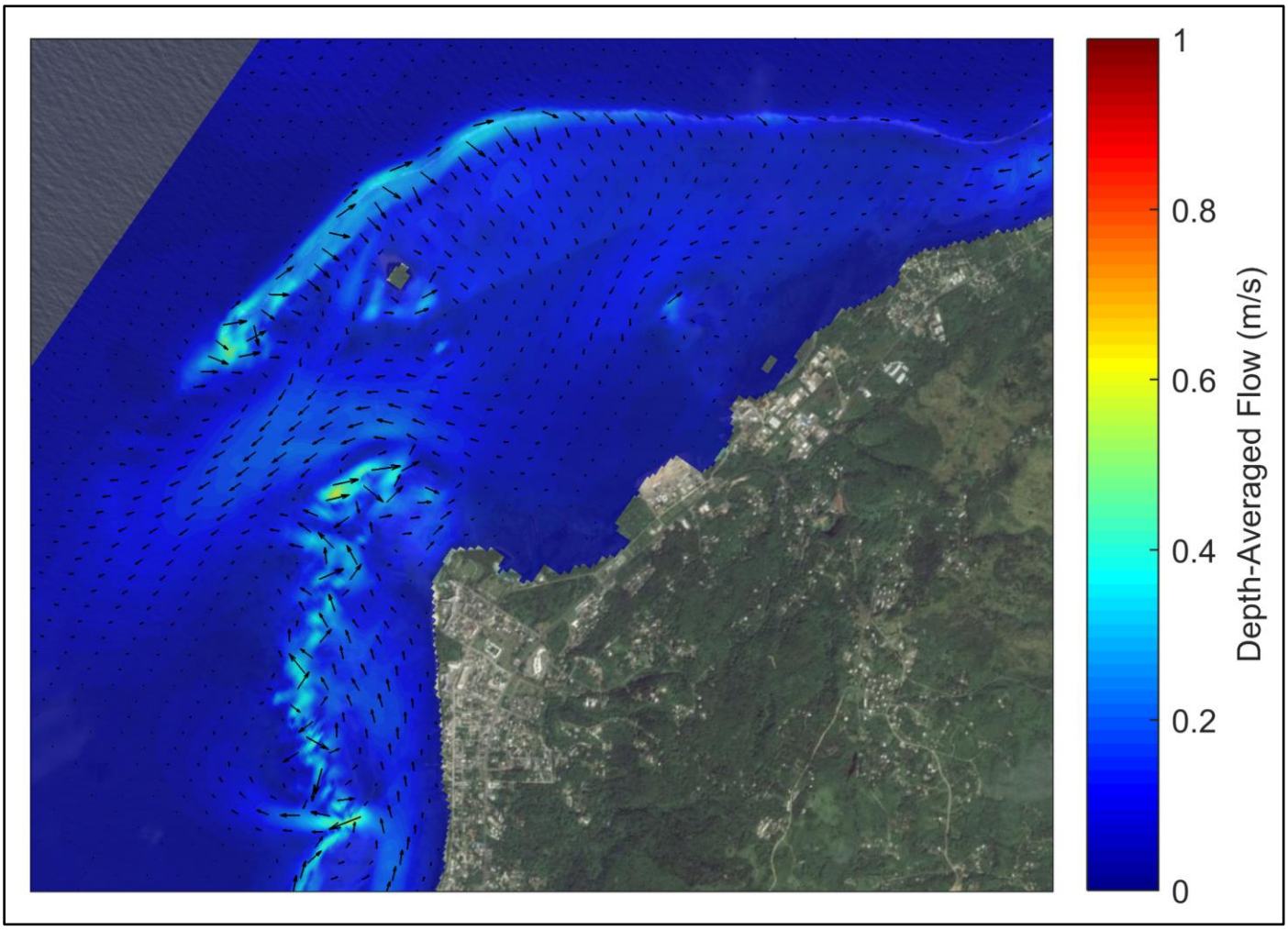

Figure 3-57. Average flows generated by typical summer westerly waves in Tanapag Lagoon.

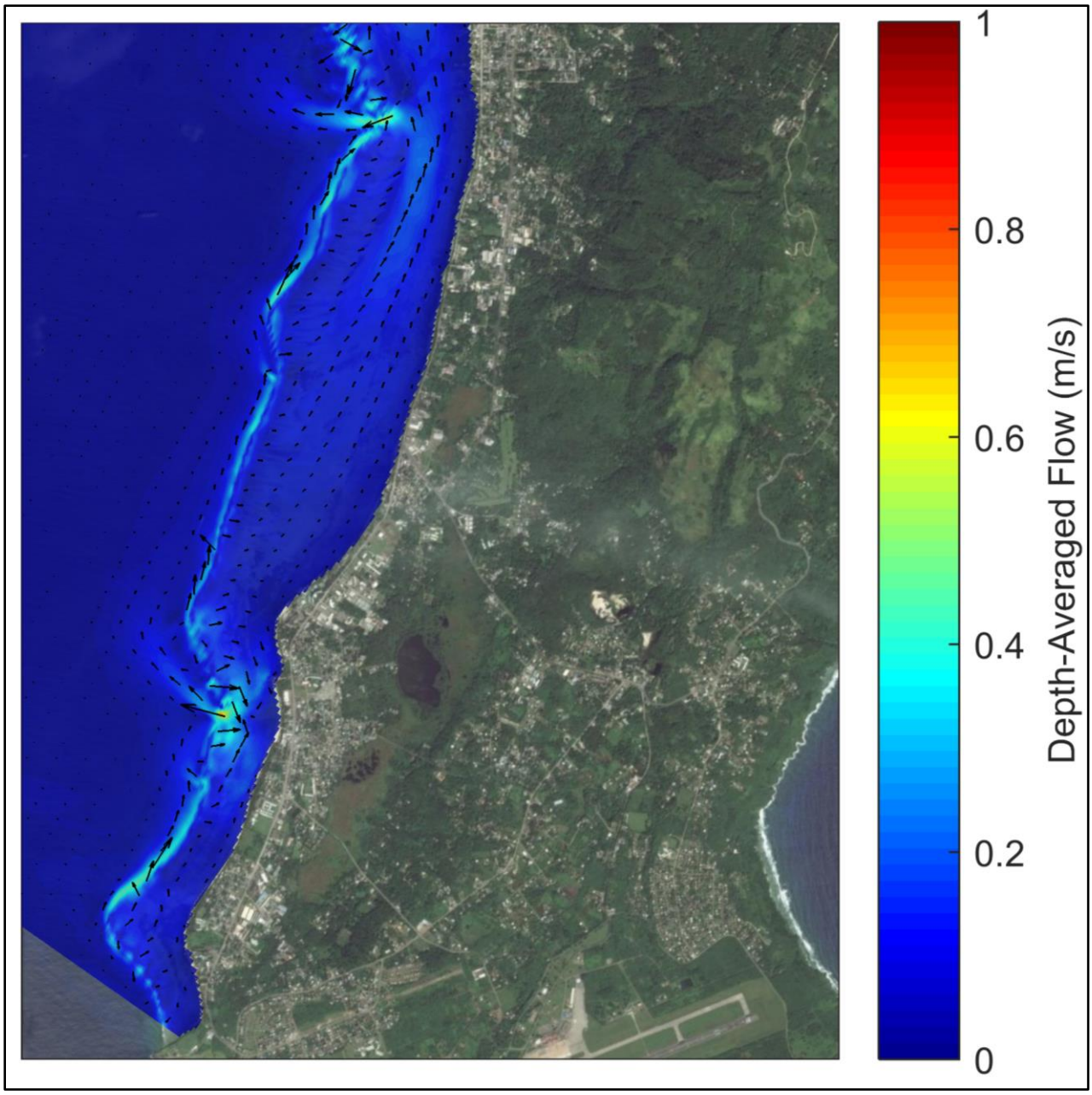

Figure 3-58. Average flows generated by typical summer westerly waves in Garapan Lagoon.

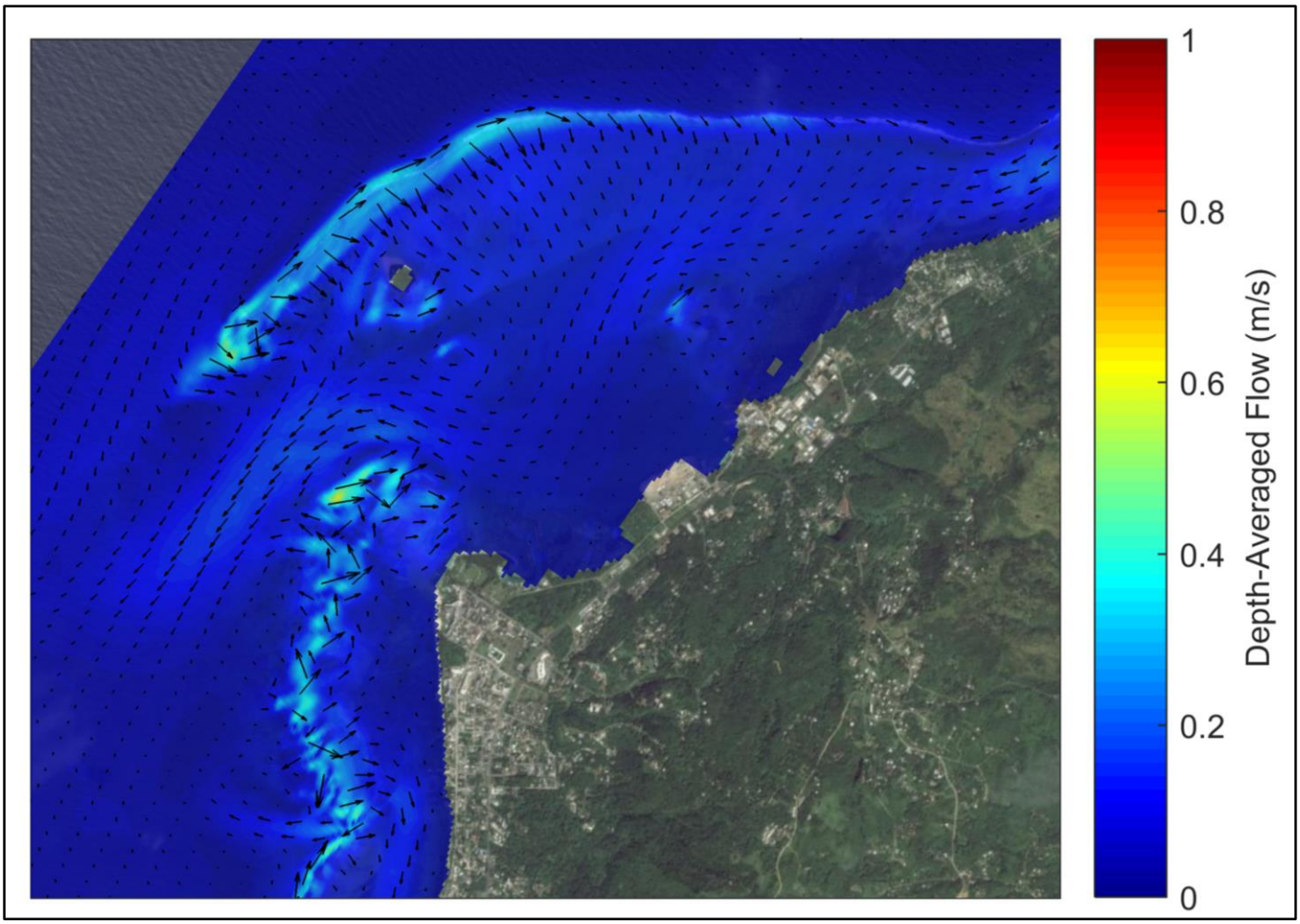

Figure 3-59. Currents during a rising tide - summer westerly wave conditions, Tanapag Lagoon.

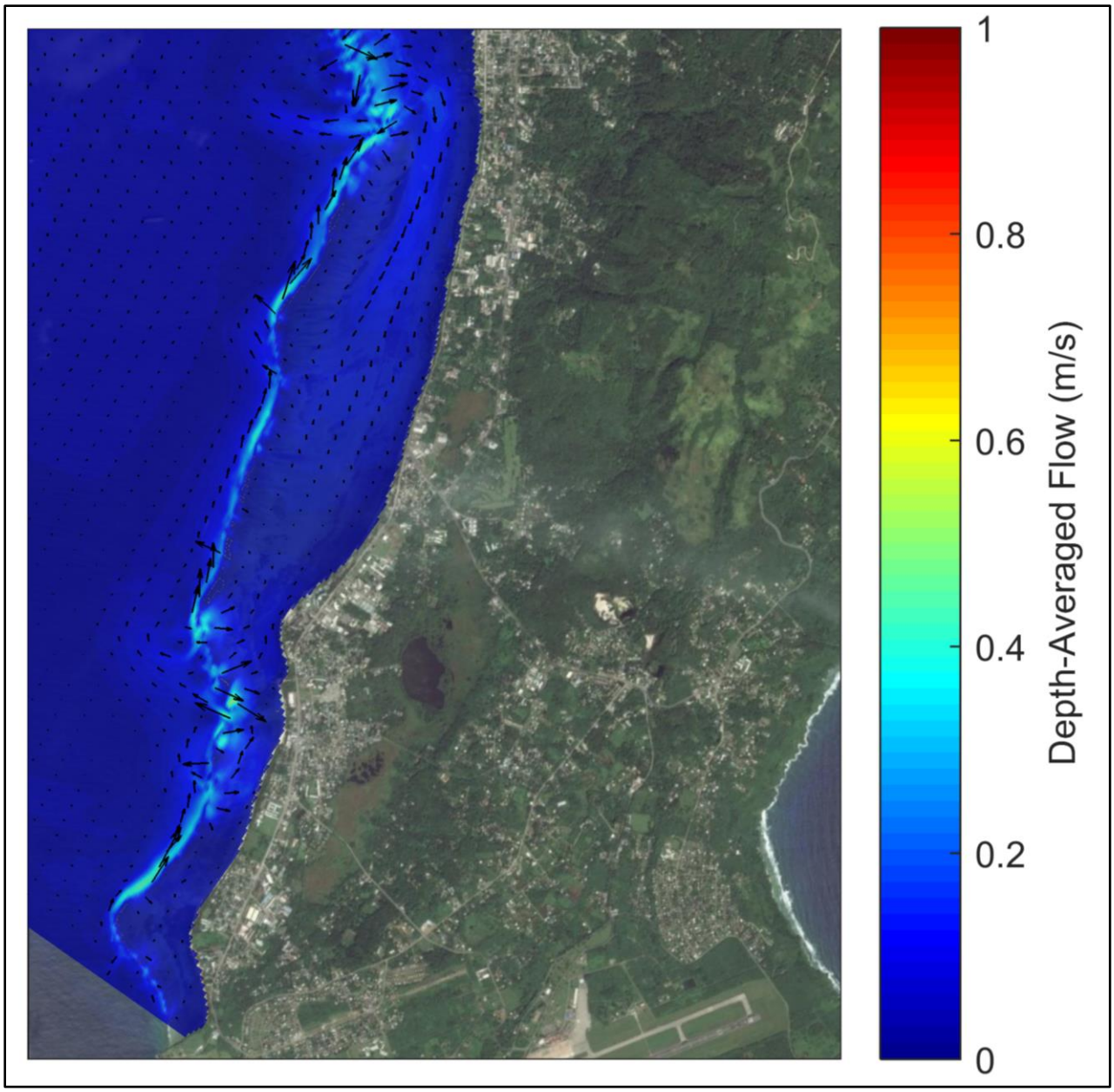

Figure 3-60. Currents during a rising tide - summer westerly wave conditions, Garapan Lagoon.

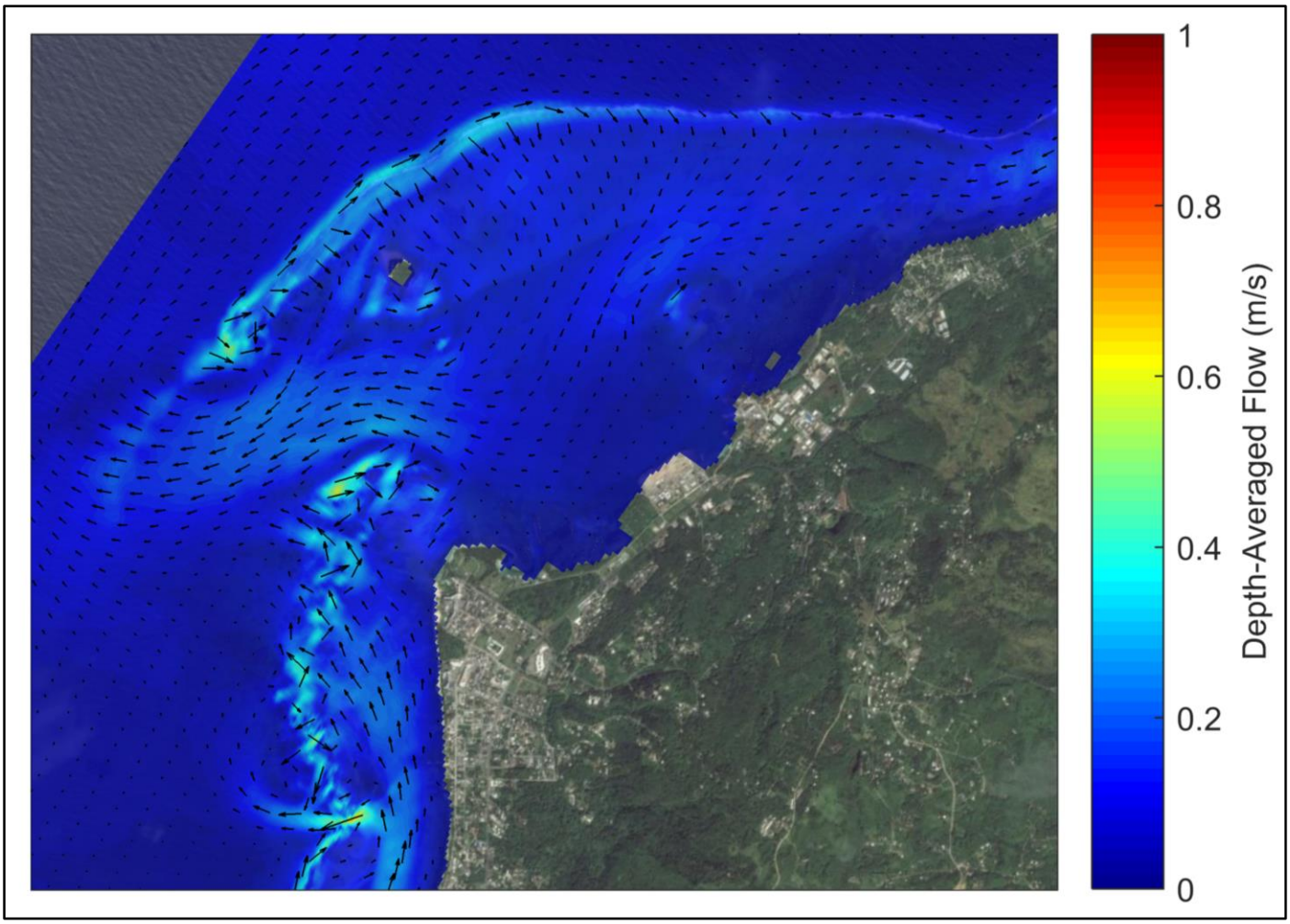

Figure 3-61. Currents during a falling tide - summer westerly wave conditions, Tanapag Lagoon.

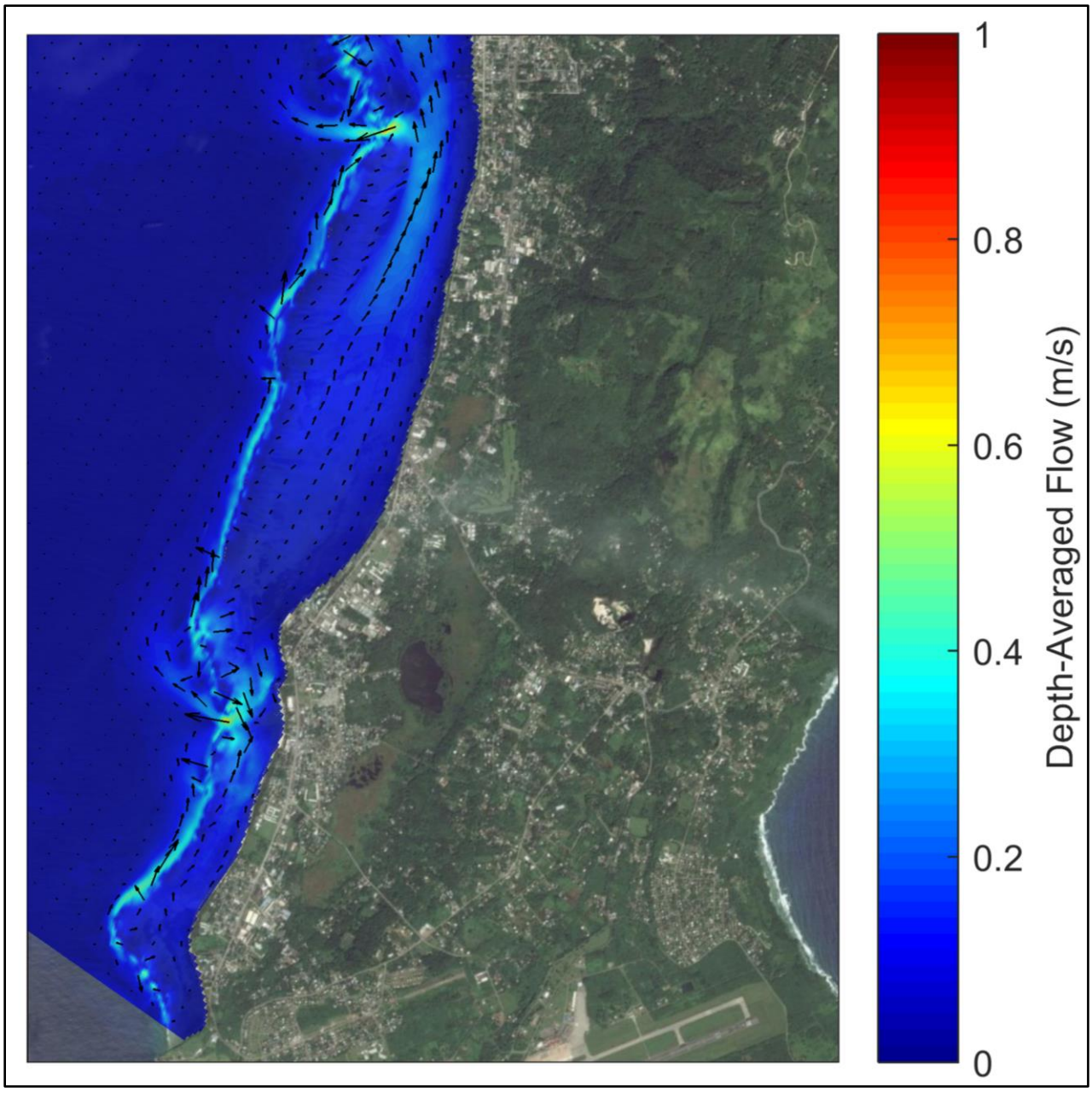

Figure 3-62. Currents during a falling tide - summer westerly wave conditions, Garapan Lagoon.

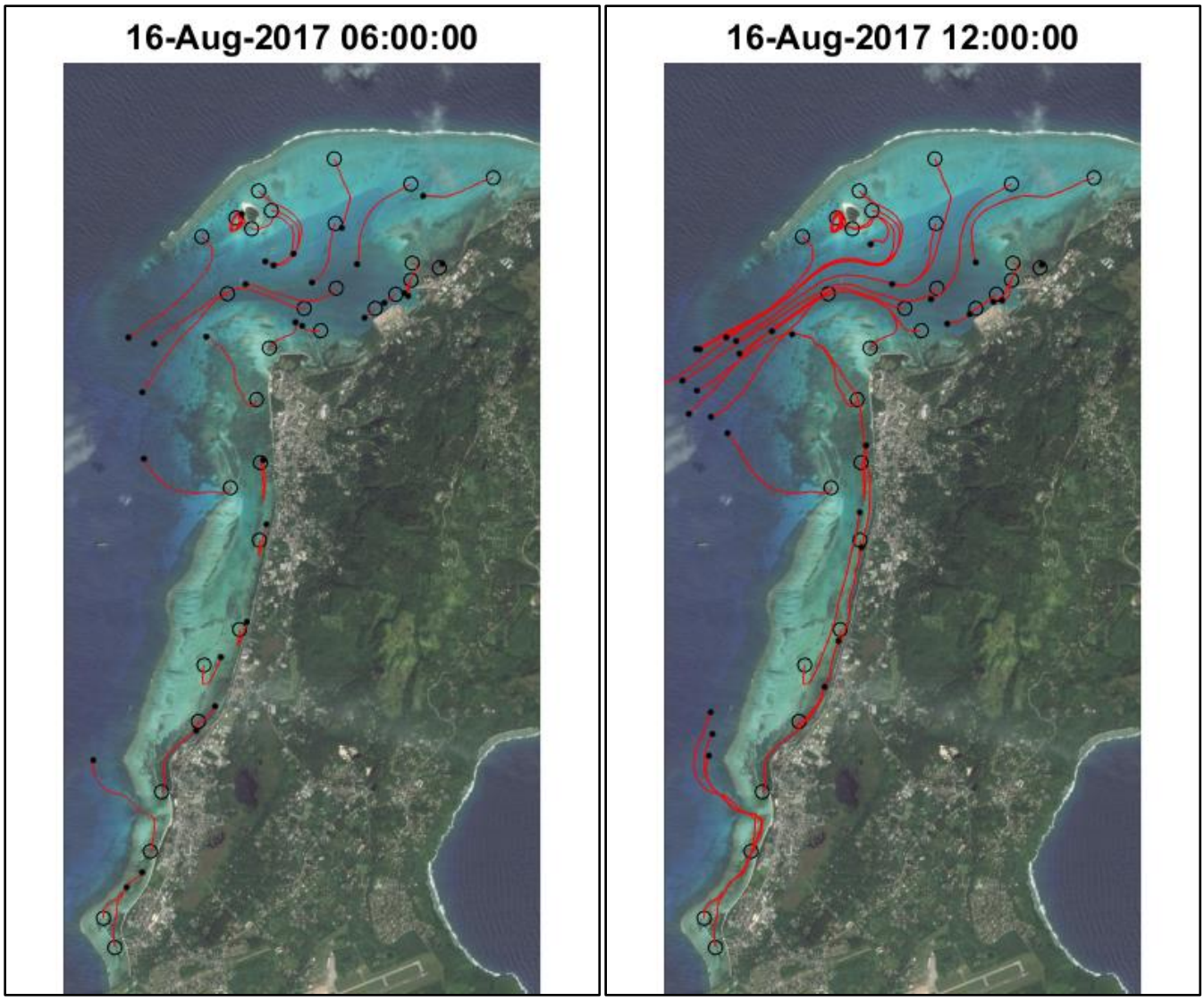

Figure 3-63. Tracer paths during typical summer westerly wave conditions.

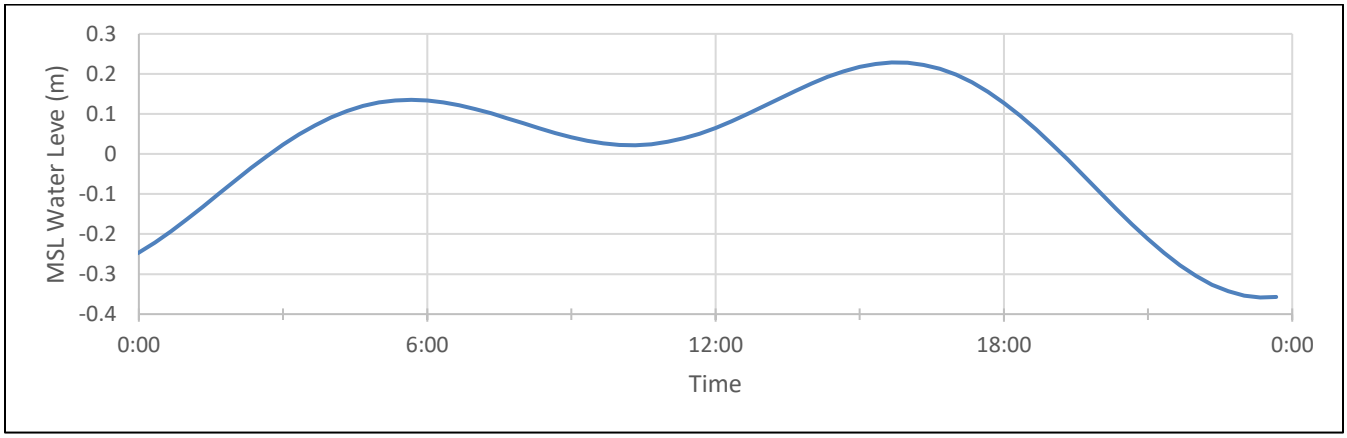

Figure 3-64. Tide level during tracer interval.

3.4.4 Case: 4: 1-Year Typhoon Wave From The Southwest

A typical typhoon passing annually to the southwest of Saipan could generate waves approaching the island from 240 degrees with deepwater wave heights of 4.3 meters and periods of 12 seconds. This wave approach is presented in Figure 3-65. The waves approach from the southwest with a direct approach to the west side of the island. As seen in the figure, the reefs along Garapan Lagoon and the southern part of Tanapag Lagoon that are oriented north-south are exposed to the greatest wave energy. The depth-averaged flow patterns in Tanapag Lagoon are shown in Figure 3-66 and Garapan Lagoon in Figure 3-67. Figure 3-66 illustrates that the waves drive flow over the reef, into the Tanapag Lagoon, and out the main channel. Velocities over the reef are greatest at sections of reef with direct exposure to the west and have speeds of approximately 0.6 – 1.0 m/s. Portions of the flow are also driven to the northeast along the reef edge before turning into Tanapag Lagoon where speeds dissipate as depths increase. Waves from the southwest can also enter directly into the lagoon and generate breaking waves to the north and south of the channel in the vicinity of Managaha Island and offshore of American Memorial Park and Garapan. These breaking waves can generate flow directed into the lagoon. In addition, the large waves that enter the channel have enough energy to reach the northeast corner of the lagoon and generate flow to the east past Pau Beach and out over the reef crest. Flows around the Port of Saipan remain small with magnitudes less than 0.04 m/s to the southwest.

Figure 3-67 illustrates that net flow within Garapan Lagoon during westerly waves is uniformly to the north from Puntan Susupe at speeds up to 0.5 m/s, and then seaward out of Light House channel at speeds of up to 1.1 m/s. A portion of the northward flow continues past Light House channel, and out the main channel. The section of the Garapan Lagoon south of Puntan Susupe drains toward the Sugar Dock channel where flow exists the lagoon with a maximum velocity of 2.0 m/s.

The flow patterns in the middle of a rising tide are shown in Figure 3-68 and Figure 3-69, and during a falling tide in Figure 3-70 and Figure 3-71. As the figures show, there is little difference in flow patterns and magnitudes relative to the average flow conditions presented in Figure 3-66 and Figure 3-67. The energy from annual typhoon waves is sufficient to overwhelm tidal flows. Cases 1, 2 and 3 indicated that during prevailing smaller wave conditions and a rising tide, currents in Garapan Lagoon generally flowed from north to south. By contrast, the annual typhoon wave event has sufficient energy to drive currents in the lagoon to the north, even during a rising tide.

Figure 3-72 presents the model calculated transport paths followed over 6 and 12 hours of tracers released into the water at select locations within the lagoon and along the shoreline during a 1-year return period wave approaching from the southwest. The tracers are released at 00:00 on a day – August 16, 2017 - with an intermediate tide between a neap and spring tide. The tide for August 16, 2017 is plotted in Figure 3-73. A tracer's instantaneous position is marked with a black dot and its path marked with a red line. Figure 3-72 illustrates the following:

- Transport is much further and more rapid than in the previous cases, driven by larger waves and stronger currents.

- Tracers released in the Tanapag Lagoon primarily flow rapidly out of the main channel. The tracers in the vicinity of the northeast corner of the lagoon flow to the northeast due to the large waves entering the main channel and breaking on the interior shoal
- Tracers released near the port travel a small distance to the southwest along the coast in weak currents
- Tracers released in the Garapan Lagoon north of Puntan Susupe flow rapidly to the north.
- There is a net transport out of the Light House channel and the Sugar Dock channel.

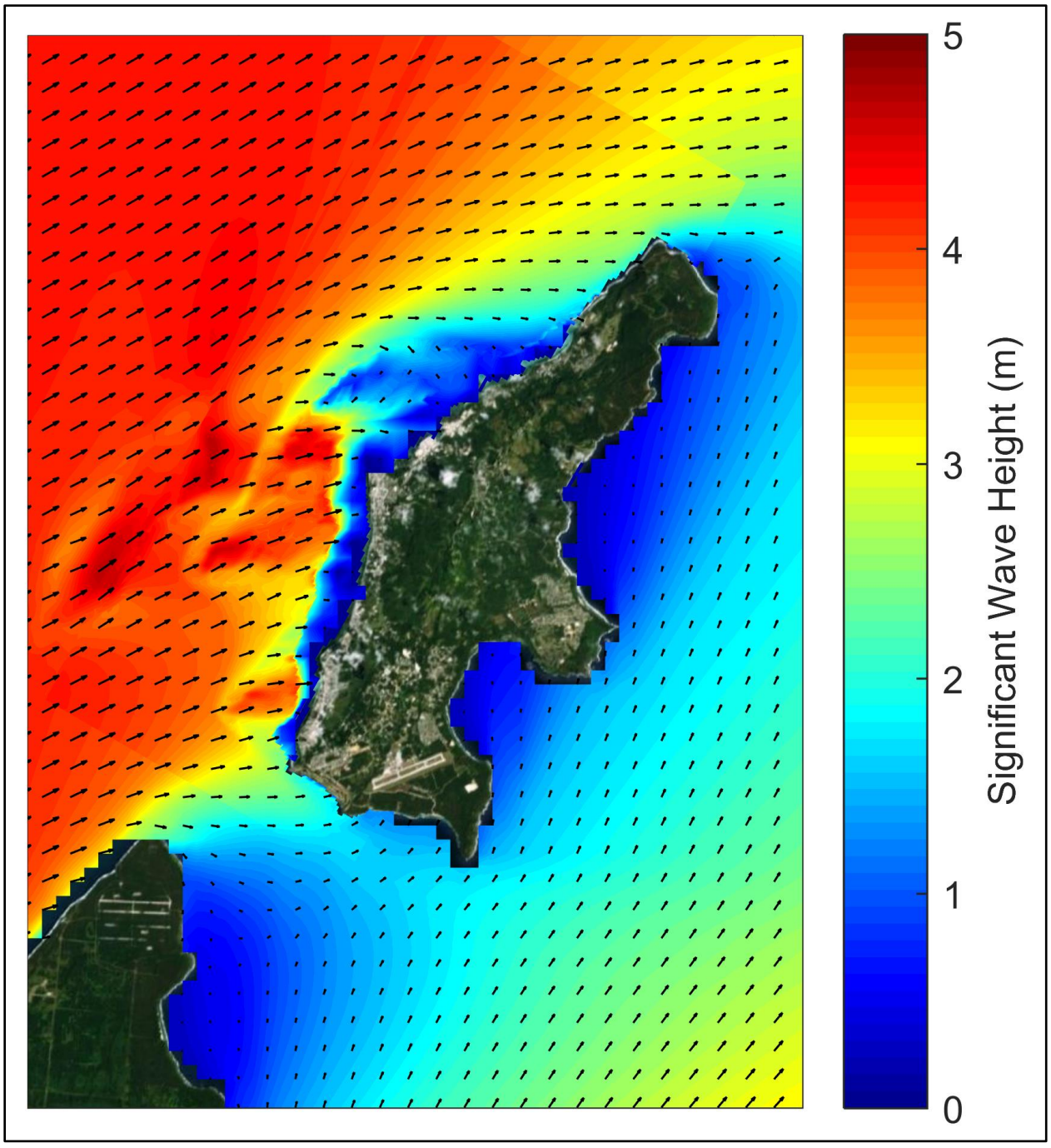

Figure 3-65. Wave patterns for a 1-year typhoon from the southwest.

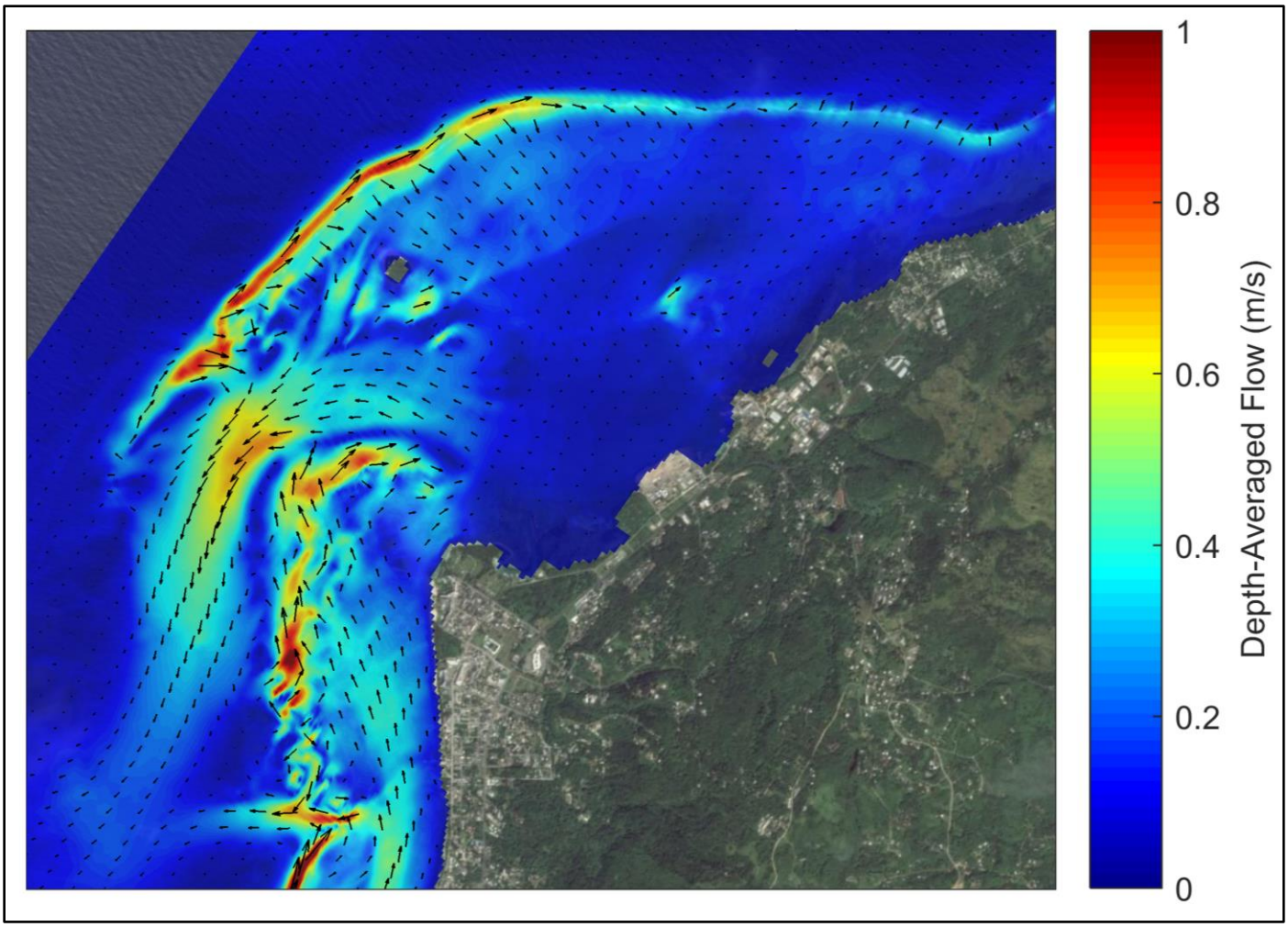

Figure 3-66. Average flow generated by 1-year typhoon wave from the southwest in Tanapag Lagoon.

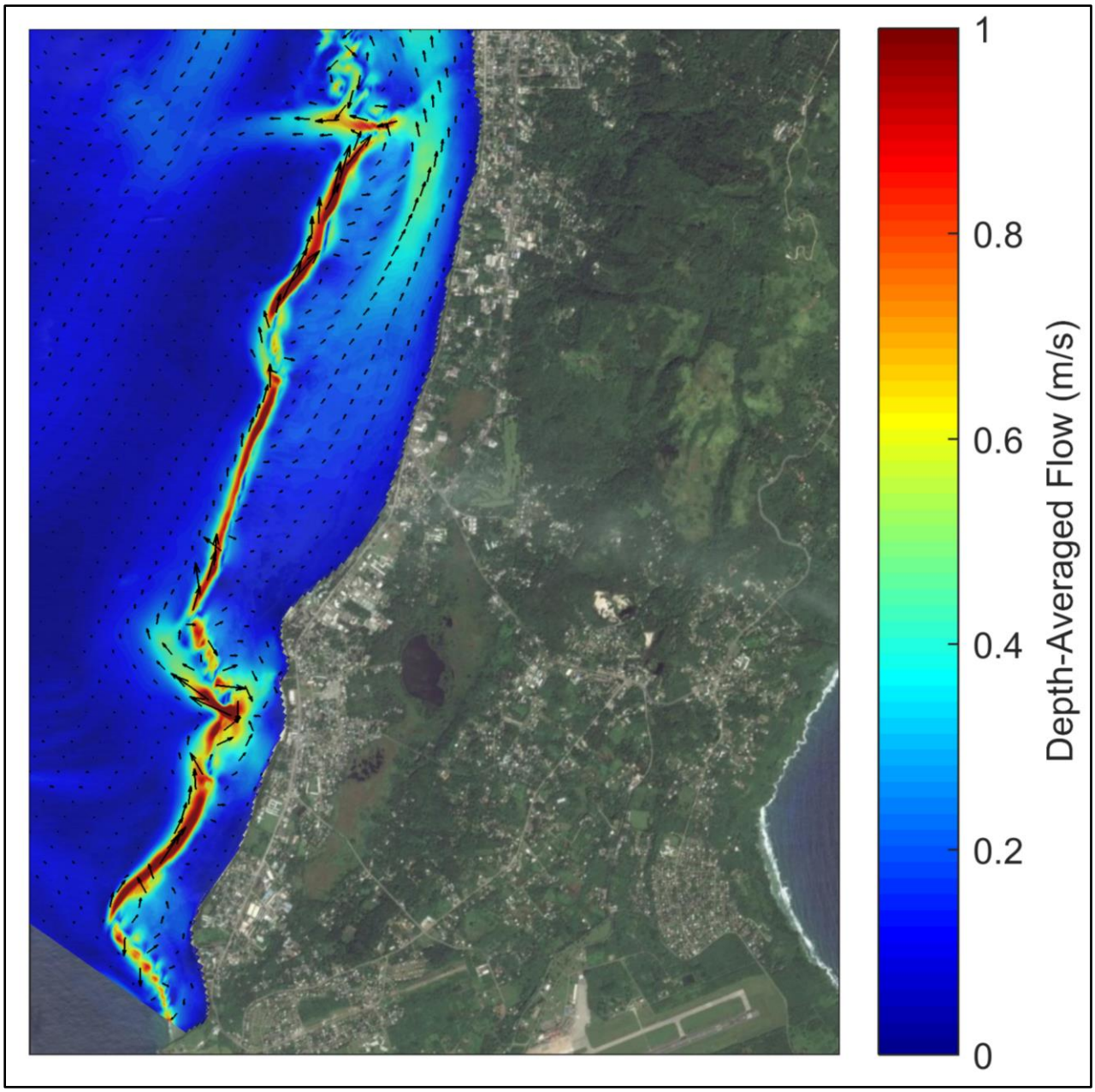

Figure 3-67. Averaged flow generated by 1-year typhoon wave from the southwest in Garapan Lagoon.

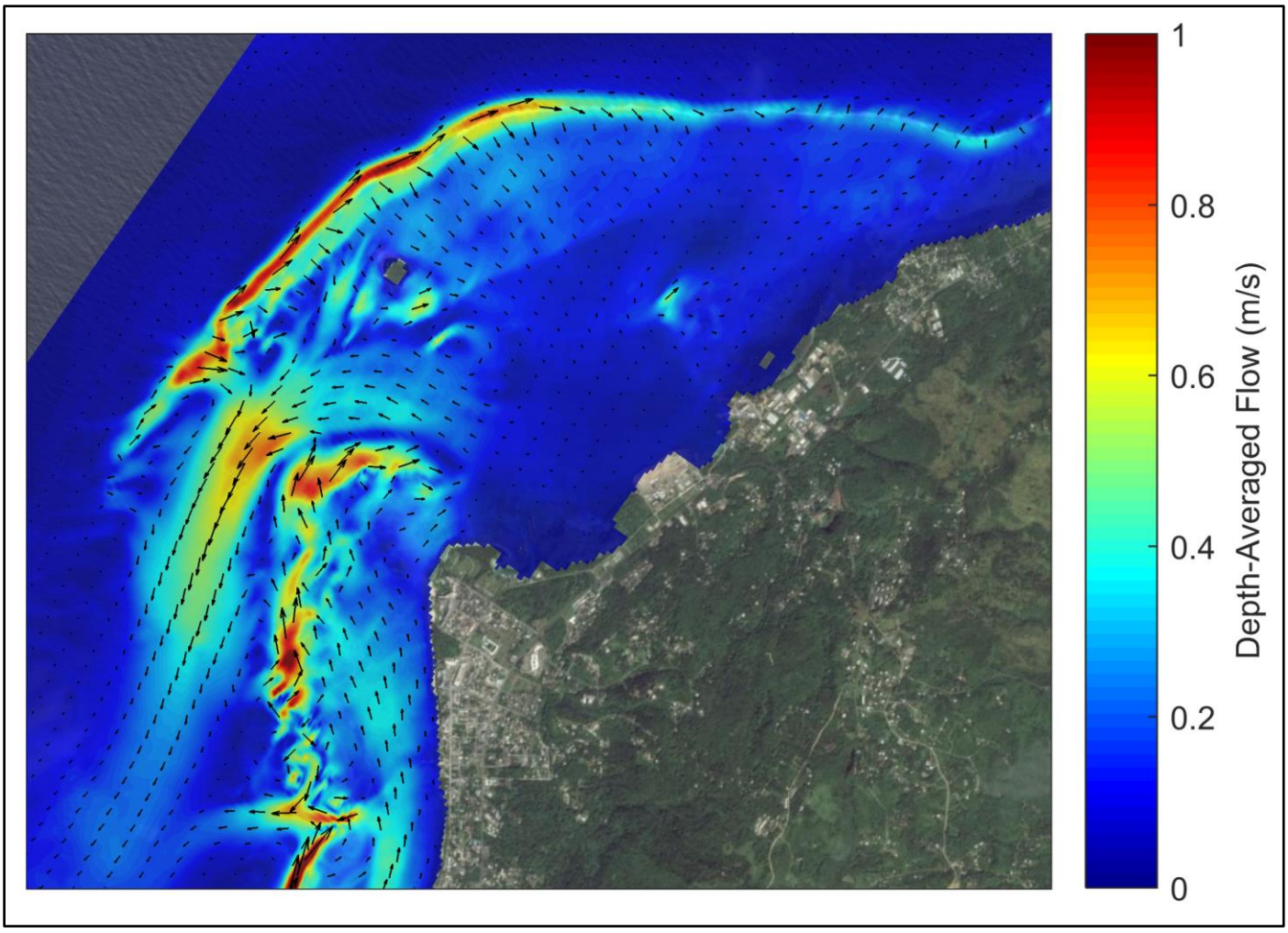

Figure 3-68. Currents during a rising tide - 1-year typhoon wave from the southwest, Tanapag Lagoon.

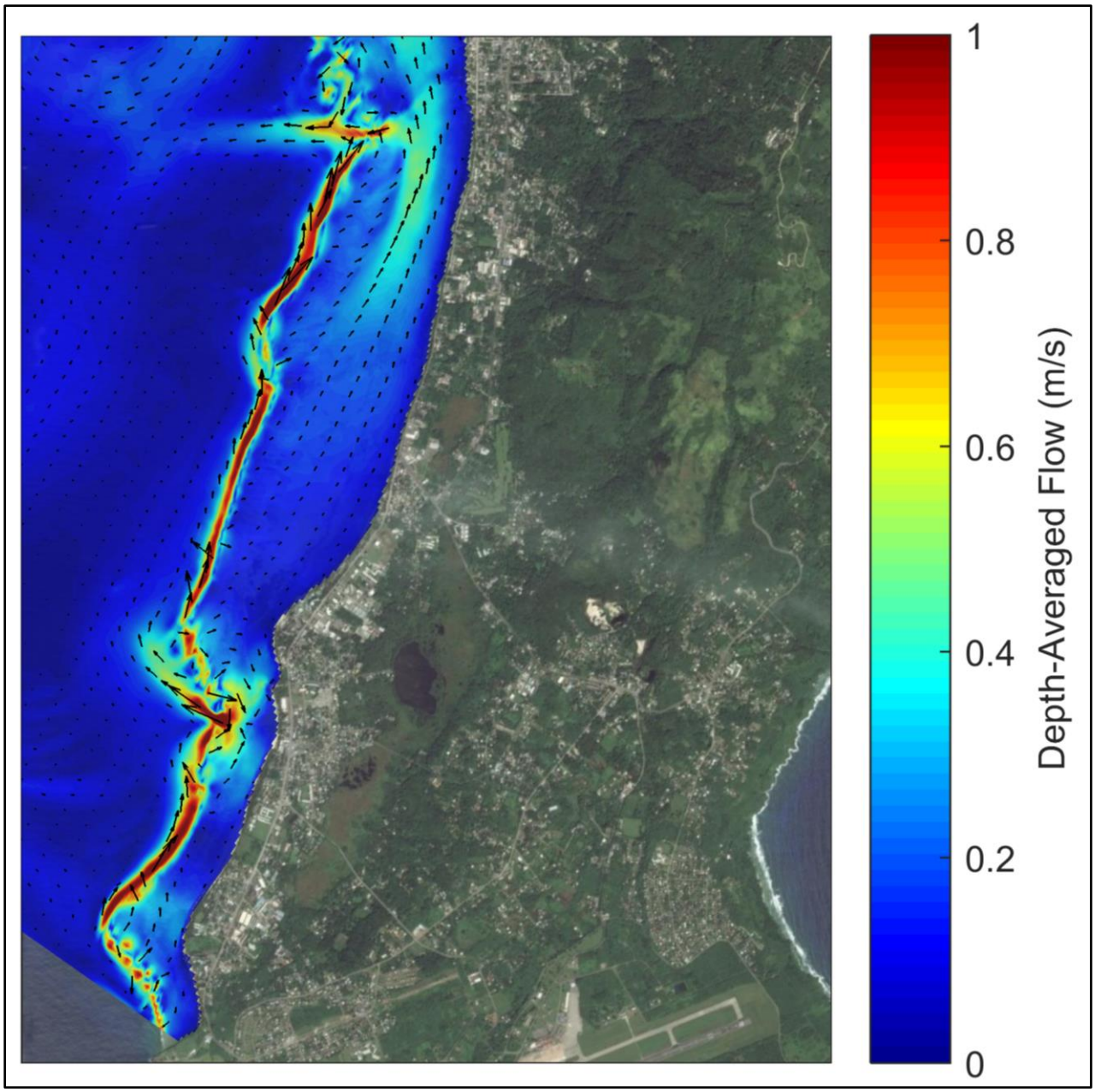

Figure 3-69 Currents during a rising tide - 1-year typhoon wave from the southwest, Garapan Lagoon.

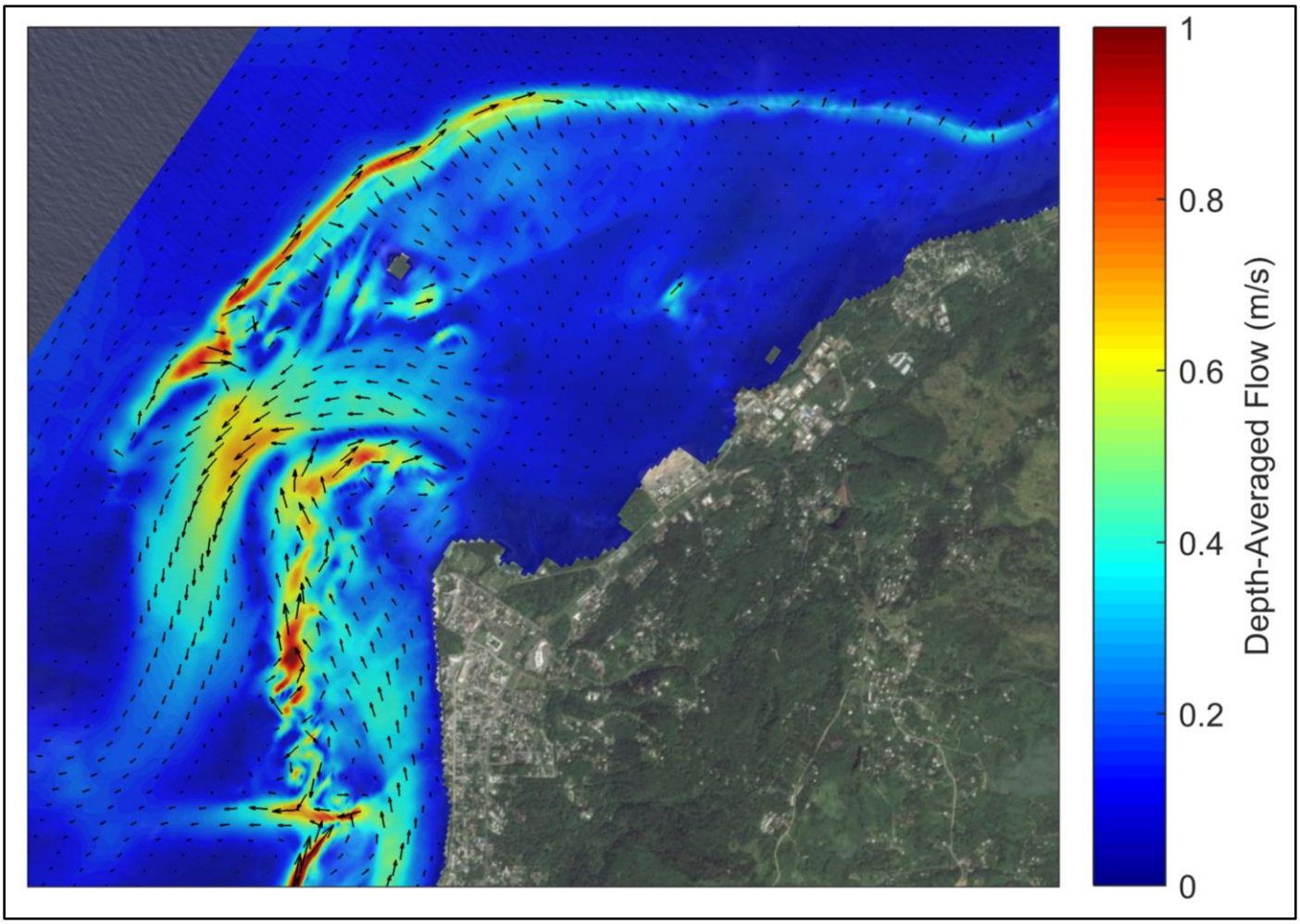

Figure 3-70. Currents during a falling tide - 1-year typhoon wave from the southwest, Tanapag Lagoon.

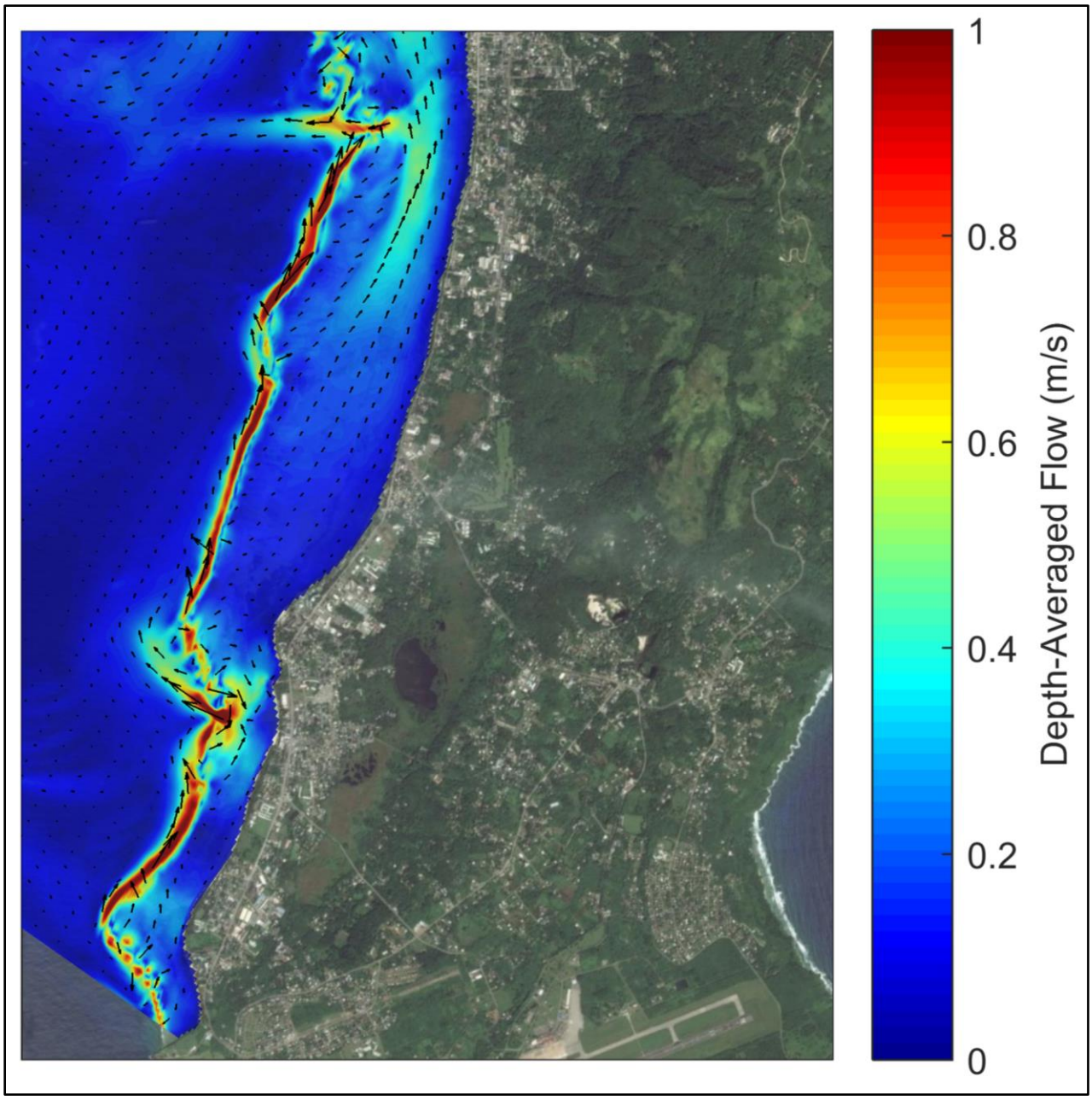

Figure 3-71. Currents during a falling tide - 1-year typhoon wave from the southwest, Garapan Lagoon.

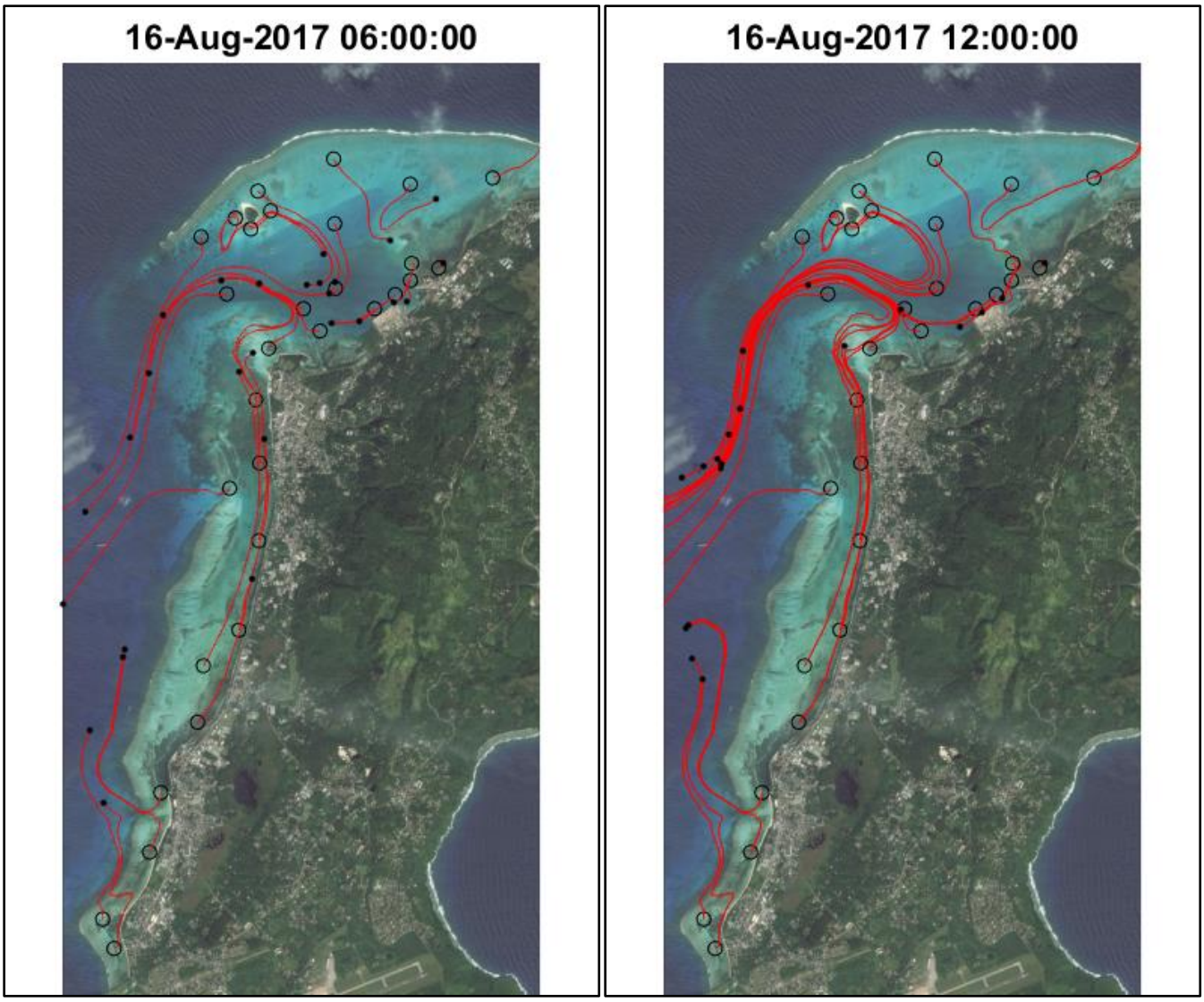

Figure 3-72. Tracer paths during typical 1-year return period typhoon wave from the southwest.

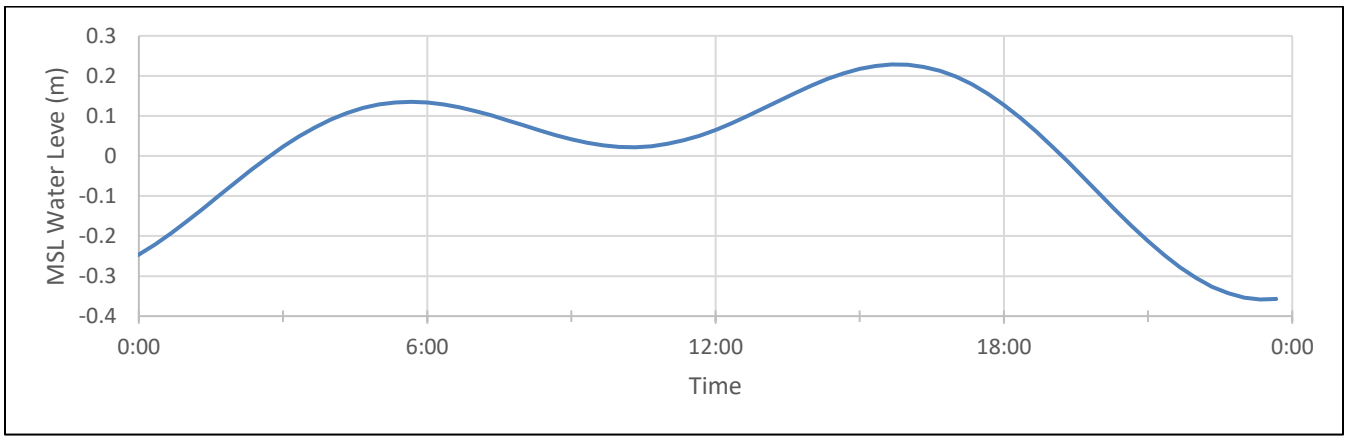

Figure 3-73. Tide level during tracer study interval

3.4.5 Case 5: 1-Year Typhoon Wave from The North-Northwest

A typical typhoon passing annually to the north of Saipan could generate waves approaching the island from 345 degrees with deepwater wave heights of 4.3 meters and periods of 12 seconds. This wave approach is presented in Figure 3-74. As seen in the figure, the typhoon waves directly impact the reefs along Tanapag Lagoon and refract with substantial energy into Garapan Lagoon. The depth-averaged flow patterns in Tanapag Lagoon are shown in Figure 3-75 and Garapan Lagoon in Figure 3-76. Figure 3-75 illustrates that waves drive strong flow over the reef, into the Tanapag Lagoon, and out the main channel. Velocities over the reef are greatest at sections of reef with direct exposure to the north and have speeds of approximately 0.75-1.50 m/s. The currents flow straight across the reef to the north, and along the reef to the southwest from Managaha Island to the main channel. Flow out of the main channel has a maximum velocity of approximately 1.05 m/s. Flows around the Port of Saipan remain small with magnitudes less than 0.02 m/s. The patch reef area to the west of Garapan experiences wave driven currents with speeds up to 0.9 m/s.

Figure 3-76 illustrates that net flow within Garapan Lagoon during north-northwest typhoon waves is uniformly to the north from Puntan Susupe at speeds up to 0.5 m/s, and then seaward out of Light House channel at speeds of up to 1.0 m/s and also to the north out of the main channel. On the outside perimeter of the reef, a rapid current flow to the southwest with a speed of approximately 0.7 to 1.0 m/s. The section of the Garapan Lagoon south of Puntan Susupe drains toward the Sugar Dock channel where flow exits the lagoon with a maximum velocity of 1.4 m/s.

The flow patterns in the middle of a rising tide are shown in Figure 3-77 and Figure 3-78, and during a falling tide in Figure 3-79 and Figure 3-80. Similar to Case 4 for southwest typhoon waves, the figures indicate that there is little difference in flow patterns and magnitudes relative to the average flow conditions presented in Figure 3-75 and Figure 3-76. The energy from an annual typhoon wave is sufficient to overwhelm tidal flows. Cases 1, 2 and 3 indicated that during prevailing, lower wave energy conditions, and a rising tide, currents in Garapan Lagoon generally flow from north to south. By contract, the annual typhoon wave event from the north-northwest has sufficient energy to drive currents in the lagoon to the north, even during a rising tide.

Figure 3-81 presents the model calculated transport paths followed over 6 and 12 hours of tracers released into the water at select locations within the lagoon and along the shoreline during a 1-year return period wave approaching from the north-northwest. The tracers are released at 00:00 on a day – August 16, 2017 - with an intermediate tide between a neap and spring tide. The tide for August 16, 2017 is plotted in Figure 3-82. A tracer's instantaneous position is marked with a black dot and its path marked with a red line. The tracer paths allow visualization of overall circulation patterns throughout the lagoon and how pollutants or other items of interest released into the water are likely to move. Figure 3-81 shows the following:

- Similar to Case 4, transport is much further and more rapid than in Cases 1, 2 and 3, driven by larger waves and stronger currents.
- Tracers released in the Tanapag Lagoon uniformly flow rapidly out of the main channel.

- Tracers released near the port travel a small distance to the southwest along the coast in weak currents.
- Tracers released in the Garapan Lagoon north of Puntan Susupe flow rapidly to the north.
- There is strong flow out of Light House and the Sugar Dock channels.

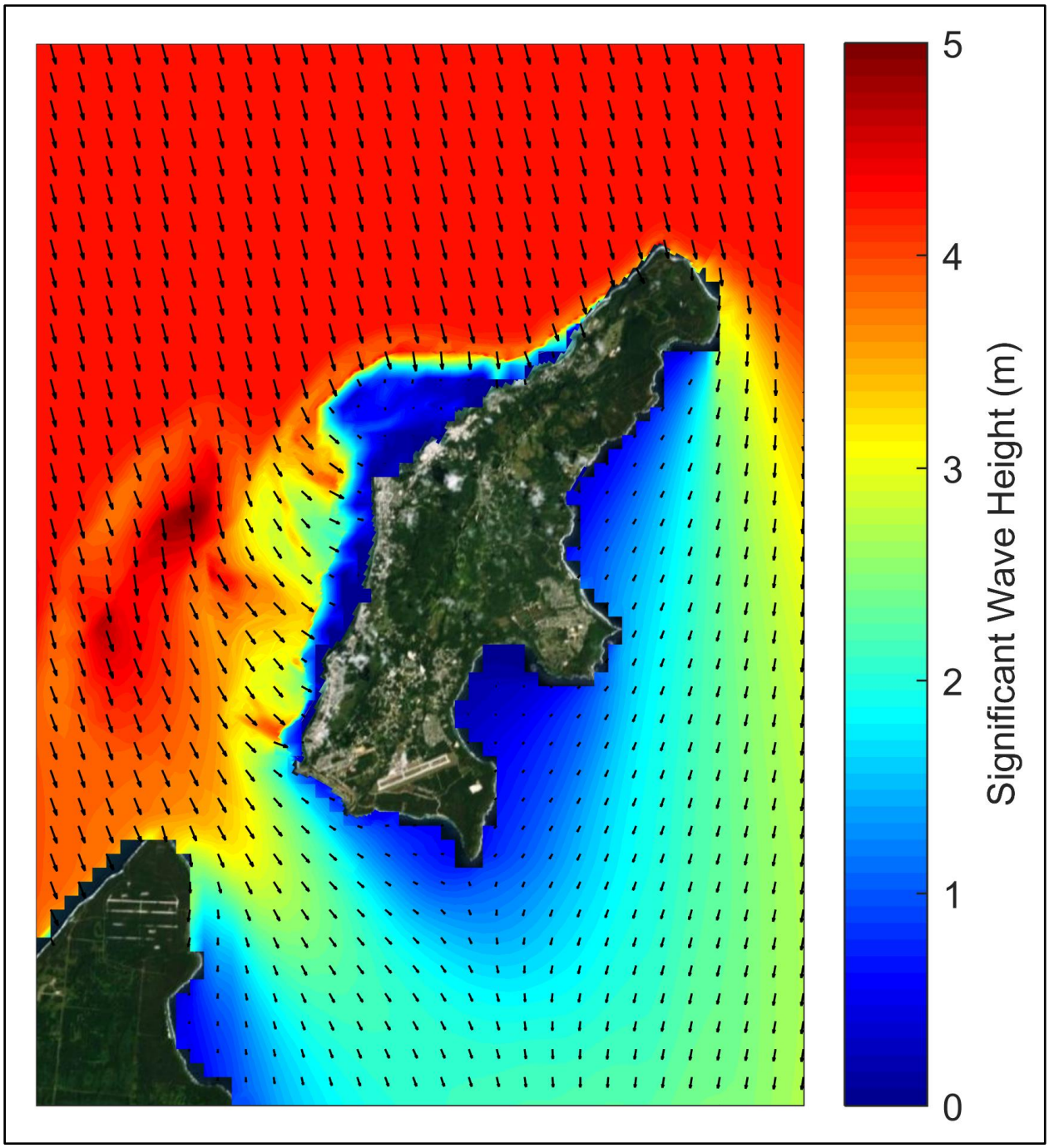

Figure 3-74. Wave pattern for a 1-year typhoon wave from the north-northwest.

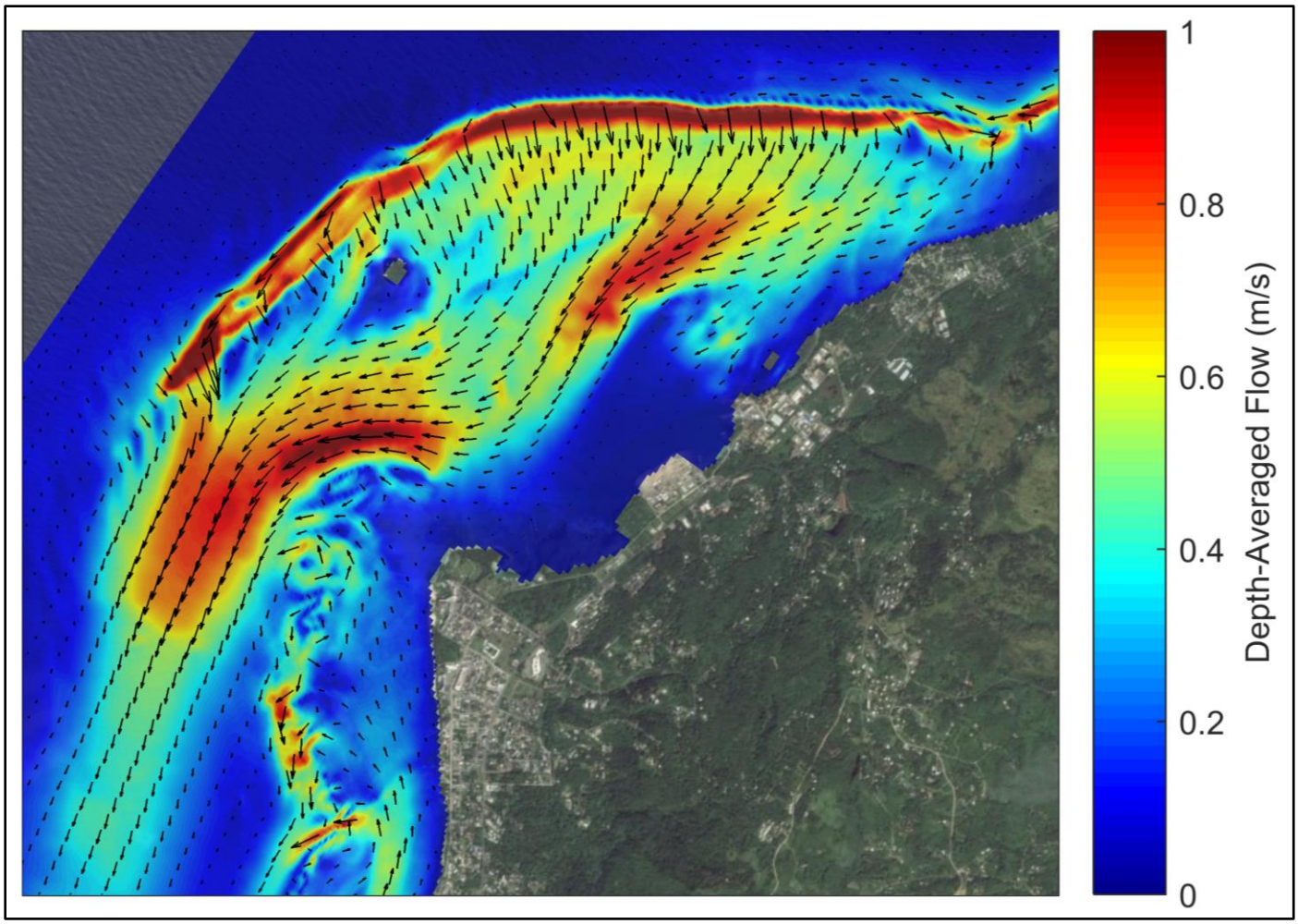

Figure 3-75. Average flow generated by 1-year typhoon wave from the north-northwest in Tanapag Lagoon.

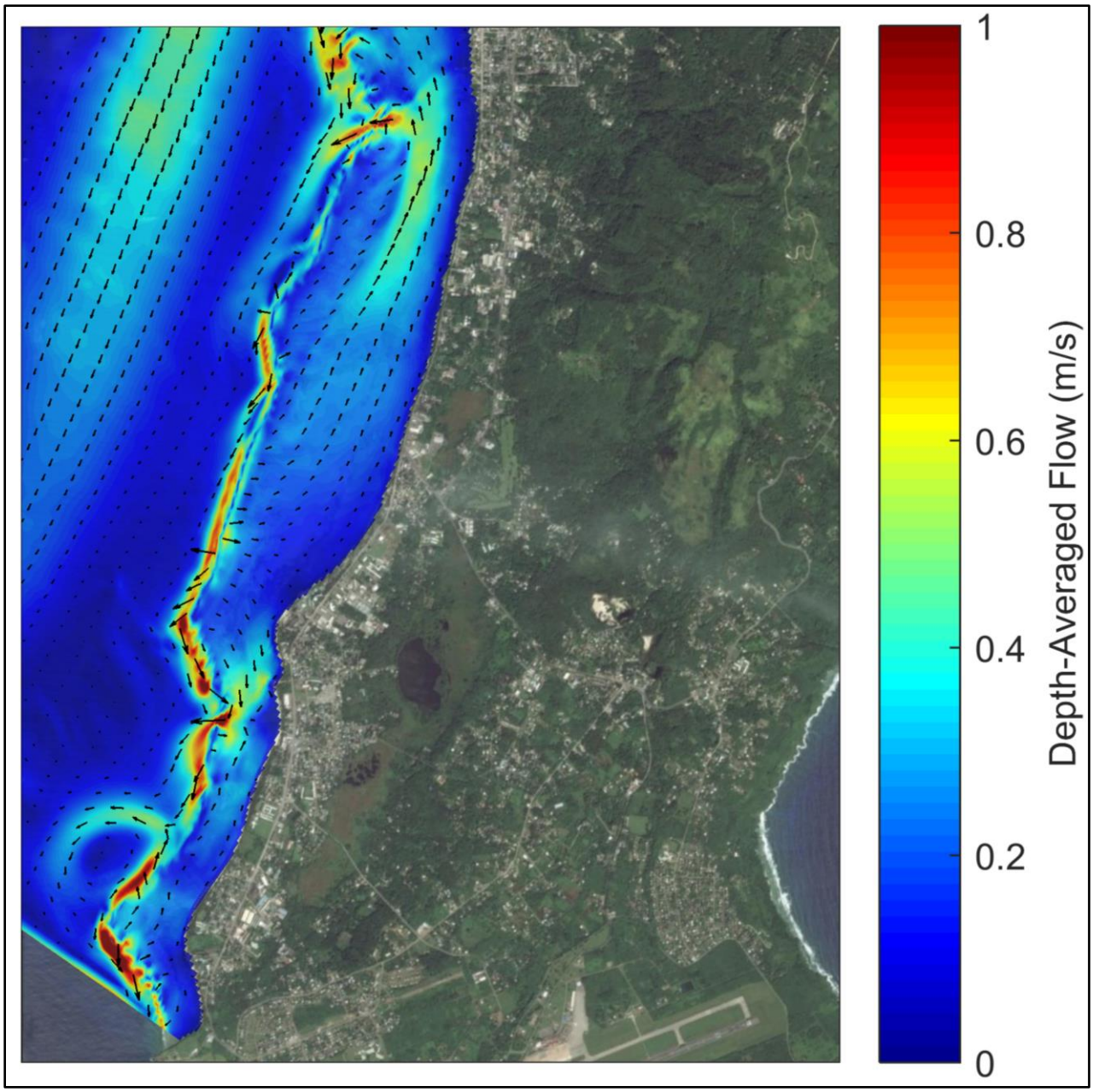

Figure 3-76. Average flows generated by 1-year typhoon wave from the north-northwest, Garapan Lagoon.

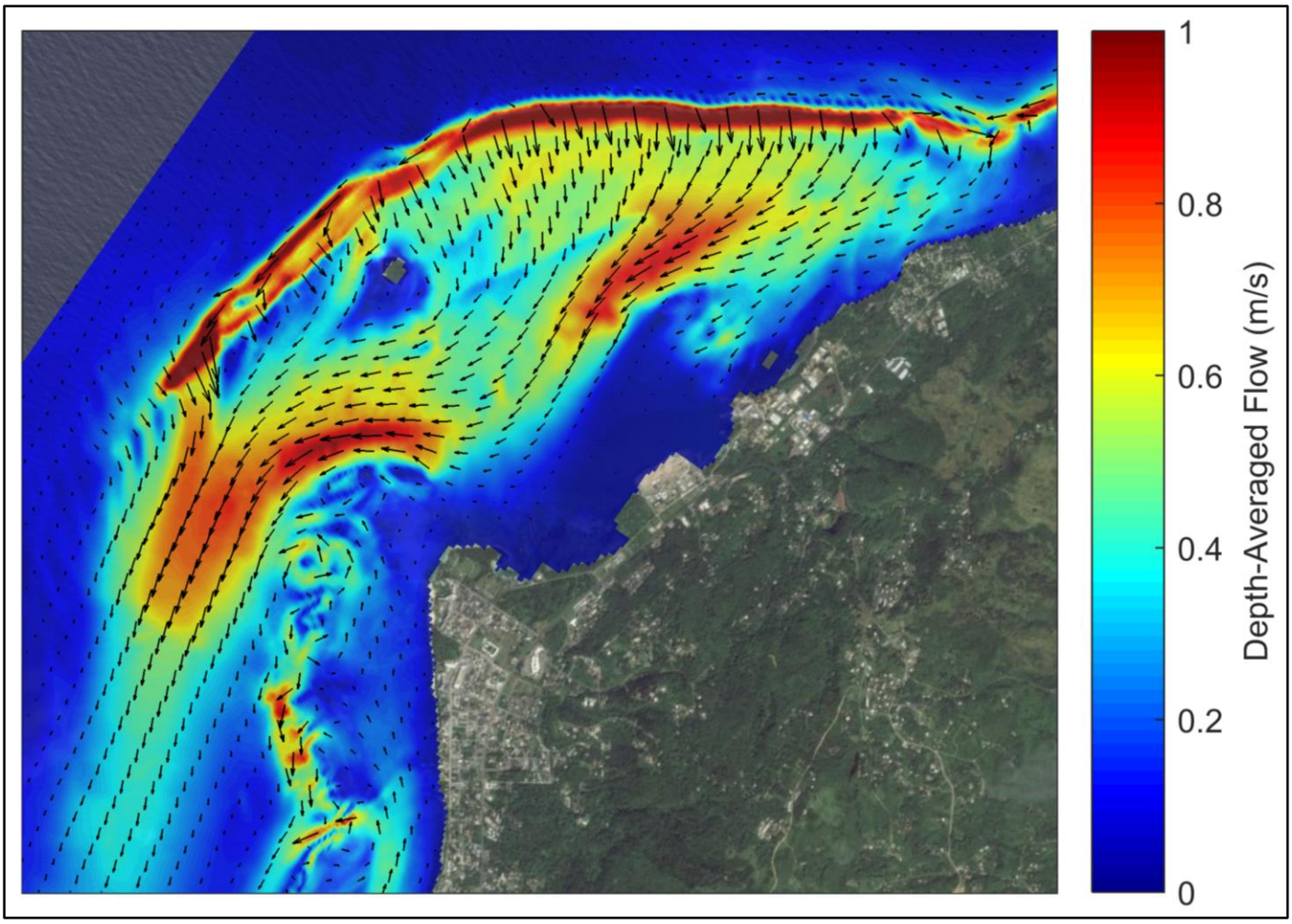

Figure 3-77. Currents during a rising tide - 1-year typhoon wave from the north-northwest, Tanapag Lagoon.

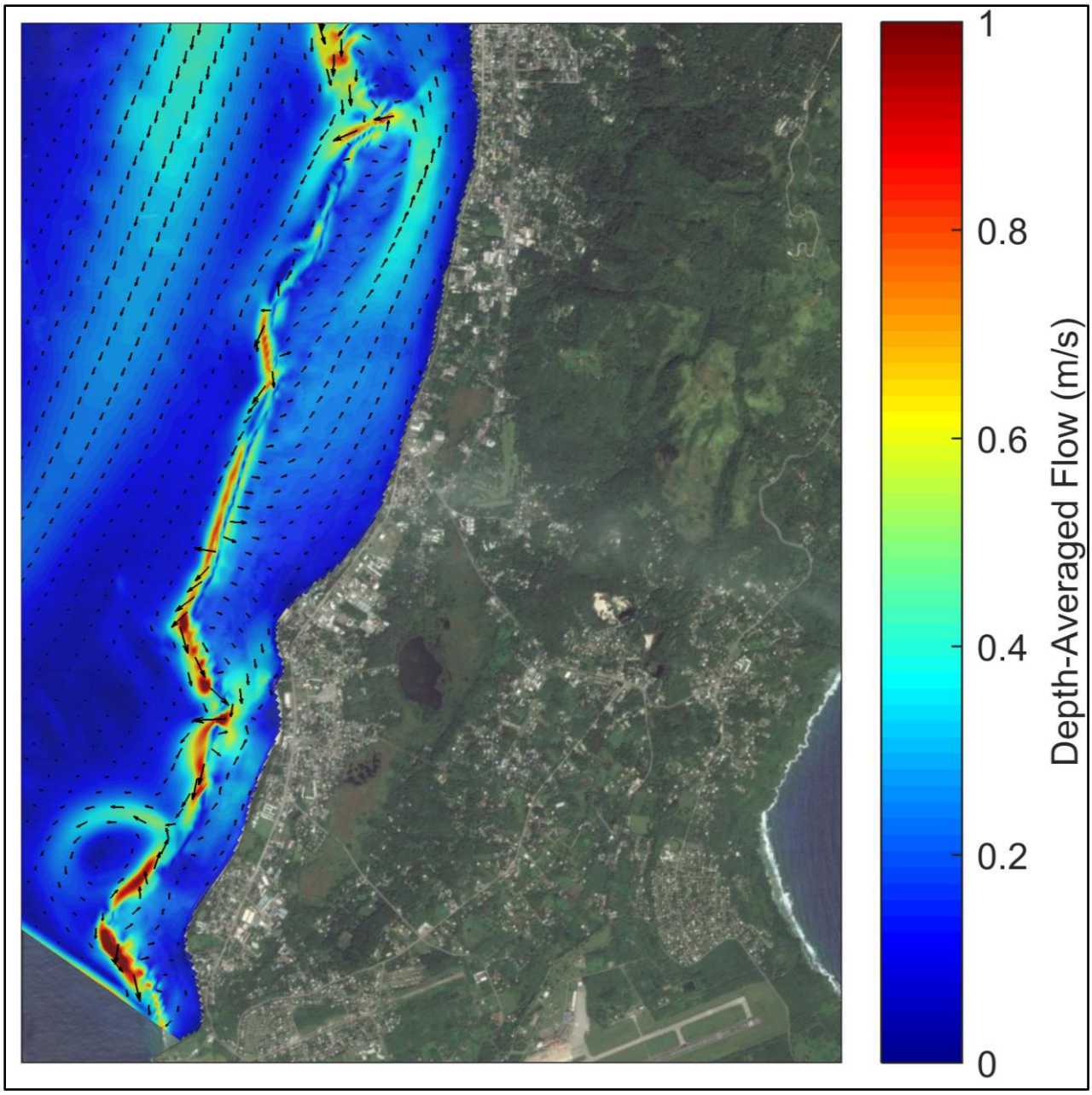

Figure 3-78. Currents during a Rising tide - 1-year typhoon wave from the north-northwest, Garapan Lagoon.

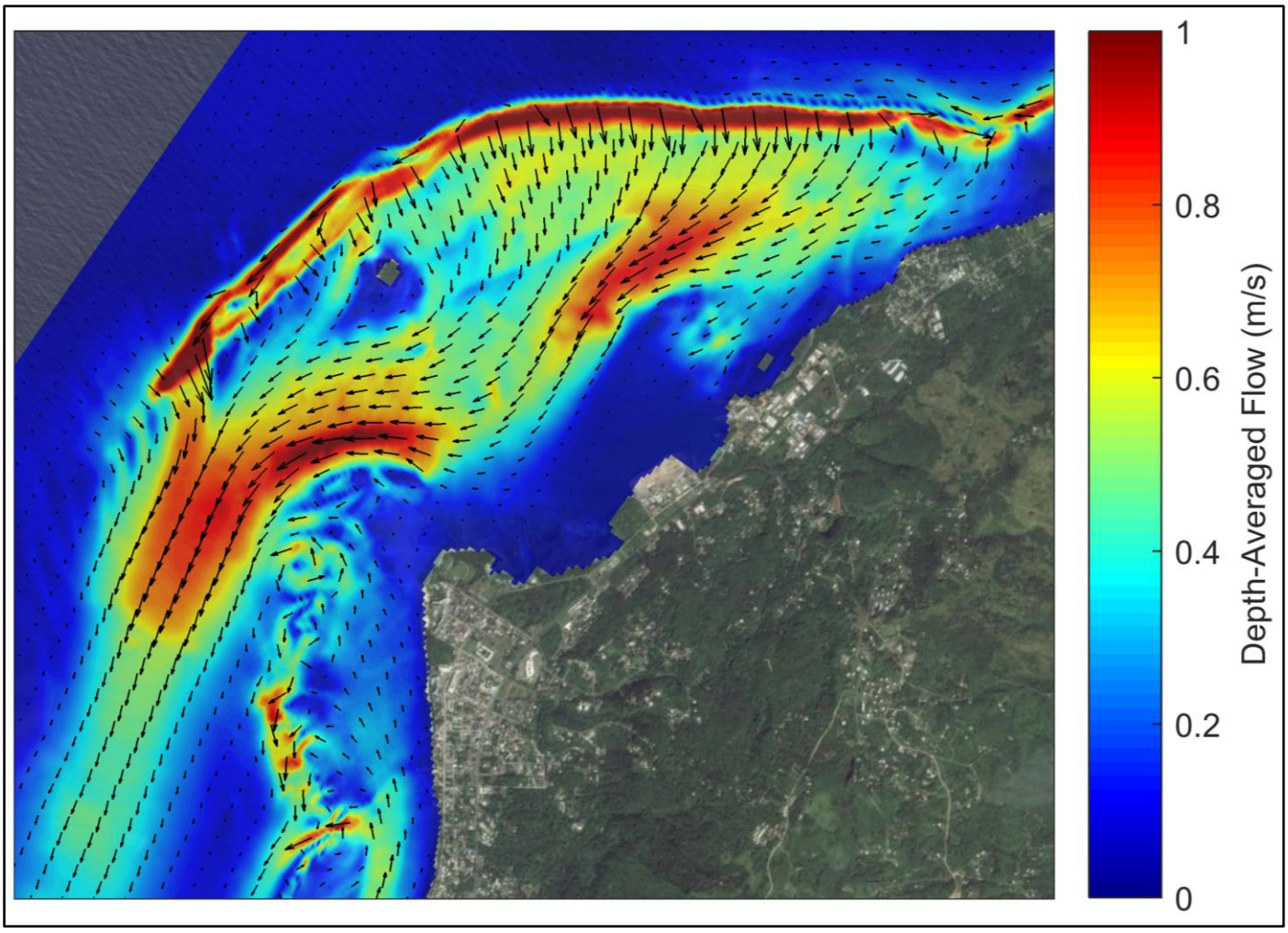

Figure 3-79. Currents during a falling tide - 1-year typhoon wave from the north-northwest, Tanapag Lagoon.

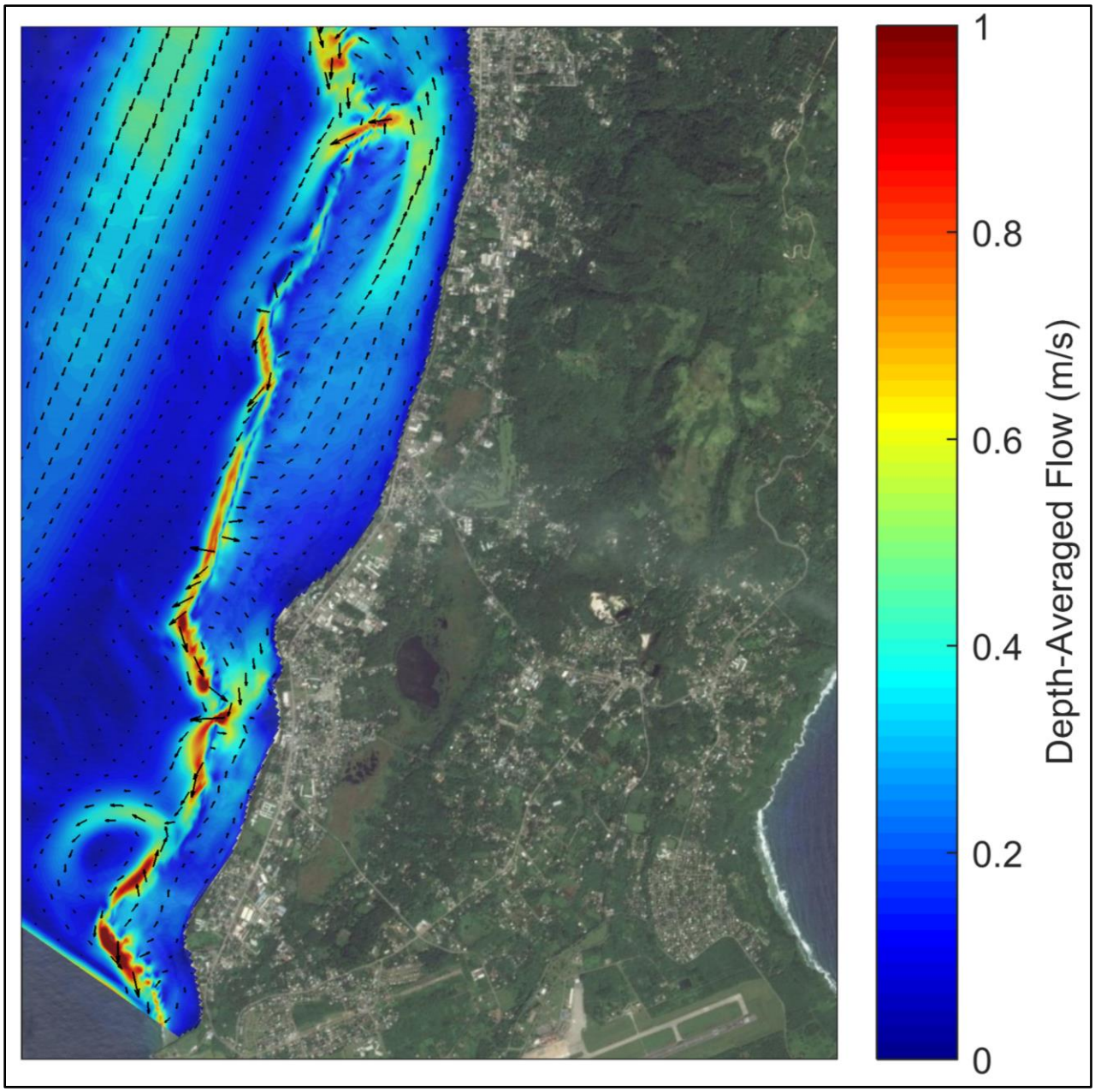

Figure 3-80. Currents during a falling tide - 1-year typhoon wave from the north-northwest, Garapan Lagoon.

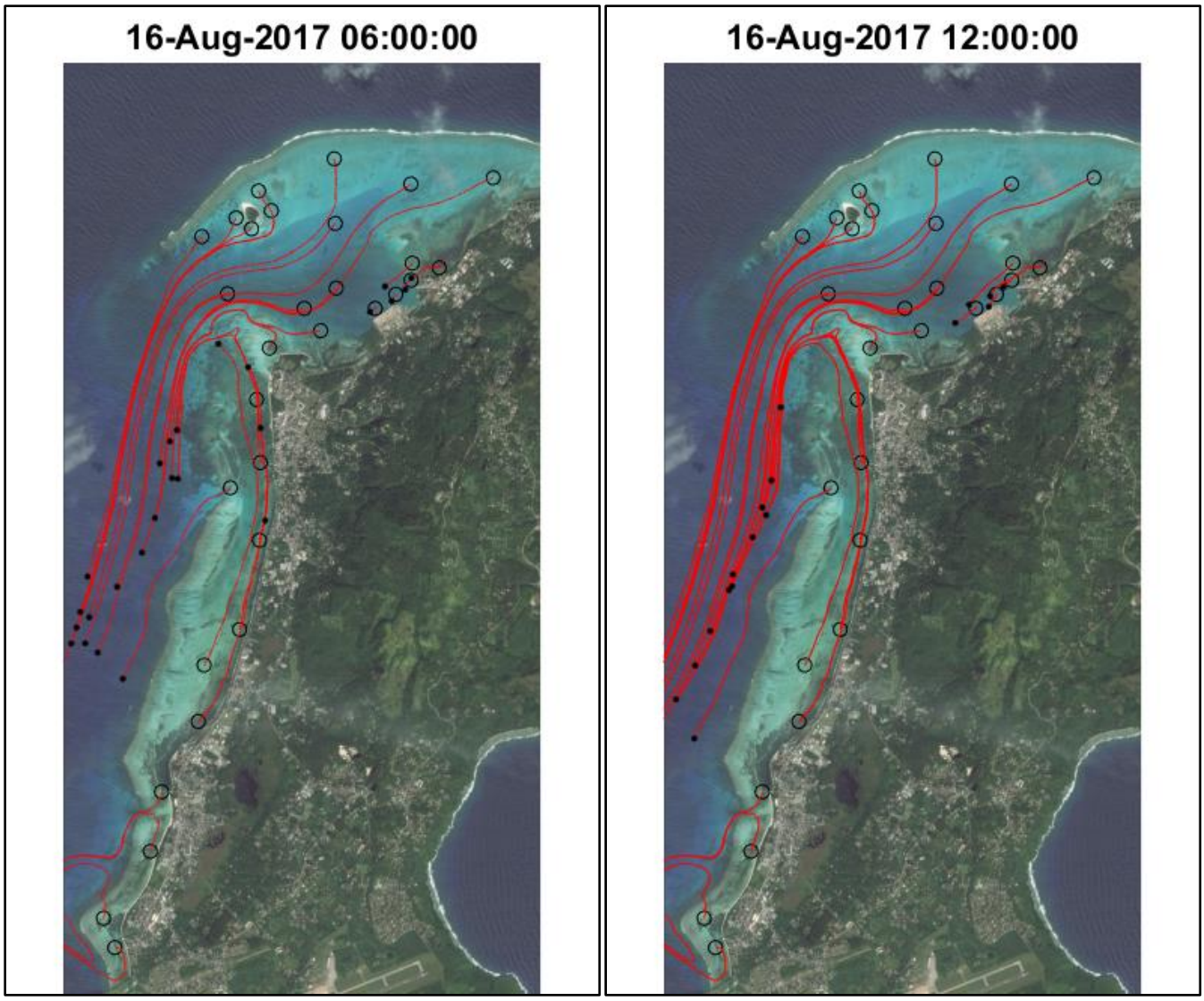

Figure 3-81 Tracer paths during typical 1-year return period typhoon wave from the north-northwest.

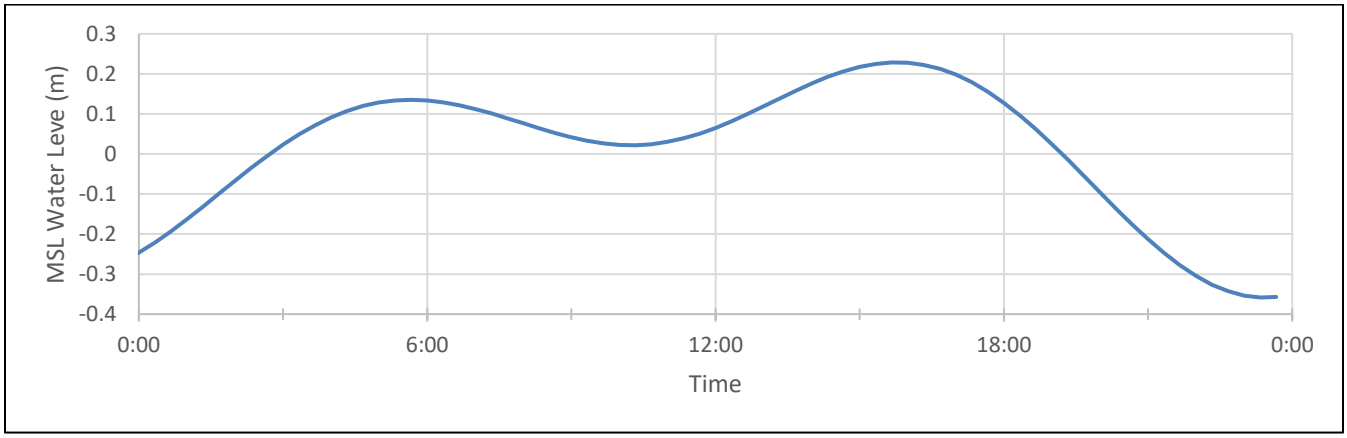

Figure 3-82. Tide level during tracer interval.

4. SUMMARY

A comprehensive study of Saipan's Western Lagoon has been completed. The study included the following components: a 30-year wave hindcast and wave climate analysis of Saipan's Western Coast, development and application of a deepwater wave model to transform deep ocean waves to the coast, development and application of a nearshore coupled wave and current model to simulate wave heights and currents within the lagoon, validation of the models with measurements recorded in the lagoon over three months during the summer of 2017, and completion of five model cases portraying the most typically occurring conditions within the lagoon. Key results of the study are outlined below.

- The hindcast and wave climate analysis revealed that the prevailing tradewind waves from the northeast are greatly reduced in wave height when the wrap around Saipan. Due to the geometry of the island, the reefs along the edge of Tanapag Lagoon are exposed to more tradewind energy than the reef that bounds the Garapan Lagoon. An analysis of hindcast wave data indicated seasonal variability in the tradewind waves with larger waves during the winter months of January to April and smaller waves during the summer months of July through October. During the summer months, there is an increase in wave energy from the west which directly impacts the west side of Saipan. Additionally, the hindcast revealed annual occurrences of large waves from passing typhoons approaching Saipan from all directions.
- The deepwater wave and nearshore coupled wave and flow models were validated using data collected by SEI during the companion field measurement program for this study. The field program included measuring waves and currents every 20-30 minutes from July through September 2017 at one location outside the lagoon, and eight locations inside the lagoon. Comparison of the model results with the measurements indicated that the numerical models are able to replicate well the wave and flow patterns in the Tanapag and Garapan Lagoons over a range of wave conditions. Both the measured data and model results show that the average flow in Tanapag Lagoon is driven primarily by waves breaking on the shallow reef resulting in a near continuous flow out of the main channel. Flow in Garapan Lagoon is driven by combination of waves and tides.
- Minor discrepancies between the measurements and model results are evident at some locations during some conditions. This is to be expected because the wave and tide driven flow in the lagoon is highly sensitive to bathymetry and reef morphology. Although the numerical models were developed to approximate as closely as possible the existing environment, the model grid size is 30 meters, and it is not possible to exactly replicate small scale bathymetric features and morphologies that may affect flow. In addition, the existing bathymetry data is inaccurate in some locations. Model results are therefore not exact simulations or predictions of what will occur, but rather approximations based on the best available information and methodologies.

- Five model cases were completed representing the most typically occurring conditions in the lagoon: typical winter tradewind wave conditions, typical summer tradewind wave conditions, typical summer westerly wave conditions, a 1-year return period typhoon wave from the southwest, and a 1-year return period typhoon wave from the north-northwest. These model cases and the field measurements show the following:
    - The average flow in the Tanapag Lagoon is driven by waves breaking on the shallow reef resulting in a near continuous westward flow out of the main channel. Larger waves drive stronger currents over the reef and out of the channel.
    - Flow in the Garapan Lagoon is driven by a combination of waves and tides. During low wave energy conditions along the reef bordering Garapan Lagoon, the tide drives flow in and out of Light House and Sugar Dock Channels and reversing currents to the north and south within the lagoon with little net transport over the course of a tide cycle.
    - During larger wave events, such as an annually occurring typhoon wave, wave-driven flow predominates in Garapan Lagoon, forcing strong currents uniformly to the north between Puntan Susupe and Garapan, and strongly seaward out of Light House and Sugar Dock channels.

Schematic portrayals of these flow patterns are presented in Figure 4-1 and Figure 4-2

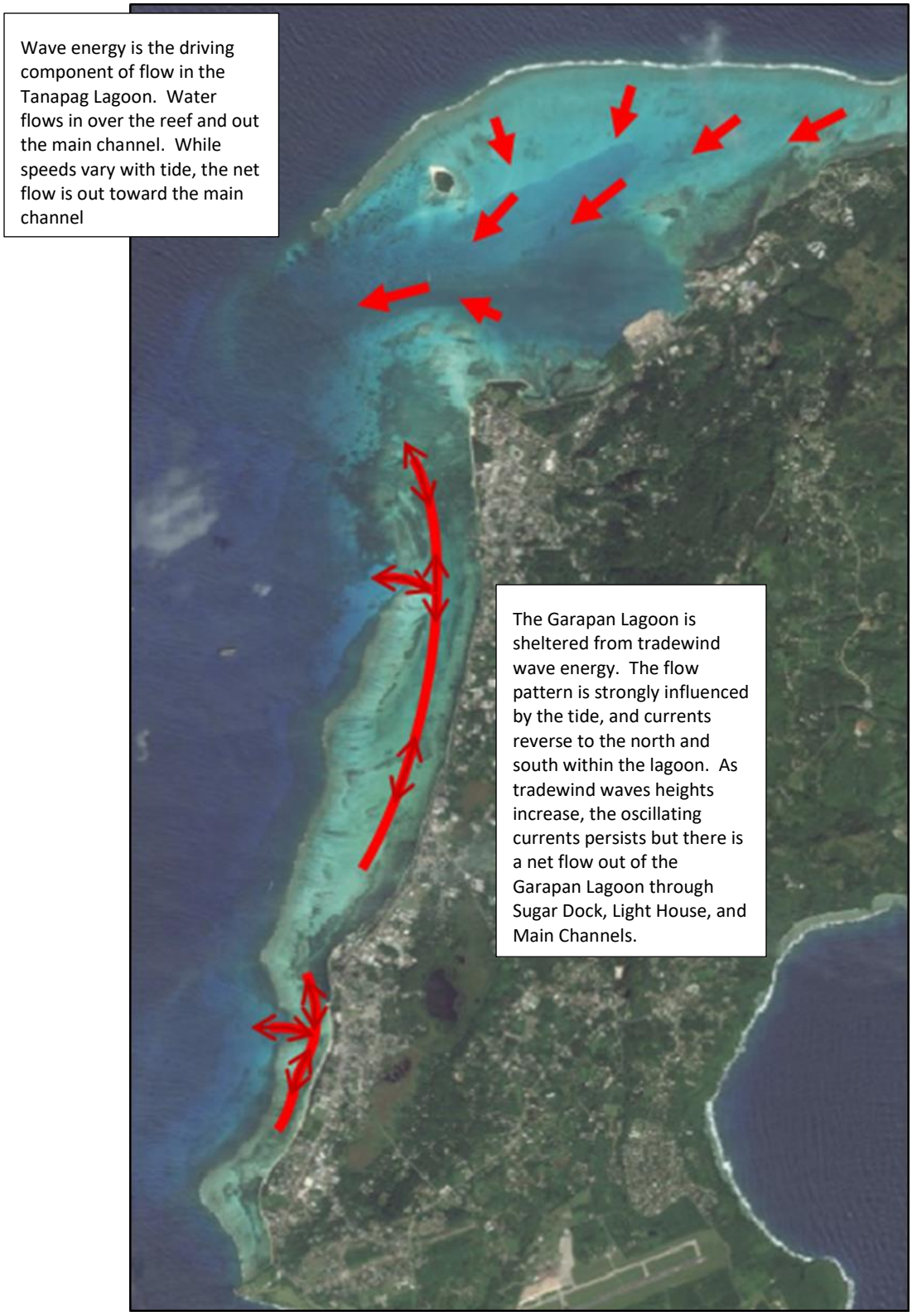

Figure 4-1. Schematic diagram of typical flow during tradewind wave conditions.

Figure 4-2. Schematic diagram of typical flow during large wave conditions.

5. REFERENCES

Coastal Data Information Program (CDIP), Scripps Institute of Oceanography, USACE. *http://cdip.ucsd.edu*. Accessed 2018.

Defense Mapping Agency, Office of Distribution Services, *Sailing Directions for the Pacific Islands, Volume I*, 1976

Deltares, 2017. Delft3D-FLOW Simulation of multi-dimensional hydrodynamic flows and transport phenomena, including sediments User Manual version 3.15.

Deltares, 2017. Delft3D-WAVE Simulation of short-crested waves with SWAN User Manual version 3.05.

Egbert, Gary D., and Svetlana Y. Erofeeva. "Efficient inverse modeling of barotropic ocean tides." Journal of Atmospheric and Oceanic Technology 19.2 (2002): 183-204.

Kamphuis, J. William. *Introduction to coastal engineering and management. Vol.* 30. World Scientific, 2010.

Lowe, Ryan J., et al. "Spectral wave dissipation over a barrier reef." Journal of Geophysical Research: Oceans 110.C4 (2005).

Lowe, Ryan J., et al. "Wave-driven circulation of a coastal reef–lagoon system." Journal of Physical Oceanography 39.4 (2009): 873-893.

Meteoblue weather. https://www.meteoblue.com/en/weather/forecast/modelclimate/saipan_northern-mariana-islands_7828758. Accessed 2019

Office for Coastal Management. National Oceanic Atmospheric Administration (NOAA) https://coast.noaa.gov/hurricanes/index.html?redirect=301ocm. Accessed 2018

Sea Engineering Inc. *Saipan Current Study: Garapan Anchorage*. 2004.

Sea Engineering Inc. *2017 Hydrodynamic Study of Saipan's Western Lagoon Data Report*. 2018.

Wave Information Studies (WIS), USACE. *http://wis.usace.army.mil*. Accessed 2015.